UNIVERSITY OF STRATHCLYDE

Department of Physics

Miniaturised opto-fluidic systems for cell manipulation and analysis

---

by Alicja Zarowna-Dabrowska

A thesis presented in fulfilment of the

requirements for the degree of

Doctor of Philosophy

November 2011

Declaration of Authorship

This thesis is the result of the author's original research. It has been composed by the author and has not been previously submitted for examination which has led to the award of a degree.

The copyright of this thesis belongs to the author under the terms of the United Kingdom Copyright Acts as qualified by University of Strathclyde Regulation 3.50.

Due acknowledgement must always be made of the use of any material contained in, or derived from, this thesis.

Frontispiece

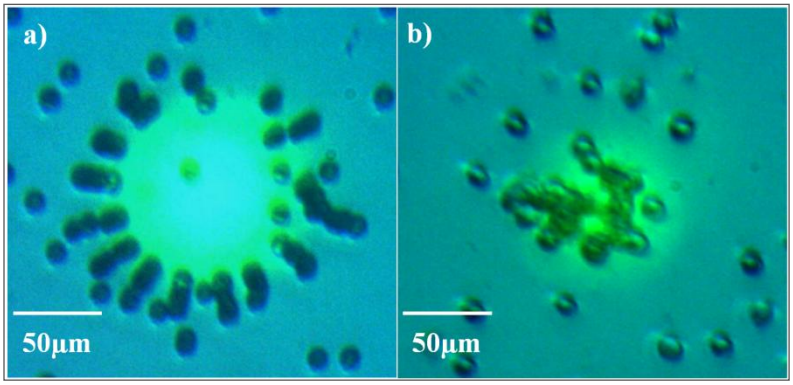

Trapping particles with miniaturised optoelectronic tweezers: a) trapping beads with 74µm diameter pixel, at 20V peak to peak voltage; b) trapping cells with 54µm pixel at 5V peak to peak voltage; both photographs were captured 40 seconds after a pixel was turned on. Movies showing these trappings are available at http://www.opticsinfobase.org/abstract.cfm?uri=oe-19-3-2720 .

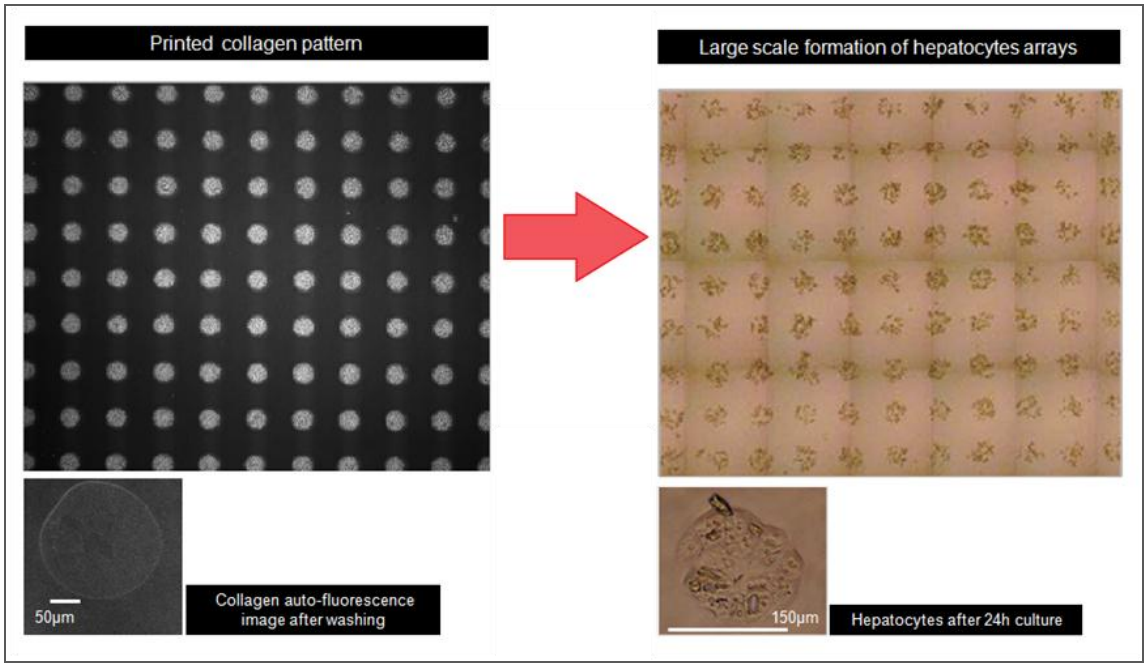

Generation of uniform microarrays of primary hepatocytes for chip based analysis on the top of printed collagen patterns created by piezoelectric printing.

Abstract

This PhD research project aimed to develop miniaturised opto-fluidic systems for cell manipulation and analysis which are essential for new medical technologies. These miniaturised systems have distinctive advantages over traditional analysis tools such as faster assays, smaller size, lower cost and much lower sample consumption.

In this work, three miniaturised systems were achieved. The first system, miniaturised optoelectronic tweezers (OET), was developed by using a CMOS-controlled GaN micro-light emitting diode (micro-LED) array as an integrated micro-light source. It was demonstrated for the first time that with the spatio-temporal and intensity controllabilities of the emission pattern, the green micro-LEDs are capable of creating reconfigurable virtual electrodes to achieve optoelectronic tweezing.

The second system, a miniaturised cell analysis platform, used piezoelectric printing to create micro-patterns of proteins onto a new type of non-adhesive surface, which was then integrated with a microfluidic device. The printed protein pattern has a higher resolution in comparison with previous reported results and remained stable even after extensive washing. Cells seeded on these patterns formed well defined micro-arrays which were successfully used for toxicity studies. The cell micro-arrays were also integrated with a microfluidic device.

The third system developed was a miniaturised local cell fluorescence analysis platform. In this system, micro-LEDs with a dedicated thin-film filter and a lens were integrated with a microfluidic network to achieve efficient local fluorescence excitation and

detection. By using this system, fluorescence from individual cells has been successfully detected.

With their distinctive advantages, the new miniaturised systems developed in this work offer a wide range of clinical and bio-applications.

Acknowledgments

I would like to thank my supervisors, Dr. Erdan Gu and Dr. Huabing Yin for their guidance, support and encouragement throughout the course of my PhD. I also wish to express my gratitude to Dr. Steven L. Neale for his support and cooperation during my work. Furthermore, I would like to thank Prof. Martin Dawson for giving me the opportunity to prepare this PhD thesis and the Scottish Consortium for Integrated Micro Photonics Systems (SCIMPS) which he led for providing financial support for the project. I also would like to thanks Prof. Jon Cooper for his support and encouragement.

Completing this work would not be possible without the precious help and support I received from many people. I would like to thank wholeheartedly, in no particular order, David Massoubre and Zheng Gong who fabricated the micro-LEDs devices, Jonathan McKendry who taught me how to use them, Bruce Rae who assisted me in experiments with CMOS devices, Min Wu and Ekaterina O. McKenna who helped me in printing experiments, Li Chen who taught me the PEG treatment, Carlos Cuestas-Ayllon who helped me with surface treatments, Gordon McPhee who helped me in cell culture and did AFM analysis, Andrew Glidle who did XPS measurements, Maaike E. Schutte who showed me how to culture primary hepatocytes, Niall P. McDonald who helped me with hepatocytes and cleanroom fabrication, Chris Syme who helped me with fluorescence measurements, Paul Hynd who prepared a lot of micro-fluidic holders, Paul Thomson who prepared PCBs for micro-LEDs, and many other people who helped me in some way.

I also wish to thank Lynda McLaughlin for her unconditional support during my PhD study, and also Lisa Flanagan and Sharon Kelly for their administrative help. A big ‘thank you’ goes to all my IoP and Glasgow University colleagues, past and present, for making those institutions such stimulating and friendly work places.

Last but not least, I would like to thank my family for their continuous encouragement and in particular my husband, Marcin, for his relentless support and love.

Content

List of Figures

Chapter 1

1. Introduction

1.1. The role of optics and photonics in the new medical technologies

Following the increasingly rapid development of science and technology, medical technologies have progressed significantly over the past decades to improve the quality of people's lives. Beyond doubt, the progress in this domain is reflected in the steady increase of life expectancy from 1960 by around one year per decade [1]. Modern technologies, for example, allowed for earlier, faster and more accurate diagnostics, which contribute to decrease the number of premature deaths. Technological progress has also allowed for production of innovative medical devices, new drugs and the development of different analysis instruments. Furthermore, new ways of imaging such as computed tomography (CT) scanners, magnetic resonance imaging (MRI) and positron emission tomography (PET) have enabled finding the dysplasia of a tissue without using "exploratory surgery" [1].

When looking from perspective of medical techniques, the role of optics and photonics is particularly important, not only in the field of imaging. Light is used to interact with bio-samples in different forms, for example, by photo-stimulation. More importantly, the whole domain called photodynamic therapy was developed based on toxic reactions induced by light. Photodynamic therapy is used with success for treatment of different tumors and dysplasia [2]. Furthermore, light absorption and emission by specifically

designed molecules called fluorophores allowed the development of fluorescence microscopy. By utilising specially designed dyes, fluorescence microscopy helps differentiate between different cell types, different molecules and their different biological states.

Looking back into the historical development of optics and its biomedical applications, the 1960s saw the development of the first lasers. These novel powerful light sources were first used in medicine in the 1970s in certain types of surgeries, replacing knives and scalpels. In the 1980s, lasers were coupled with microscopes and allowed for the development of powerful fluorescence imaging methods. In the 1990s, fibre optics helped develop modern laparoscopic surgery, colonoscopy, gastroscopy and endoscopy. As a result, surgery and diagnostics of organs previously inaccessible or of difficult access could be achieved. For example, "colonoscopy can detect intestinal polyps before they become cancerous. Another example is the repair of torn ligaments and tissues in knees and other joints" [1]. Recently, evanescent wave analysis and optical trapping techniques have been developed rapidly allowing for characterising forces and interactions between bio-molecules in micro-scale, such as interactions between different molecular motors, the phenomena of DNA transcription, protein folding, etc. [3].

1.2. Semiconductor solid state light sources as an attractive alternative for new medical technologies

However, from today's perspective the medical technologies mentioned above used bulky and expensive light sources, such as lamps and lasers. Some of the optics in these tools are still based on the technologies and designs developed 30 years ago. By contrast, novel semiconductor solid state light sources have been developed in recent years. One of the major new semiconductor light sources is that of light emitting diodes (LEDs). LEDs have very good light-emitting characteristics such as high light output power (mW-W) and are an attractive alternative to big lasers and lamps in many medical and biological applications. The physics and light emitting mechanism of LEDs will be described in detail in the next Chapter.

Thanks to this new semiconductor optoelectronics, medical tools can be made smaller, portable or implantable and more energy efficient. Semiconductor optoelectronic devices can generate, transmit, modulate and detect light over a wide range of wavelengths, from ultraviolet (UV), through visible to near infrared. These capabilities are very useful for bio-applications as UV light is absorbed by proteins and nucleic acids, while visible light is absorbed by molecular probes and aromatic compounds. Thus, the semiconductor light sources can be used for synthesis of molecules, fluorescence studies and bio-sample manipulation. Furthermore, their small device geometry facilitates the integration with different bio-instruments. A few examples of micro-systems using semiconductor optoelectronics and the background of previous relevant work will be reviewed in detail in the following sections.

1.3. The existing bio-micro-tools and platforms with a light source

Over the last decade, families of bio-micro-tools, frequently referred to as ‘lab-on-a-chip,’ were developed. However, when a light source is required for the analysis, the tools have generally still employed bulky and expensive lasers and lamps (see Fig. 1.1). Thus, this kind of tool could perhaps be described as ‘chip-in-the-lab’ rather than ‘lab-on-a-chip’.

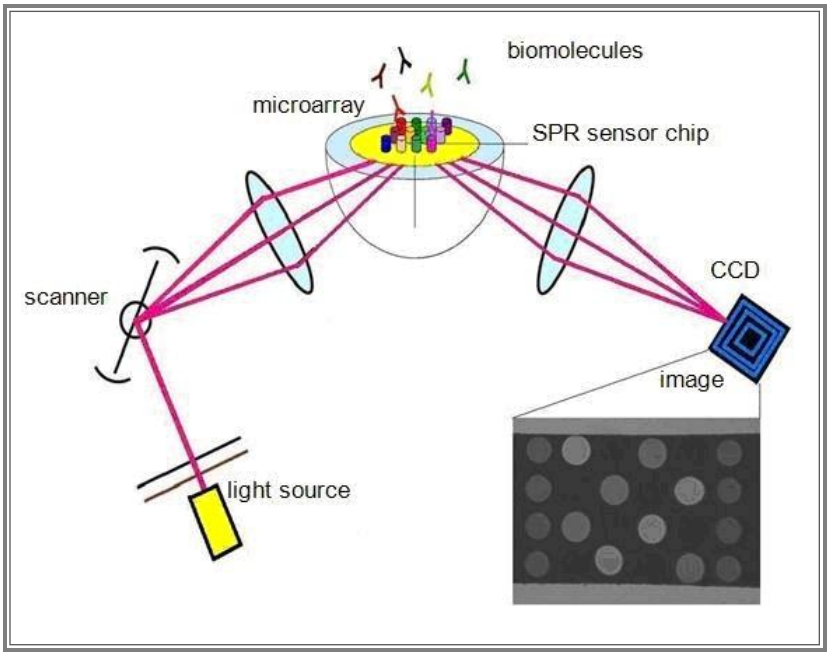

Fig. 1.1 Schematic of an example of a ‘lab-on-a-chip’ device for scanning arrays of antibodies to analyse human immune response; the ‘light source’ here is a laser; from [4].

In recent years, a few bio-micro-analysis tools used integrated semiconductor lasers as a light source. Among the examples of real integrated micro-devices, a ‘bio-cavity lasers’ approach was developed, whereby healthy and unhealthy cells were differentiated by inducing changes in the cavity laser spectrum due to the difference of the cell’s refractive index [5]. Different cell types were analysed and distinguished by a

miniaturised flow cytometry test made inside miniaturised laser cavity (Fig. 1.2). The main challenge for developing this device was sample hosting. First, as the bio-sample adhered to the glass and semiconductor material surfaces, the sample was contaminated and the reliability of the assay decreased. Second, the semiconductor material (gallium arsenide) used was not bio-compatible – arsenide ions are toxic for biological samples. These problems have been resolved by adequate coating of the sample chamber and the device application was under test for clinical use.

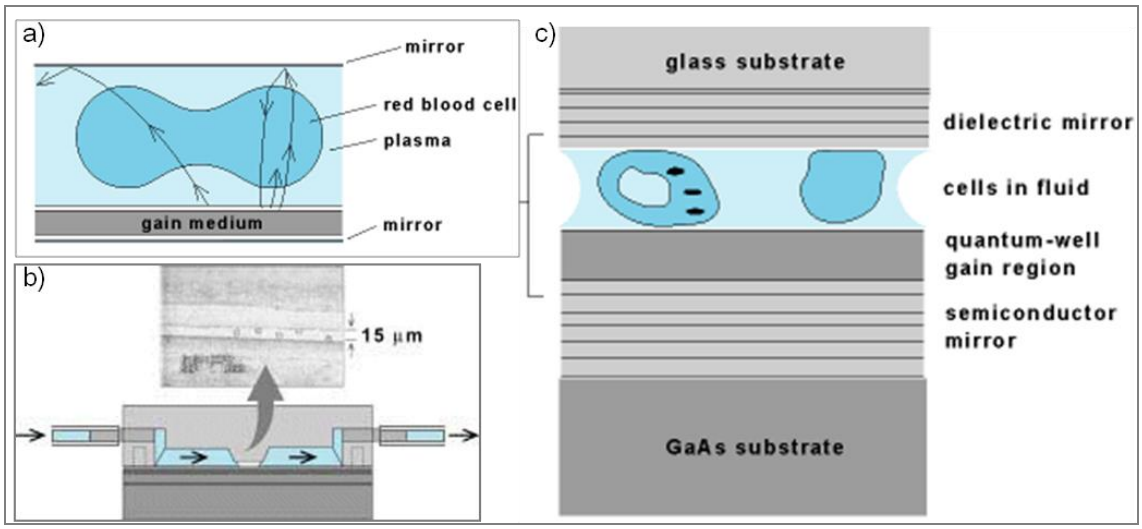

Fig. 1.2 Schematic of the bio-cavity laser: a) a red blood cell acts as a waveguide to resonate light between the two mirrors; b) bio-cavity for flow cytometry, showing the cross section of the semiconductor wafer where a 15-µm groove has been etched; the red blood cells are shown flowing in single channel; c) cross section of the bio-cavity laser; from [5].

Other promising optical micro-devices used micro-wells made in semiconductor materials [6]. This work used a semiconductor laser emitting at 630nm, and the wells were etched inside the semiconductor wafer with a femtosecond laser. The wells have diameters from 36µm to 268µm. Next, red fluorescent beads, 2.5µm in diameter and

absorbing at 630nm and emitting at 660nm, were placed inside the etched wells. Localised fluorescence emission from the beads confined inside microwells was induced (Fig. 1.3) [6]. However, further fluorescent tests with bio-samples have not been reported.

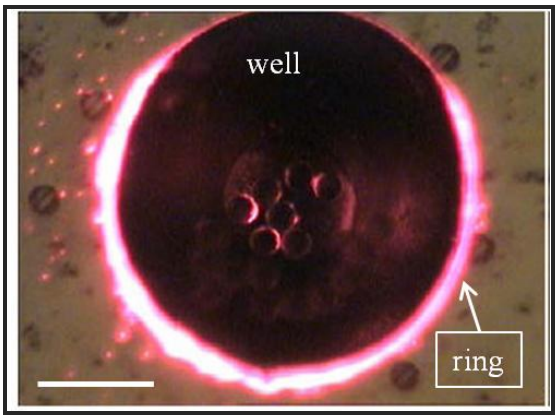

Fig. 1.3 A micro-well created at the surface of a semiconductor wafer. A ring illumination within a microfluidic well was used to quantify latex micro-beads. The scale bar is 10μm; from [6].

In another setup for bio-molecule analysis, having the potential of being a fully integrated device, the light was projected from a Vertical Cavity Surface Emitting Laser (VCSEL) to the sample chamber as shown in Fig. 1.4 [7]. A VCSEL is a microcavity semiconductor laser emitting mW power with a beam perpendicular to the surface of the chip. The surface plasmon resonance (SPR) method was used for sample detection. SPR relies on the change in the refractive index of the reflecting surface induced by binding a molecule to this surface [7].

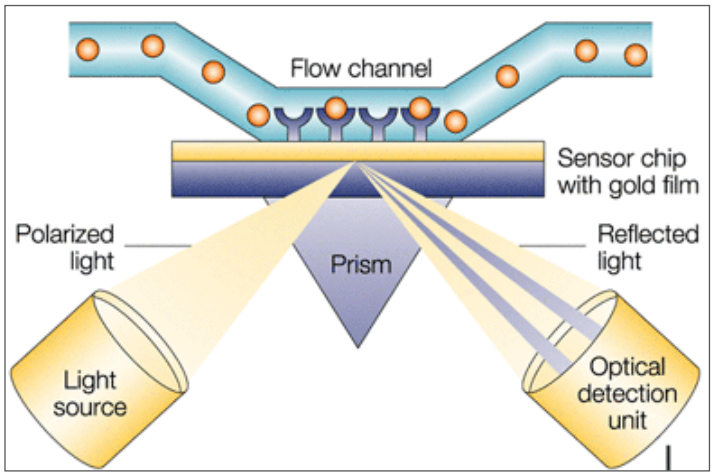

Fig. 1.4 Scheme of a surface plasmon resonance (SPR) device. SPR detects changes in the refractive index in the immediate vicinity of the surface layer of a sensor chip. The SPR angle shifts when micro-particles or biomolecules are bound to the surface, which changes its density and results in changes in the refractive index of the surface layer; from [7].

Usually, in this kind of device, the light is projected onto the reflecting surface through a prism as shown in Fig. 1.4. However, the light can also be coupled onto the reflecting surface through a plasmonic crystal structure [8]. When a micro-particle or molecule is attached to the reflecting surface, the layer density changes, which changes its refractive index. Thus the reflected light angle changes, indicating particle attachment [8, 9]. However, it has not been reported whether this particular device was used successfully for detection of biomolecules.

Another group demonstrated the integration of microfluidic channels with a semiconductor laser for achieving micro-particle manipulation and trapping [10]. These microfluidic channels were made out of SU8 polymer and monolithically integrated on the top of the laser emitting surface. The polystyrene bead manipulation and cell trapping inside these channels are shown in Fig. 1.5 [10].

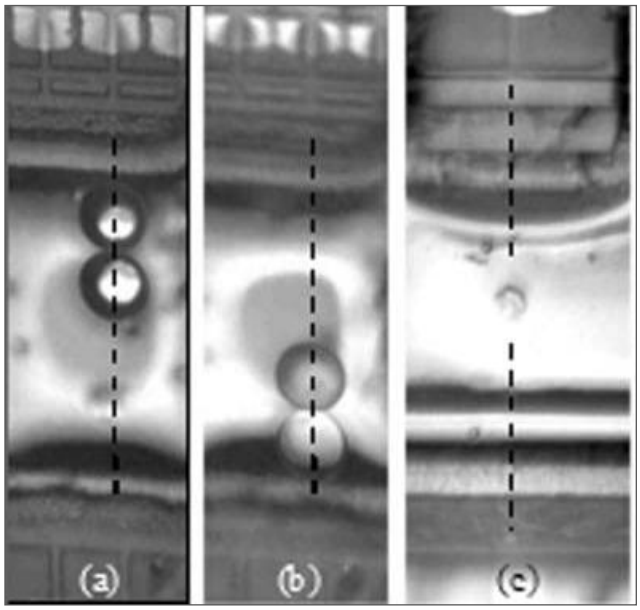

Fig. 1.5 Particles trapping inside SU8 microfluidic channels. The dashed lines in these images show the axes of the laser beam. (a), (b) two 20μm diameter polymer spheres pushed from one side to the other as relative beam powers are varied; (c) one cell "trapped"; from [10].

In this work, even though the light beam was divergent, polystyrene beads and cells were effectively manipulated inside the microfluidic channels due to the high light intensities used (tens of mW in infrared wavelengths). However, high light intensity may pose problems such as heat generation which would interfere with the viability of cells in a longer study.

Another recently developed micro-device combines photonics and bio-technology to achieve a bio-micro-actuator as shown in Fig. 1.6 [11]. In this device, drosophila heart muscle was transfected with a gene of Channelrhodopsin-2 (ChR-2). ChR-2 absorbs light at blue wavelengths and generates electrons provoking an electrical impulse. When these transfected muscle cells are illuminated with blue light, the light is absorbed, the

electric impulse is generated and the muscle contracts under this stimulus. The muscle cells were seeded on a special poly(dimethylsiloxane) (PDMS) structure and the muscle contraction made the PDMS structure change its shape.

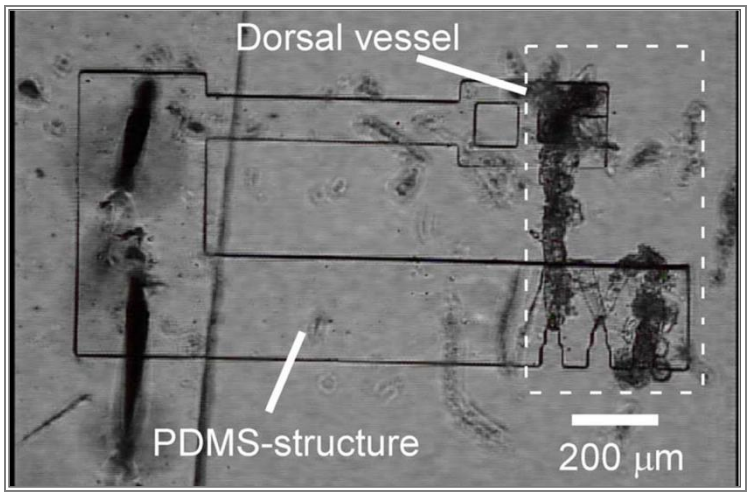

Fig. 1.6 Microscopic image of the assembled bio-micro-actuator; from [11].

The light source used in this work was a 470nm indium gallium nitride LED (M470L2, Thorlabs), controlled by an external driver (LEDD2L, Thorlabs). However, as the LED light was projected onto the PDMS structure through microscope lenses, the whole system was quite bulky.

In this thesis work, three novel miniaturised systems for bio-applications were developed using new light sources and technologies. By integrating the novel semiconductor optoelectronics micro-light emitting diode (micro-LED) arrays the following micro-systems were developed: miniaturised optoelectronic tweezers, a cell analysis platform and a tool for local cell fluorescence analysis. The motivation for the development of these devices is presented in the next sections.

1.4. Micro-light emitting diodes: advantages and existing system applications

The gallium nitride micro-LED devices have been developed in the Institute of Photonics and by other groups for a variety of applications. Micro-LED arrays consist of many micro-scale LED pixels which can be fabricated with different pixel shapes, sizes and layouts. The details of micro-LED characteristics and operation will be presented in the next Chapter. The emission wavelengths and output powers of micro-LEDs are suitable for inducing the polymerization of some organic materials as well as for exciting fluorescence from biological samples. For example, the micro-LEDs have been successfully used for micro-fluorimetry, whereby time resolved fluorescence emission of Rhodamine dyes and colloidal quantum dots were measured with a single photon avalanche diode (SPAD) detector integrated on a Complementary Metal-Oxide-Semiconductor (CMOS) chip [12, 13]. The structure of the micro-fluorimetric device and measurement results are shown in Fig. 1.7.

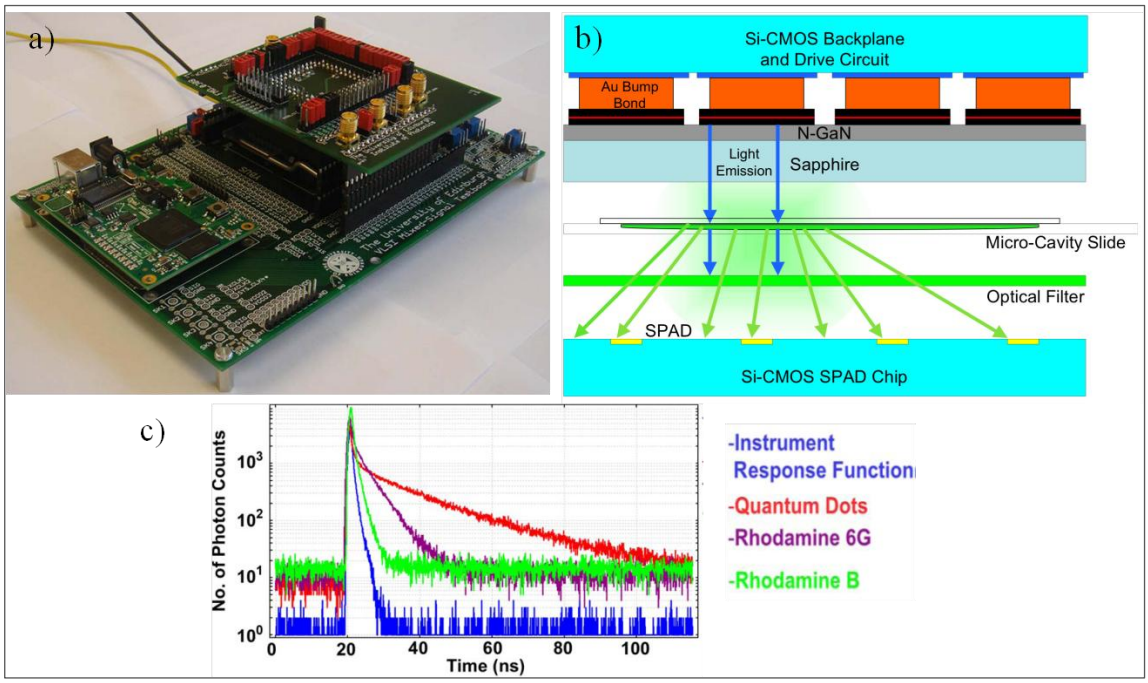

Fig. 1.7 Fluorescence life-time measurements with a micro-LED device; a) picture of the micro-system; b) schematic of the experimental set up; c) quantum dots and Rhodamine dye fluorescence life-time measurements; from [12].

This application is important for the development of a miniaturised 'all-in-one' fluorescence life-time measurement tool. Today, this type of measurement is typically done by systems with a bulky laser source operating in sub-nanosecond regime.

Micro-LED devices were also successfully used for mask-free photolithography and direct writing [14, 15]. For example, UV micro-LED devices with and without an integrated lens array were used to create micro-photoresist patterns (Fig. 1.8 I (a) and (b)) [14]. Also, UV micro-LED pixels projected through a de-magnifying setup were used to create very fine lines and dots in NO A81 photoresist (Fig. 1.8 II a) and b)) [15]. In the last application, the projected light power density was as high as 8.8 W/cm^2 and

the smallest created dot had a diameter of 8µm (10:1 demagnification). Recently, micro-LEDs with a pixel size of 5µm was used successfully to write the structures smaller than 1µm (again with 10:1 demagnification) [16]. These results are significant for the development of mask-less photolithography with nanometre resolution.

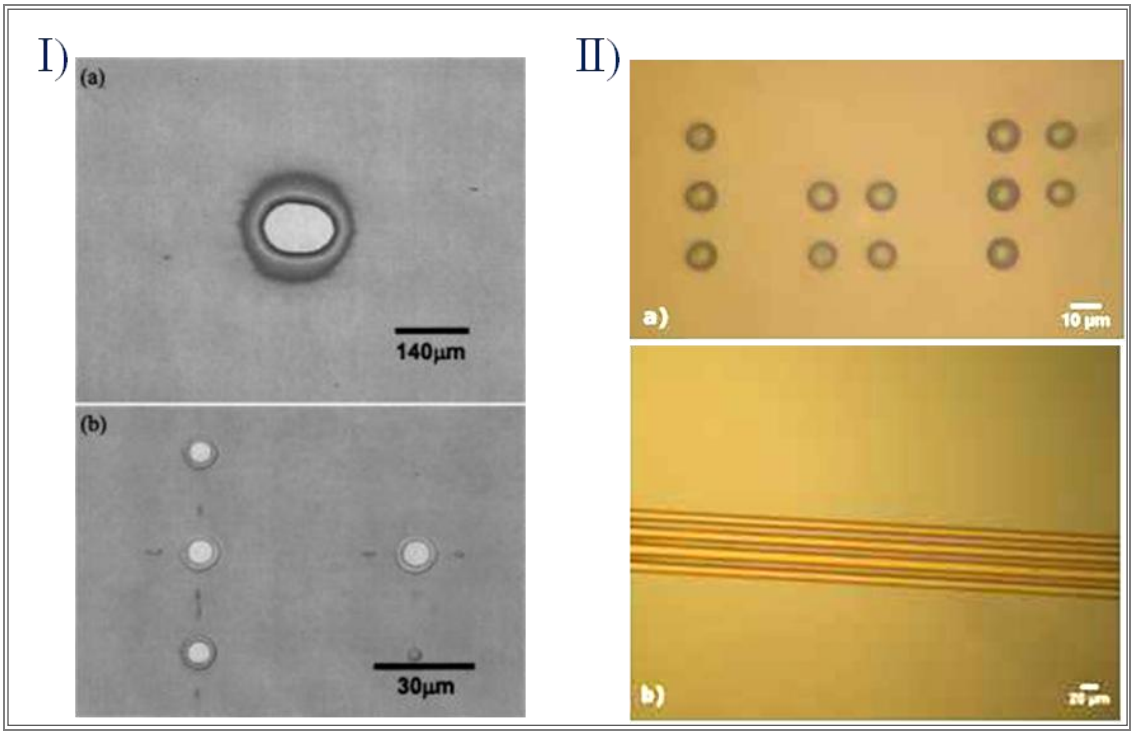

Fig. 1.8 Mask-less photolithography with micro-LEDs: I) micro-wells created in photoresist with matrix-addressable micro-LED arrays: (a) a well created with a bare LED device, 2 pixels switched-on 60µm apart; (b) wells created in photoresist with the micro-LED with integrated micro-lenses, LED pixels 30µm apart; II) patterns created with CMOS controlled micro-LEDs by using a projection setup: a) 8µm diameter dots forming an IoP logo; b) 8µm wide lines; from [14, 15].

Among further applications, micro-LED devices have also been 'coupled' with organic structures to form organic/inorganic hybrid optoelectronic devices [17]. For these hybrid devices, specially synthesised organic materials were inkjet printed on the top of micro-

LED pixels to achieve efficient colour conversion (Fig. 1.9). Based on these hybrid devices, high brightness micro-colour displays can be developed.

Fig. 1.9 Inkjet printed organic semiconductor material on micro-LED pixels. Optical micrographs of two LED pixels: bare UV micro-LED pixel (left) and the LED pixel with integrated light emitting polymer structure (right). The scale bar represents 50μm; from [17].

In bio-applications, blue micro-LED devices were used successfully in structured illumination microscopy [18]. For this application, specially designed micro-stripe LED devices were used with custom designed software to obtain sectioned images with enhanced contrast between the sample and the background. The images of pollen grain obtained with a micro-stripe LED source in comparison with standard wide field and confocal images are shown in Fig. 1.10.

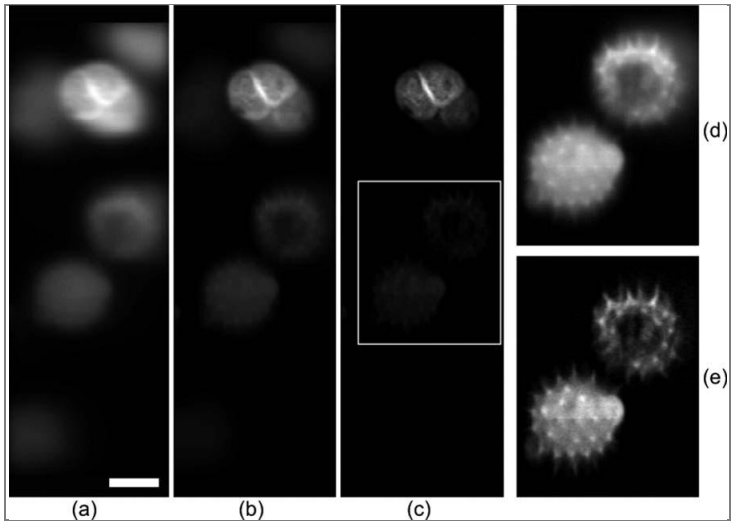

Fig. 1.10 Images of a stained pollen grain cluster: (a) reconstructed wide field, (b) conventional slit confocal, (c) improved slit confocal with a micro-stripe LED; (d), (e) zooms of the highlighted pollen grains from images (b) and (c), respectively. Scale bar is 6 μm; from [18].

Compared with conventional confocal microscopes with bulky light sources and complicated optics, these results demonstrated the potential to achieve a high resolution and low-cost sectioning imaging tools with a micro-LED light source.

Micro-LED devices have also been used for photo-induced nerve cell stimulation, called ‘optogenetics’ [19]. In this application, micro-LED light was projected to a cell container with a projection setup. The micro-LED array light photo-activated a fluorophore, Channelrhodopsin-2 (ChR-2) incorporated into neurons by transfection (Fig. 1.11 a and b) [20]. Once activated, the fluorophore stimulated an electrical response from living neurons cells.

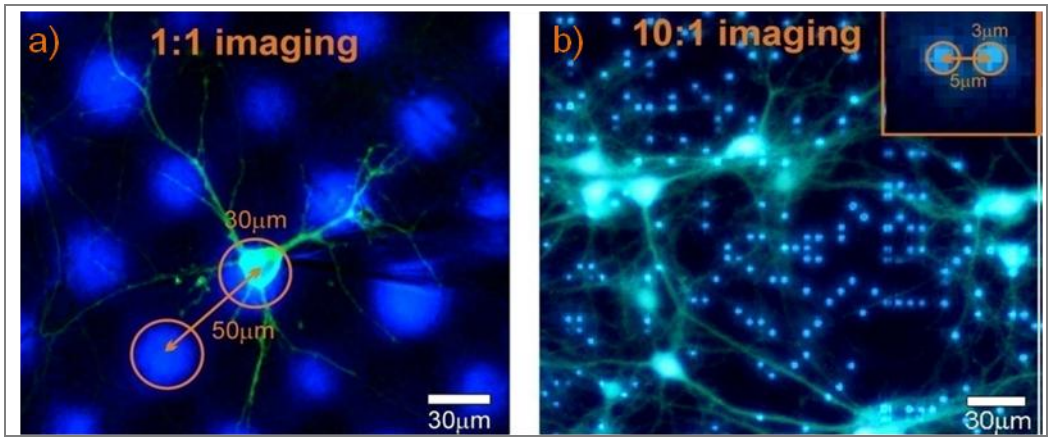

Fig. 1.11 ChR-2 excitation in cultured neuron cells with a blue micro-LED array; a) when the micro-LED array was projected as a 1:1 image; b) when the same array image was de-magnified through a projection system; from [20].

As compared to previous studies of neural photo-stimulation, it was shown that by using ChR-2, the minimum optical power required for neuron stimulation was decreased down to a safe level for the cells. Importantly, matrix addressed pixels of micro-LED array allowed for two-dimensional multisite excitation of neurons. This approach was further developed in cultured and sliced neurons, which allowed for controlling their electrophysiological responses in vitro [20]. The developed optogenetics technique can be used to create a retinal prosthesis for degenerated photoreceptors [21].

1.5. Use of micro-LED devices in this work

In this thesis work, the micro-LED devices were used as a light source for two new micro-systems: miniaturised optoelectronic tweezers (mini-OET), described in Chapter 3; and a miniaturised system for local fluorescence excitation described in Chapter 6. In both applications, micro-LED light was projected to the sample chamber with a small lens. Unlike the previous systems, these two systems are compact and portable.

More specifically, micro-LEDs were used to generate local virtual micro-electrodes in photoconductive material in the miniaturised optoelectronic tweezers (OET). The manipulation technique using OET will be presented in detail in the next section and compared with other virtual tweezing techniques. In previous OET applications, light from an external light source was projected onto a device to generate a micro-light pattern, such as a digital micromirror device (DMD), and then coupled into the sample chamber. By contrast, in this research, virtual electrodes were induced directly by the micro-LED array.

1.6. Bio-molecule manipulation

Generally, virtual tweezing uses different physical mechanisms such as atomic attraction, acoustic wave depletion or magnetic, light or electric field gradients to generate localised forces. The forces generated are then used to manipulate micro/nano objects. Different manipulation techniques have been developed over the past decades such as Atomic Force Microscopy (AFM) [22], acoustic traps [23], magnetic tweezers [24], optical tweezers [25] and dielectrophoresis [26].

In particular, AFM is a measurement technique allowing for the measurement of forces as small as 10pN, imaging objects with a resolution of Ångstroms and detecting events happening in a millisecond time scale. It involves detecting changes in laser reflection on the AFM head hosting a cantilever. Changes in the reflection pattern show cantilever micro/nano displacements and allow for measuring the topography of a surface (Fig. 1.12 a) [27]. In contact mode, AFM can also be used to manipulate the samples. Importantly, such manipulation can be done in three dimensions (Fig. 1.12 b) [28].

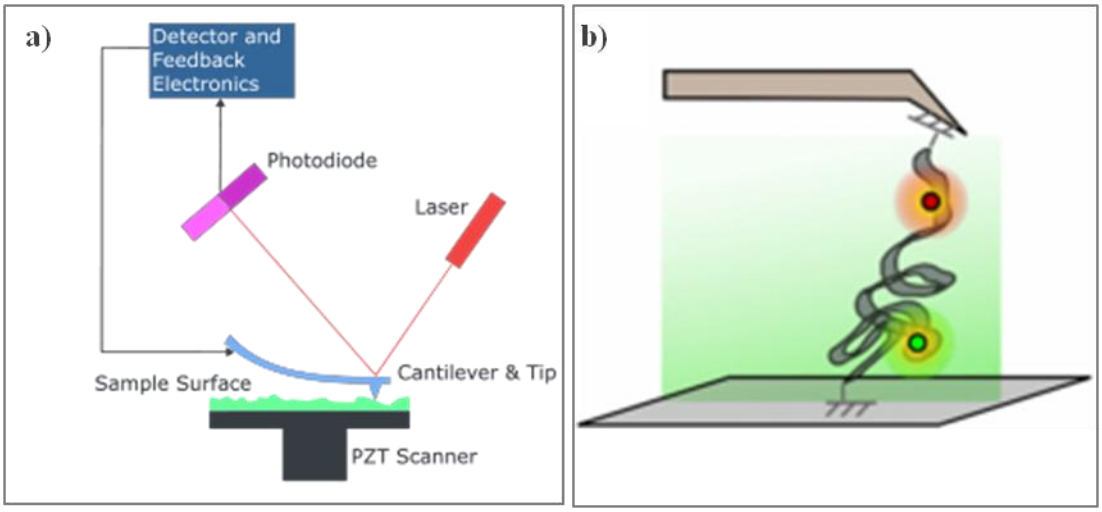

Fig. 1.12 Principles of AFM: a) measurement – laser reflection on the AFM head, hosted on a cantilever, shows cantilever micro displacements and allows for measuring the topography of a surface; b) principle of AFM manipulation – a bead labeled with a molecule needs to be attached to the AFM cantilever and will be displaced with the cantilever [28].

AFM was invented by Binnig, Quate and Gerber in 1986 and the first commercial AFM machine was made in 1989 [27]. Advantages of the AFM are that it is operated in ambient temperature and that the analysis can be done in liquid conditions, which facilitates work with bio-objects. The disadvantages of the AFM are the following: long acquisition time (several minutes) and limited scanning area ~ 150µm x 150µm. During the AFM measurements there can be a cross-talk between different scanning axes, which introduces artifacts. The hysteresis of the piezoelectric cantilever can also induce artifacts. Moreover, the AFM is not well adapted for measurements of steep walls or deep holes. Finally, the miniaturisation of AFM is limited.

The second technique, an acoustic trap, uses two or more standing surface acoustic waves to trap particles. The holding action of a field of ultrasonic standing waves on

particles was first described in 1982 by Dion [29]. Two sound waves of the same wavelength, emitted from sources placed opposite to each other at a distance of multiple wavelengths, will annihilate in a particular point of space called pressure node. This point becomes an acoustic trap (Fig. 1.13) [30].

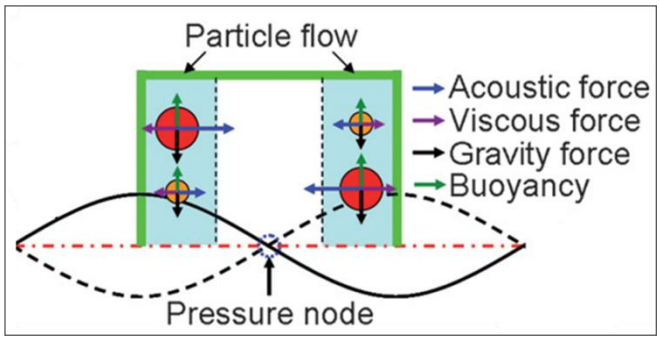

Fig. 1.13 Principle of trapping with acoustic waves and respective forces distribution, from [30].

For acoustic trapping, the sound waves generate pressure which can move very small objects, such as cells. The objects will move until they will reach the trap. This technique is non-destructive and independent of optical properties of the sample. The frequency used for trapping depends on the material used for micro-transducer fabrication and of the length of the wavelength required for trapping. However, fabrication of micro-transducers of a special configuration is necessary for each of the different applications [31].

The third technique, the magnetic trap, uses a magnetic field gradient to manipulate particles such as magnetic beads and measures the forces exerted on them (Fig. 1.14) [28].

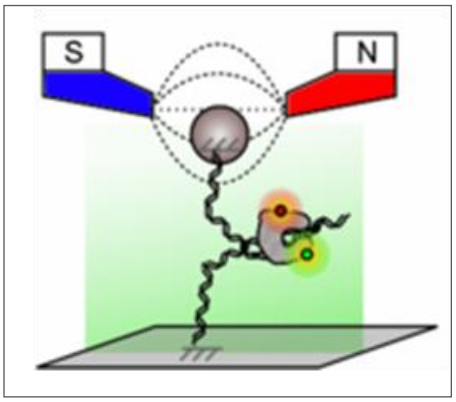

Fig. 1.14 Principles of manipulation in magnetic tweezers, from [28].

The first demonstration of magnetic tweezers in biology was reported in 1950 by Crick and Hughes [32]. They probed the physical properties of cells with large magnets and magnetic particles. Later, magnetic tweezers were used for single molecule micro-manipulation, rheology of soft matter and for studies of force-regulated processes in living organisms. Magnetic tweezers can measure femto-newton forces and also apply torsions. This technique is easily accessible for research laboratories, as many magnetic beads of different sizes are commercially available and the beads are easily imaged with a microscope to monitor micro-displacements. The disadvantage of this technique is the need for labelling the magnetic beads [33].

The fourth technique, optical tweezers, originally called a "single-beam gradient forces trap", uses a highly focused laser beam to create attractive or repulsive force in the range of pico-newtons. It relies on refractive index mismatch of the microscopic objects (Fig. 1.15) [34]. It can hold particles of sizes ranging from nanometres to micrometres and it allows for their nanometre displacement.

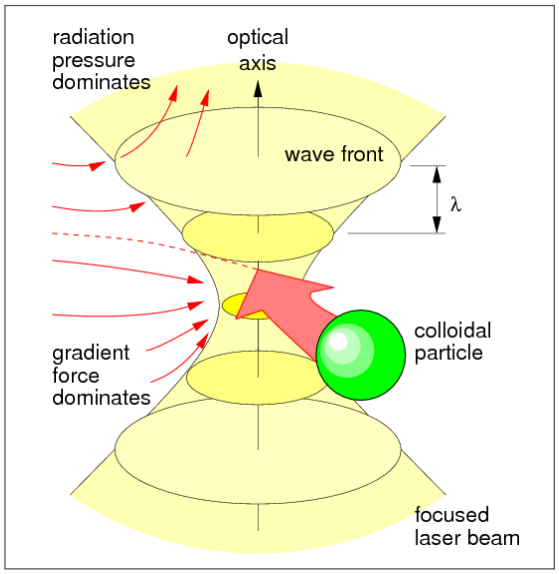

Fig. 1.15 Optical tweezers principle, from [34].

Optical tweezers were demonstrated for the first time in 1986 by Ashkin [35]. He showed that a dielectric particle could be trapped in the focal point of a laser beam focused with a high numerical aperture lens. A year later, Ashkin used an infrared laser to trap cells avoiding excessive heating and photo-damage of a biological sample [36]. Following this experiment, optical tweezers became an important tool for manipulation and sorting of biological objects as well as characterization of the forces created by bio-motors [3]. However, this technique needs to use high numerical aperture lenses and high power light sources ("1mW is necessary to trap 1µm particle" [37]), which limits the manipulation area (for example to an area of 100 x 100 μm^2 for 100 x oil immersion lenses) and makes multiple trapping difficult. In addition, such systems are generally bulky and only a few particles can be manipulated at the same time [37].

The fifth technique, dielectrophoresis (DEP), is well known to be used for manipulation and discrimination between different particles in suspensions. DEP was first used to

move neutral polarisable matter in a non-uniform electric field in 1950 by Pohl [38]. When a neutral dielectric particle was submerged into a non uniform electric field, it was polarized, a dipole moment was induced in the particle and the particle moved due to the interaction with the field (Fig. 1.16) [39].

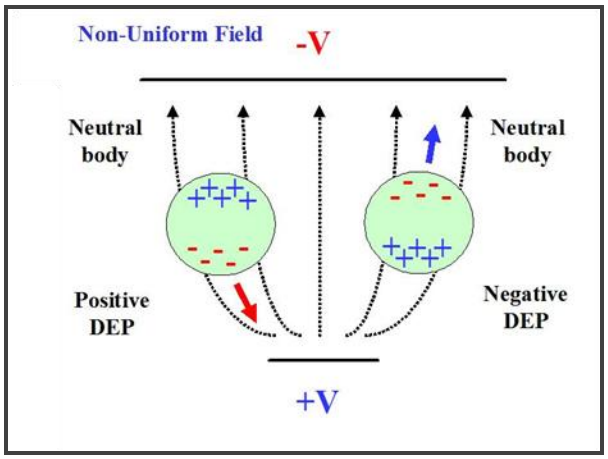

Fig. 1.16 Principle of DEP trapping of neutral particles, from [39].

Dielectrophoresis relies on frequency-dependent dielectric properties of the materials and was used for manipulation of particles of different materials. Only low voltages were used for manipulation, which facilitated integration with other components [26].

The dielectrophoresis force can be described by Eq. (1.1).

$$F = 2\pi r^3 \varepsilon_m \mathrm{Re}[k(\omega)]\nabla E^2 \qquad (1.1)$$

Where r is the radius of the particle, ε_m is the permittivity of the medium, Re[k(ω)] is the real part of the Clausius-Mossotti factor, and ∇E^2 is the gradient of the electric field square [26]. The Clausius-Mossotti factor indicates the particle response to the electric field and will be defined in detail in Chapter 2. More importantly, as indicated by Eq. (1.1), the force due to the dielectrophoresis is proportional to the gradient of the

electrical field squared. Consequently large forces are achieved when this gradient is high: when the difference of the electrical field between two places is big, and the surface on which it happens is small. To achieve high electrical gradients, very small electrodes were made by micro-fabrication methods. Dielectrophoresis has been used for trapping, sorting and patterning of micro-objects, such as cells, bacteria, viruses, DNA, proteins, nanoparticles, carbon nanotubes, nanowires, and liquid droplets [26]. Moreover, high throughput DEP trapping was demonstrated using a Complementary Metal-Oxide-Semiconductor (CMOS) device [40].

However, in reality, the micro-fabrication facility to make small patterned electrodes for DEP is not easily accessible for many biology laboratories [41]. Consequently, an alternative method was developed recently to create localised electrical field gradients without the need of patterned electrodes. This technique is called optoelectronic tweezers (OET) [42]. The non-uniform electric field in the OET device is generated using a combination of light patterns and a photoconductive layer [42]. As shown in Fig. 1.17, OET consists of two plates. Thin photoconductive layers, made of amorphous silicon (a-Si:H), are placed in between the two conducting plates, made out of indium tin oxide (ITO) coated glass slides. An AC voltage is applied across these two plates and a conductive liquid is placed between them. In the dark, the impedance of the photoconductive layer is higher than the impedance of the liquid and the voltage is dropped across this photoconductive layer. However, under illumination, the impedance of the photoconductor drops substantially and the voltage is applied onto the liquid. When the photoconductor is illuminated with a light pattern, virtual electrodes are created in the photoconductor, which generates a high electric field gradient in the liquid

above the photoconductive layer. By turning on and altering the light pattern, particle trapping and manipulation can be achieved [42].

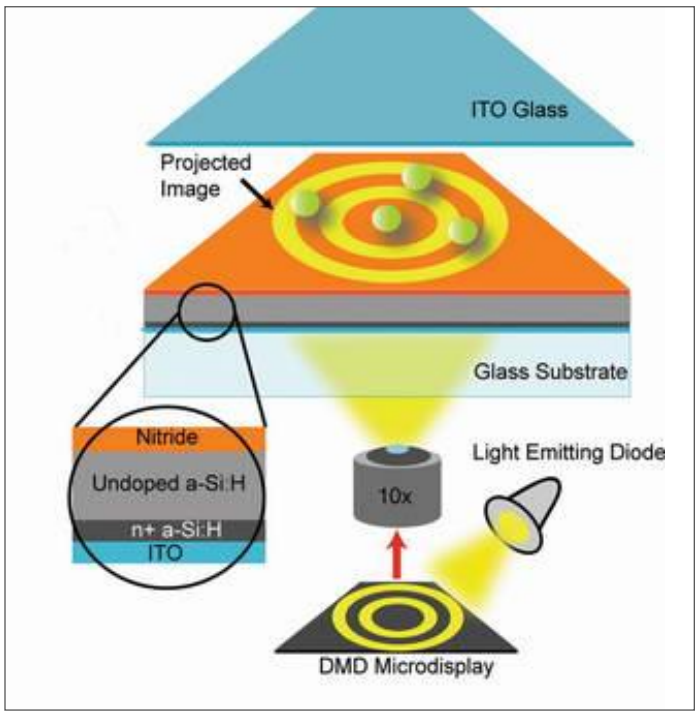

Fig. 1.17 Schematic of optoelectronic tweezers device; from [42].

The advantage of this technique over standard dielectrophoresis is that the electrode's dimensions can be changed continuously just by changing the light pattern. The advantages of the OET over optical tweezers are that 100,000 times less optical power density is needed to trap and move particles [42]. In addition, more particles can be manipulated individually and in parallel by OET compared with the AFM, magnetic tweezers or optical tweezers methods [42]. Chiou et al. demonstrated that more than 15,000 particles could be manipulated on a 1.0 x 1.3 mm^2 area at the same time [42]. The OET traps have been compared to optical traps and have been found to be 470 times stiffer for a similar light intensity [43]. Furthermore, the optical properties of the

particles do not constrain the manipulation. Also, for OET, the particles do not need to be labelled to be susceptible to the induced forces, as was the case for magnetic tweezers. Compared to other micro-manipulation techniques cited above, the OET also offers the unique opportunity to integrate the micro-LED light source to develop a miniaturised tweezing system.

Disadvantages of OET are that it is a 2D manipulation and that the trapping is not as strong as that with an AFM tip or with magnetic trapping. There are also limitations on the liquids that the particles can be suspended in, e.g. the liquid conductivity has to be within a certain range determined by the conductivity of the photoconductor electrode.

So far, the light pattern that creates the virtual electrodes in OET was achieved by using either a Digital Micro-mirror Device (DMD) [42] or Liquid Crystal Display (LCD) [44] on which a laser or halogen lamp was projected. However, these DMD and LCD devices are quite bulky, and have limited prospects for achieving a multi-functional OET or a miniaturised OET device. In our approach, micro-light patterns are created by a micro-pixelated light-emitting diode (micro-LED) array which is controlled by an integrated complementary metal–oxide–semiconductor (CMOS) chip. This miniaturised OET system is described in detail in Chapter 3.

1.7. Microfluidic devices

The micro-systems developed in this thesis work addressed several issues raised by previous work for developing miniaturised devices, such as the integration of the light source with the sample chamber and sample hosting. To achieve the system miniaturisation for local fluorescence excitation as well as fast and efficient sample

delivery during the experiments, a micro-LED array was integrated with a microfluidic network. The advantages of using microfluidic devices will be described in this section.

Microfluidic devices are indispensable parts of many micro-systems for bio-applications. They can be defined as devices which operate small volumes of samples using little energy. Typically, the fluid volumes are in the range of pico to micro litres and the dimensions of the microfluidic channels and sample chambers are in the nanometre to micron ranges. A more detailed description of the microfluidic device characteristics will be presented in Chapter 2.

Due to several advantages of microfluidic devices, many bio-applications involving them were developed over the past years, as for instance real time polymerase chain reaction (PCR) of bacteria, viruses and cancer cells [45, 46], biochemical assays [47], immunoassays based on antigen-antibody reactions [48], detection of cancer cells and bacteria by dielectrophoresis [49, 50], DNA extraction from blood samples [51], single cell analysis [52], ion channel screening [53]. Today, microfluidics has become a classic 'enabling technology' which is used as a tool to solve specific problems, such as precise sample delivery or sample evaporation issues [54]. Microfluidic devices are also used in a wider context in a variety of applications such as capillary electrophoresis, water or food quality testing, point of care diagnostic, bio-threat detection, protein crystallisation or synthesis of fine chemicals [54]. Some of the technologies are already commercialised by companies such as Affymetrix offering the GeneChip®; others start to 'penetrate' the industrial market. Currently, there are more than 200 microfluidics

companies in the world [55]. Microfluidic technology has become omnipresent in various fields of research and manufacture.

In this work, we developed a novel tool which integrated microfluidic network with a micro-LED device allowing for localised two-dimensional analysis of cell fluorescence in a miniaturised and portable format. This device can be used for immediate analysis as well as for a long term study. This work will be presented in Chapter 6.

Importantly, in our miniature systems, the microfluidic network including the bio-sample hosting chamber does not directly contact the semiconductor material used for making the micro-LED light source and the microfluidic component can be easily separated from the LED light source. This arrangement will protect the bio-samples from possible toxic effects of the semiconductor material and also facilitates the system sterilisation and sample residue cleaning. In addition, the microfluidic component is disposable; we can easily dismount it and use the LED light source repeatedly. In our integrated systems, we use low power micro-LEDs as a light source, minimising the interference with cell viability. We also found that the integrated micro-systems are robust and can withstand standard cell culture conditions. The previous systems do not have these advantages.

The second tool presented in this thesis using microfluidic technology involved creation of cell micro-arrays inside a microfluidic device. The motivation for this work is presented in the following section.

1.8. Cell micro-arrays

Cell micro-arrays are important in medical technology development as they can replace the multi-well plate method and thus significantly reduce the amount of samples used in medical tests. Also, cell micro-arrays combined with microfluidic devices adds the capability of high throughput analysis and makes the sample manipulation easier.

So far, several methods have been employed to create micro-arrays of cells. The most commonly used approach consists of first patterning micro-structures or molecules in micro-format and second, of seeding different types of cells on top of the patterned substrates [56].

The pre-patterned structures can be micro-pillars [57], wells [58] and chambers [59] which physically separate the cells. These methods were capable of creating uniform cell micro-patterns, however they had some disadvantages. Physical separation allows for studying single cell populations, but prevents observation of influences between different cell types. Moreover, it was proven that extracellular matrix (ECM) proteins, such as collagen and poly-L-lysine, and connective tissue cells are very important in maintaining cell function in vitro [60]. However, the physical barrier technique did not allow implementation of proteins. Consequently, it limited the scope for the subsequent analysis.

By using polymerisation of hydrogels [61, 62] or collagen with embedded cells [63, 64], cells could be immobilised, providing a possible approach to create cell patterns. However, as the cells were randomly located within the gel, these techniques do not offer the controllability of cell spatial position and do not allow for comparison of cell

interactions with different bio-interfaces. Due to the above reasons, a different method is required to create cell patterns.

Moreover, patterning of ECM proteins and attaching cells on the top of the protein pattern showed improved cell functionality *in vitro* [65]. These results suggested that patterning of proteins first could be a better way to create subsequent cell patterns and ensure cell-friendly environment.

Inspired by the above results, we used protein patterned substrates to create cell micro-arrays in this work. We used piezoelectric printing to create protein patterns on the non-adhesive surfaces. Cells were then seeded on these patterns and created well defined cell micro-arrays. In this way, a reliable single-step method to create a cell micro-array was developed.

The cell micro-arrays created were tested for activity in specific toxicity test and the activity results are comparable with those obtained from the cells seeded in a standard multi-well plate. The protein printing and cell micro-array formation will be presented in Chapters 4 and 5, respectively. Piezoelectric printing of bio-samples as compared to other patterning methods will be described briefly in the next section and the details of this technique will be presented in Chapter 2.

1.9. Protein patterning by piezoelectric printing

So far, non-invasive and flexible patterning of proteins at predefined locations has remained a challenge [66, 67]. Previous patterning methods involved alternate chemical patterning and surface modification processes, and they remained very complicated depending on the protein type being used.

In previous studies, the techniques used to create micro-patterns included photolithography [59, 60, 68], microcontact printing [67] and soft lithography [69]. These methods present several advantages, such as micron size resolution and the possibility of generation of complex structures. However, they involve multistep processes performed in the cleanroom, which is not easily available for many of the biology laboratories [41]. In addition, photolithography involves patterning of the photoresist on top of a protein layer which requires removal of resist with organic solvents. We have found that in the case of proteins, the use of organic solvents, such as acetone, compromises non-adhesiveness of the areas surrounding the protein pattern and influences the adhesiveness of cells on the pattern (data not shown). Moreover, the patterns created by photolithography are defined by photo-masks made from quartz glass coated with a chromium layer. Not only does this method involves high cost, but also, once designed and produced, the mask is not modifiable.

In the case of soft lithography or microcontact printing, patterns in the form of micro-stamps are created in different materials, such as poly(dimethylsiloxane) (PDMS), which are then coated with thin protein layer and are used as a medium to transfer protein pattern to other substrates. We found that it was very difficult to achieve uniform pressure applied onto the PDMS medium. Consequently, the quality and particularly reproducibility of the final protein pattern were poor. Given these disadvantages, we wanted to explore a simple, one step method which would ensure production of a robust and reliable protein pattern and a consequent cell pattern.

To achieve this aim, we have used and developed piezoelectric printing of proteins. Piezoelectric printing is a very flexible and precise robotic deposition technique that delivers small droplets with controlled volumes in non-contact mode [70]. It also offers a high degree of flexibility in pattern layout, concentration range, operation sequences and possibility of multilayer deposition or superposition of different materials. It often uses solutions in their physiological form and it is a high throughput technique.

The printing technology has been established already in the field of DNA microarrays [71] and has been rapidly expanding in the emerging fields of proteomics [72, 73] and, more recently, cell microarrays [72, 74]. Fig. 1.18 shows some examples of bio-samples printed by other groups.

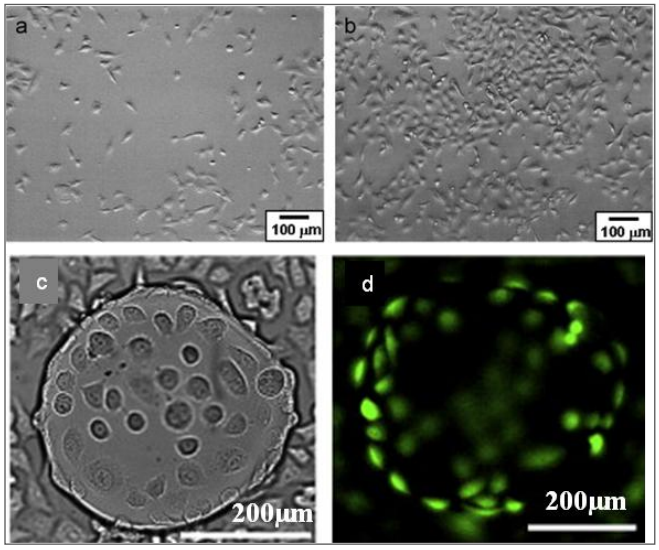

Fig. 1.18 Use of printing for cell cultures: a) and b): direct printing of cells. Optical micrographs of fibrosarcoma cells after 24 hours in culture following printing in two different conditions: at two waveform amplitude: a) 40V and b) 60V; c) and d): Images of a HeLa cell culture 48 hours after seeding on printed polymer hydrogel microarray: c) bright field image of a hydrogel feature with cells, d) fluorescent image of cells attached to a hydrogel spot. From [73, 74].

Fig. 1.18 a and b present the cells printed by Saunders et al. Unfortunately, the printed cells did not form any distinctive pattern. Fig. 1.18 c and d present cells seeded on a pre-patterned hydrogel microarray. However, it can be seen that the growth of these cells was not restricted only to the hydrogel dots, which decreased the contrast between the cell array and the background. The high cell pattern definition is important for the subsequent cell fluorescence analysis.

Moreover, only a few of previous works have generated a protein pattern on a surface which, at the same time, would allow for selective cell adhesion, would maintain its specific functions and would be suitable for use with microfluidics networks [69]. The work presented here will address these issues. We demonstrate for the first time that our printed protein patterns remain stable on the surface even after several washing steps. Moreover, the definition and resolution of the printed protein patterns were higher than those shown in previous work thanks to the advanced printing machines used. With the high quality protein pattern and the non-adhesive background, our cell microarrays obtained after seeding on the protein pattern were of better quality in comparison with previous cell patterns. Moreover, this is the first time that the microarray of cells created on the top of printed proteins was integrated with a microfluidic device for further analysis.

1.10. Outline of this thesis

This thesis will present the work and results on novel portable miniaturised bio-systems achieved by using a new light source, micro-LEDs, and technologies such as optoelectronic tweezing, microfluidics and piezoelectric printing. In Chapter 2, the

physics background and principles of these novel components and technologies are presented in detail.

Three different micro-systems were developed. The first system, miniaturised OET, is described in Chapter 3. The results of this work were published and the corresponding paper is attached at the end of this thesis [75].

The second system involved reliable cell micro-arrays fabricated on a glass substrate and integrated with a microfluidic device. Chapter 4 describes piezoelectric printing of proteins. The printed protein patterns were used for subsequent cell micro-array formation. In Chapter 5, the results on the selective cell adhesion on the protein patterns and biological assays performed on the cell patterns are presented. The results of this work are accepted for publication in Colloids and Surfaces B: Biointerfaces (the accepted version of the corresponding paper is attached at the end of this thesis).

The third micro-system involved the integration of micro-LEDs with a microfluidic device for achieving two-dimensional cell fluorescence analysis. The development of this integrated device is presented in Chapter 6.

Finally, Chapter 7 presents conclusions of the thesis work and proposes some future works and further applications of the micro-systems developed.

References

1. L. K. Altman, "So Many Advances in Medicine, So Many Yet to Come," The New York Times **2006/12/26**, 2006/2012/2026 (2006).
2. Z. Huang, "A review of progress in clinical photodynamic therapy," Technol. Cancer Res. Treat. **4**, 283-293 (2005).
3. A. D. Mehta, M. Rief, J. A. Spudich, D. A. Smith, and R. M. Simmons, "Single-molecule biomechanics with optical methods," Science **283**, 1689-1695 (1999).
4. J. Kelly, "Lab-on-a-Chip Promises Fast Profile of RA Patients' Autoantibodies," Muscoskeletal Report, 2645 (2007).
5. P. L. Gourley, "Biocavity laser for high-speed cell and tumour biology," J. Phys. D-Appl. Phys. **36**, R228-R239 (2003).
6. H. D. Summers, D. R. Matthews, R. J. Errington, K. L. Njoh, P. J. Smith, A. D. Goater, J. P. H. Burt, N. H. Rizvi, A. Menachery, and D. J. Morris, "Semiconductor light-emitting devices with in-built bioreaction chambers - art. no. 64410Y," in *Imaging, Manipulation, and Analysis of Biomolecules, Cells, and Tissues V*, D. L. Farkas, R. C. Leif, and D. V. Nicolau, eds. (Spie-Int Soc Optical Engineering, Bellingham, 2007), pp. Y4410-Y4410.
7. M. A. Cooper, "Optical biosensors in drug discovery," Nat. Rev. Drug Discov. **1**, 515-528 (2002).
8. O. Levi, W. Suh, M. M. Lee, J. Y. Zhang, S. R. J. Brueck, S. H. Fan, and J. S. Harris, "Integrated biomedical nanosensor using guided resonance in photonic crystal structures - art. no. 60950N," in *Nanobiophotonics and Biomedical*

Applications III, A. N. Cartwright, and D. V. Nicolau, eds. (Spie-Int Soc Optical Engineering, Bellingham, 2006), pp. N950-N950.

9. J. A. De Feijter, J. Benjamins, and F. A. Veer, "Ellipsometry as a Tool to Study the Adsorption Behavior of Synthetic and Bio Polymers at the Air Water Interface," Biopolymers **17**, 1759-1772 (1978).

10. S. Cran-McGreehin, T. F. Krauss, and K. Dholakia, "Integrated monolithic optical manipulation," Lab Chip **6**, 1122-1124 (2006).

11. K. Suzumura, K. Funakoshi, T. Hoshino, H. Tsujimura, K. Iwabuchi, Y. Akiyama, and K. Morishima, "A light-regulated bio-micro-actuator powered by transgenic Drosophila melanogaster muscle tissue," in *2011 IEEE 24th International Conference*, Tokyo Univ. of Agric. & Technol., ed. (Tokyo, Japan;, 2011), pp. 149 – 152.

12. B. R. Rae, K. R. Muir, Z. Gong, J. McKendry, J. M. Girkin, E. Gu, D. Renshaw, M. D. Dawson, and R. K. Henderson, "A CMOS Time-Resolved Fluorescence Lifetime Analysis Micro-System," Sensors **9**, 9255-9274 (2009).

13. B. R. Rae, C. Griffin, J. McKendry, J. M. Girkin, H. X. Zhang, E. Gu, D. Renshaw, E. Charbon, M. D. Dawson, and R. K. Henderson, "CMOS driven micro-pixel LEDs integrated with single photon avalanche diodes for time resolved fluorescence measurements," J. Phys. D-Appl. Phys. **41**, 094011 (2008).

14. C. W. Jeon, E. Gu, and M. D. Dawson, "Mask-free photolithographic exposure using a matrix-addressable micropixellated AlInGaN ultraviolet light-emitting diode," Applied Physics Letters **86**, 221105 (2005).

15. D. Elfstrom, B. Guilhabert, J. McKendry, S. Poland, Z. Gong, D. Massoubre, E. Richardson, B. R. Rae, G. Valentine, G. Blanco-Gomez, E. Gu, J. M. Cooper, R. K. Henderson, and M. D. Dawson, "Mask-less ultraviolet photolithography based on CMOS-driven micro-pixel light emitting diodes," Opt. Express **17**, 23522-23529 (2009).

16. B. Guilhabert, "Maskless Fabrication of GaN-based Light-Emitting Diodes," in *IEEE 23rd Photonics Annual Meeting* (IEEE, Denver, USA, 2010).

17. M. Wu, "Hybrid GaN/organic device fabrication by inkjet printing," PhD Thesis in *Physics* (Strathclyde, Glasgow, 2009), p. 203.

18. V. Poher, G. T. Kennedy, H. B. Manning, D. M. Owen, H. X. X. Zhang, E. Gu, M. D. Dawson, P. M. W. French, and M. A. A. Neil, "Improved sectioning in a slit scanning confocal microscope," Opt. Lett. **33**, 1813-1815 (2008).

19. V. Poher, N. Grossman, G. T. Kennedy, K. Nikolic, H. X. Zhang, Z. Gong, E. M. Drakakis, E. Gu, M. D. Dawson, P. M. W. French, P. Degenaar, and M. A. A. Neil, "Micro-LED arrays: a tool for two-dimensional neuron stimulation," J. Phys. D-Appl. Phys. **41**, 094014 (2008).

20. N. Grossman, V. Poher, M. S. Grubb, G. T. Kennedy, K. Nikolic, B. McGovern, R. B. Palmini, Z. Gong, E. M. Drakakis, M. A. A. Neil, M. D. Dawson, J. Burrone, and P. Degenaar, "Multi-site optical excitation using ChR2 and micro-LED array," J. Neural Eng. **7**, 016004 (2010).

21. P. Degenaar, N. Grossman, M. A. Memon, J. Burrone, M. Dawson, E. Drakakis, M. Neil, and K. Nikolic, "Optobionic vision-a new genetically enhanced light on retinal prosthesis," J. Neural Eng. **6**, 035007 (2009).

22. H. Xie, D. S. Haliyo, and S. Regnier, "A versatile atomic force microscope for three-dimensional nanomanipulation and nanoassembly," Nanotechnology **20**, 215301 (2009).

23. Y. Yamakoshi, Y. Koitabashi, N. Nakajima, and T. Miwa, "Yeast cell trapping in ultrasonic wave field using ultrasonic contrast agent," Jpn. J. Appl. Phys. Part 1 - Regul. Pap. Brief Commun. Rev. Pap. **45**, 4712-4717 (2006).

24. G. Vieira, T. Henighan, A. Chen, A. J. Hauser, F. Y. Yang, J. J. Chalmers, and R. Sooryakumar, "Magnetic Wire Traps and Programmable Manipulation of Biological Cells," Phys. Rev. Lett. **103**, 128101 (2009).

25. D. J. Stevenson, F. Gunn-Moore, and K. Dholakia, "Light forces the pace: optical manipulation for biophotonics," J. Biomed. Opt. **15**, 041503 (2010).

26. R. Pethig, "Review Article-Dielectrophoresis: Status of the theory, technology, and applications," Biomicrofluidics **4**, 022811 (2010).

27. G. Binnig, C. F. Quate, and C. Gerber, "Atomic Force Microscope," Phys. Rev. Lett. **56**, 930-933 (1986).

28. J. Hohlbein, K. Gryte, M. Heilemann, and A. N. Kapanidis, "Surfing on a new wave of single-molecule fluorescence methods," Phys. Biol. **7**, 031001 (2010).

29. J. L. Dion, A. Malutta, and P. Cielo, "Ultrasonic Inspection of Fiber Suspensions," J. Acoust. Soc. Am. **72**, 1524-1526 (1982).

30. J. J. Shi, H. Huang, Z. Stratton, Y. P. Huang, and T. J. Huang, "Continuous particle separation in a microfluidic channel via standing surface acoustic waves (SSAW)," Lab Chip **9**, 3354-3359 (2009).

31. C. R. P. Courtney, C. K. Ong, B. W. Drinkwater, P. D. Wilcox, C. Demore, S. Cochran, P. Glynne-Jones, and M. Hill, "Manipulation of microparticles using phase-controllable ultrasonic standing waves," J. Acoust. Soc. Am. **128**, E195-E199 (2010).

32. F. H. C. Crick, and A. F. W. Hughes, "The physical properties of cytoplasm : A study by means of the magnetic particle method Part I. Experimental," Experimental Cell Research **1**, 37-80 (1950).

33. "Magnetic tweezers," http://en.wikipedia.org/wiki/Magnetic_tweezers.

34. D. Grier, "Optical Tweezers," (2011), http://www.physics.nyu.edu/grierlab/figures/tweezer.png.

35. A. Ashkin, J. M. Dziedzic, J. E. Bjorkholm, and S. Chu, "Observation of a Single-Beam Gradient Force Optical Trap for Dielectric Particles," Opt. Lett. **11**, 288-290 (1986).

36. A. Ashkin, J. M. Dziedzic, and T. Yamane, "Optical Trapping and Manipulation of Single Cells Using Infrared-Laser Beams," Nature **330**, 769-771 (1987).

37. C.-M. Ho, *Micro/nano technology systems for biomedical applications: Microfluidics, Optics, and Surface Chemistry* (OUP Oxford 2010).

38. H. A. Pohl, "The motion and precipitation of suspensoids in divergent electric fields.," J. Appl. Phys. **22**, 869–871. (1950).

39. J. M. Sung, "Dielectrophoresis and Optoelectronic Tweezers for Nanomanipulation," (2007), http://large.stanford.edu/courses/2008/ph210/sung2/.

40. N. Manaresi, A. Romani, G. Medoro, L. Altomare, A. Leonardi, M. Tartagni, and R. Guerrieri, "A CMOS chip for individual cell manipulation and detection," IEEE J. Solid-State Circuit **38**, 2297-2305 (2003).

41. J. Fink, M. Thery, A. Azioune, R. Dupont, F. Chatelain, M. Bornens, and M. Piel, "Comparative study and improvement of current cell micro-patterning techniques," Lab Chip **7**, 672-680 (2007).

42. P. Y. Chiou, A. T. Ohta, and M. C. Wu, "Massively parallel manipulation of single cells and microparticles using optical images," Nature **436**, 370-372 (2005).

43. S. L. Neale, M. Mazilu, J. I. B. Wilson, K. Dholakia, and T. F. Krauss, "The resolution of optical traps created by light induced dielectrophoresis (LIDEP)," Optics Express **15**, 12619-12626 (2007).

44. H. Hwang, Y. J. Choi, W. Choi, S. H. Kim, J. Jang, and J. K. Park, "Interactive manipulation of blood cells using a lens-integrated liquid crystal display based optoelectronic tweezers system," Electrophoresis **29**, 1203-1212 (2008).

45. D. L. House, C. H. Chon, C. B. Creech, E. P. Skaar, and D. Q. Li, "Miniature on-chip detection of unpurified methicillin-resistant Staphylococcus aureus (MRSA) DNA using real-time PCR," J. Biotechnol. **146**, 93-99 (2010).

46. A. Rasooly, "Moving biosensors to point-of-care cancer diagnostics," Biosens. Bioelectron. **21**, 1847-1850 (2006).

47. V. Srinivasan, V. K. Pamula, and R. B. Fair, "Droplet-based microfluidic lab-on-a-chip for glucose detection," Anal. Chim. Acta **507**, 145-150 (2004).

48. Y. Q. Luo, F. Yu, and R. N. Zare, "Microfluidic device for immunoassays based on surface plasmon resonance imaging," Lab Chip **8**, 694-700 (2008).

49. H. S. Moon, K. Kwon, S. I. Kim, H. Han, J. Sohn, S. Lee, and H. I. Jung, "Continuous separation of breast cancer cells from blood samples using multi-orifice flow fractionation (MOFF) and dielectrophoresis (DEP)," Lab Chip **11**, 1118-1125 (2011).

50. Y. S. Liu, T. M. Walter, W. J. Chang, K. S. Lim, L. J. Yang, S. W. Lee, A. Aronson, and R. Bashir, "Electrical detection of germination of viable model Bacillus anthracis spores in microfluidic biochips," Lab Chip **7**, 603-610 (2007).

51. M. Mahalanabis, H. Al-Muayad, M. D. Kulinski, D. Altman, and C. M. Klapperich, "Cell lysis and DNA extraction of gram-positive and gram-negative bacteria from whole blood in a disposable microfluidic chip," Lab Chip **9**, 2811-2817 (2009).

52. S. Lindstrom, and H. Andersson-Svahn, "Overview of single-cell analyses: microdevices and applications," Lab Chip **10**, 3363-3372 (2010).

53. E. Dahan, V. Bize, T. Lehnert, J. D. Horisberger, and M. A. M. Gijs, "Rapid fluidic exchange microsystem for recording of fast ion channel kinetics in Xenopus oocytes," Lab Chip **8**, 1809-1818 (2008).

54. H. Becker, "Hype, hope and hubris: the quest for the killer application in microfluidics," Lab Chip **9**, 2119-2122 (2009).

55. L. Kim, "FluidicMEMS, PERSPECTIVES ON MICROFLUIDICS AND BIOMEMS TECHNOLOGY," (2011), http://fluidicmems.com/list-of-microfluidics-lab-on-a-chip-and-biomems-companies/.

56. D. I. Rozkiewicz, Y. Kraan, M. W. T. Werten, F. A. de Wolf, V. Subramaniam, B. J. Ravoo, and D. N. Reinhoudt, "Covalent microcontact printing of proteins for cell patterning," Chem.-Eur. J. **12**, 6290-6297 (2006).

57. Y. C. Toh, C. Zhang, J. Zhang, Y. M. Khong, S. Chang, V. D. Samper, D. van Noort, D. W. Hutmacher, and H. R. Yu, "A novel 3D mammalian cell perfusion-culture system in microfluidic channels," Lab Chip **7**, 302-309 (2007).

58. A. Khademhosseini, J. Yeh, G. Eng, J. Karp, H. Kaji, J. Borenstein, O. C. Farokhzad, and R. Langer, "Cell docking inside microwells within reversibly sealed microfluidic channels for fabricating multiphenotype cell arrays," Lab Chip **5**, 1380-1386 (2005).

59. M. J. Powers, K. Domansky, M. R. Kaazempur-Mofrad, A. Kalezi, A. Capitano, A. Upadhyaya, P. Kurzawski, K. E. Wack, D. B. Stolz, R. Kamm, and L. G. Griffith, "A microfabricated array bioreactor for perfused 3D liver culture," Biotechnol. Bioeng. **78**, 257-269 (2002).

60. J. W. Lussi, D. Falconnet, J. A. Hubbell, M. Textor, and G. Csucs, "Pattern stability under cell culture conditions - A comparative study of patterning methods based on PLL-g-PEG background passivation," Biomaterials **27**, 2534-2541 (2006).

61. M. J. Mahoney, and K. S. Anseth, "Contrasting effects of collagen and bFGF-2 on neural cell function in degradable synthetic PEG hydrogels," J. Biomed. Mater. Res. Part A **81A**, 269-278 (2007).

62. W. G. Koh, L. J. Itle, and M. V. Pishko, "Molding of hydrogel multiphenotype cell microstructures to create microarrays," Anal. Chem. **75**, 5783-5789 (2003).

63. Y. C. Toh, S. Ng, Y. M. Khong, V. Samper, and H. Yu, "A configurable three-dimensional microenvironment in a microfluidic channel for primary hepatocyte culture," Assay Drug Dev. Technol. **3**, 169-176 (2005).

64. B. M. Gillette, J. A. Jensen, B. X. Tang, G. J. Yang, A. Bazargan-Lari, M. Zhong, and S. K. Sia, "In situ collagen assembly for integrating microfabricated three-dimensional cell-seeded matrices," Nat. Mater. **7**, 636-640 (2008).

65. S. N. Bhatia, U. J. Balis, M. L. Yarmush, and M. Toner, "Effect of cell-cell interactions in preservation of cellular phenotype: cocultivation of hepatocytes and nonparenchymal cells," Faseb J. **13**, 1883-1900 (1999).

66. S. W. Rhee, A. M. Taylor, C. H. Tu, D. H. Cribbs, C. W. Cotman, and N. L. Jeon, "Patterned cell culture inside microfluidic devices," Lab Chip **5**, 102-107 (2005).

67. A. Tourovskaia, X. Figueroa-Masot, and A. Folch, "Long-term microfluidic cultures of myotube microarrays for high-throughput focal stimulation," Nat. Protoc. **1**, 1092-1104 (2006).

68. H. B. Yin, N. Pattrick, X. L. Zhang, N. Klauke, H. C. Cordingley, S. J. Haswell, and J. M. Cooper, "Quantitative comparison between microfluidic and microtiter plate formats for cell-based assays," Anal. Chem. **80**, 179-185 (2008).

69. B. J. Kane, M. J. Zinner, M. L. Yarmush, and M. Toner, "Liver-specific functional studies in a microfluidic array of primary mammalian hepatocytes," Anal. Chem. **78**, 4291-4298 (2006).

70. J. Sumerel, J. Lewis, A. Doraiswamy, L. F. Deravi, S. L. Sewell, A. E. Gerdon, D. W. Wright, and R. J. Narayan, "Piezoelectric ink jet processing of materials

for medical and biological applications," Biotechnology Journal **1**, 976-987 (2006).

71. T. Okamoto, T. Suzuki, and N. Yamamoto, "Microarray fabrication with covalent attachment of DNA using Bubble Jet technology," Nat. Biotechnol. **18**, 438-441 (2000).

72. L. Pardo, W. C. Wilson, and T. J. Boland, "Characterization of patterned self-assembled monolayers and protein arrays generated by the ink-jet method," Langmuir **19**, 1462-1466 (2003).

73. R. Zhang, A. Liberski, R. Sanchez-Martin, and M. Bradley, "Microarrays of over 2000 hydrogels - Identification of substrates for cellular trapping and thermally triggered release," Biomaterials **30**, 6193-6201 (2009).

74. R. E. Saunders, J. E. Gough, and B. Derby, "Delivery of human fibroblast cells by piezoelectric drop-on-demand inkjet printing," Biomaterials **29**, 193-203 (2008).

75. A. Zarowna-Dabrowska, S. L. Neale, D. Massoubre, J. McKendry, B. R. Rae, R. K. Henderson, M. J. Rose, H. B. Yin, J. M. Cooper, E. D. Gu, and M. D. Dawson, "Miniaturized optoelectronic tweezers controlled by GaN micro-pixel light emitting diode arrays," Opt. Express **19**, 2720-2728 (2011).

Chapter 2

2. Physics background and technologies used

This Chapter describes the physics background and the components and technologies used to create miniaturised cell analysis tools. The components and technologies included micro-light emitting diode (micro-LED) arrays, optoelectronic tweezing, microfluidic devices and piezoelectric printing. Micro-LED arrays will be described first and they were used for miniaturised optoelectronic tweezing described in Chapter 3 and for localised fluorescence excitation described in Chapter 6. After the presentation of micro-LEDs, optoelectronic tweezing principles will be described. This will be followed by the presentation of microfluidic devices which were used to create a cell toxicity analysis tool (described in Chapter 5) and integrated fluorescence analysis tool (described in Chapter 6). Finally, the Chapter will describe piezoelectric printing which was used to create micro-arrays of proteins (see Chapter 4).

2.1. Micro light emitting diodes (micro-LEDs)

2.1.1. History of the light emitting diodes (LED)

We can observe light emission from LEDs thanks to electroluminescence. The physics of this phenomenon will be described in detail in the next section of this Chapter. Electroluminescence was discovered in 1907 by H. J. Round, when he was working in Marconi Labs. He detected light emission from a silicon carbide crystal [1]. The first report explaining the phenomena of visible light emitted by semiconductor materials was

published by O. V. Losev in 1927. Later, infrared emission from gallium arsenide (GaAs) crystals was reported in 1955, and in 1962 first red LED was made. Further development was made in the late sixties and early seventies, with development of growing techniques of nitrogen doped gallium phosphate materials (GaP) and resulted in the introduction of yellow, green and blue emitting LEDs [2].

Then, the first violet emitting LED was obtained from magnesium doped GaN crystals in the early seventies [3]. However, further optimisation of nitride based LED technology happened only in early nineties and was done by Akasaki and Nakamura [4, 5].

The LEDs available nowadays emit light of different colours and power ranges which results in the growing popularity of this technology. Modern LED devices are used in an increasing variety of sectors. Low power LEDs are used as indicators in aviation, the automobile industry and traffic signalling. High optical power LEDs are used for lighting, large displays and TV screens. Text and video displays were developed thanks to LED. Fast operation of the LEDs allowed for the development of the advanced communications technology [6]. Infrared LEDs are widely used for remote control in domestic appliances. Compared to the traditional incandescent light sources for lighting applications, LEDs offer lower energy consumption, longer lifetime as well as better robustness and reliability. Consequently, even though the fabrication cost for similar light output is still higher than those of fluorescent or halogen light sources, LED lighting is increasingly used for interior lighting. Moreover, the recent ban on the high power incandescent bulbs has further stimulated the development of LED technologies.

2.1.2. Principles of light emitting diodes

Light emitting diodes are made of semiconductor materials. A semiconductor is a material which has conductivity value between a well conducting metal and non-conducting insulator. The conductivity of a material is defined by its ability to permit electrical charges, e.g. electrons to flow. In semiconductors, electrons occupying the valence band are bound to atoms – these electrons do not contribute to material conductivity. However, electrons occupying the conduction band are free to move through the material, and thus contribute to conductivity. The levels of energy between valence and conduction bands are forbidden for an electron. These forbidden levels are also called the bandgap. A material is defined as an insulator if all its electrons are strongly bound to its atoms. As a consequence, the difference of energy level between valence and conduction bands is relatively large (>5eV) and there are no free electrons in the conduction band. By contrast, a conductor is a material in which the valence and conduction bands partially overlap. Consequently, some of the valence electrons can move freely through the material. In semiconductor materials, the bandgap is relatively small (~1eV). The energy of the electrons in the valence band can be easily increased to the energy of the conduction band by thermal or optical excitation (in combination with doping – see below).

In pure semiconductors, when the energy of a valence electron increases, the electron can be ‘freed’ from the atomic bonds and becomes a conduction band electron, leaving behind a vacancy, or ‘hole’. This hole can be occupied by another electron from the valence band. Thus, a hole can be considered as a positive charge moving through the

material. Excitation of an electron from the valence band to the conduction band involves the generation of a hole. As a consequence, pure semiconductors can be conductive under external excitation while retaining overall charge neutrality.

Another way to induce conductivity in semiconductors is to dope them with elements which have a different number of valence electrons. For example, silicon (Si) is a semiconductor from Group IV in the periodic table, having four valence electrons. In a pure state, Si atoms usually form a crystal lattice. Each Si atom is bound to the 4 adjacent atoms by sharing their valence electrons. Consequently, there are no free electrons as shown in Fig. 2.1 a. In this configuration, all electrons are in the valence band and the silicon is not conductive.

However, if Si is doped with another element with a different number of valence electrons, the resultant structure will become conductive. For example, Si can be doped with indium (In) atoms with 3 valence electrons. As In atoms have only 3 electrons to share with the neighbouring 4 Si atoms, one valence electron is missing in the structure (Fig. 2.1 b). Then atoms can 'accept' electrons resulting in holes in the valence band. This type of material is called a positive (p-type) semiconductor and has mobile positive charges (holes) and immobile negative ions (acceptors).

Alternatively, if the Si is doped with an element having more than 4 valence electrons, such as phosphorus (P) with 5 valence electrons, the surplus of electrons stays free and can easily move to other atoms (Fig. 2.1 c). This type of material is called a 'negative' (n-type) semiconductor. Such a semiconductor has mobile negative charges (electrons) and immobile positive ions, which are called 'donors'.

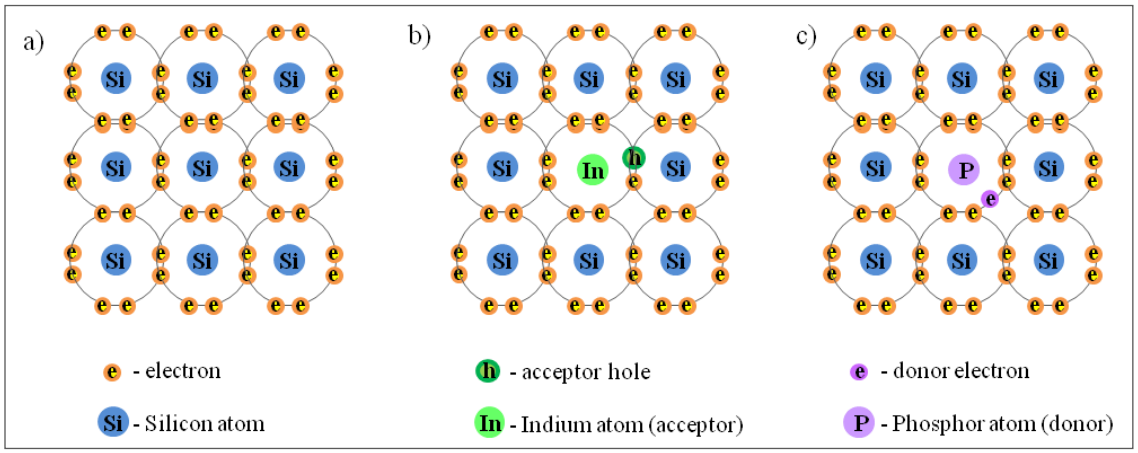

Fig. 2.1 Structure of silicon crystal; a) undoped; b) positively doped Si with one In atom; b) negatively doped Si with one P atom; from [7].

Such p-type and n-type semiconductors, which will be further described in the following sections, are vital for producing light emitting diodes.

2.1.3. Electroluminescence

In light emitting diodes, mobile electrons from the conduction band recombine with holes in the valence band. When electrons recombine with holes, the energy of the electrons can be released in the form of photons. This effect is called electroluminescence.

The energy of the emitted photon depends of the energy gap of the doped semiconductor. The scheme of the energy levels in a doped semiconductor is presented in Fig. 2.2 [7]. The energy level of acceptor, E_a, is slightly higher than the energy of the top of the valence band. As a consequence, the energy gap between the acceptor level and valence band is very small, and even at room temperature electrons from the valence band are thermally excited to the acceptor energy level leaving free holes in the valence band. Similarly, the energy level of donor, E_d, is slightly lower than the energy of the

conduction band. The donor's electrons are easily excited to the conduction band where they contribute to the semiconductor conductivity.

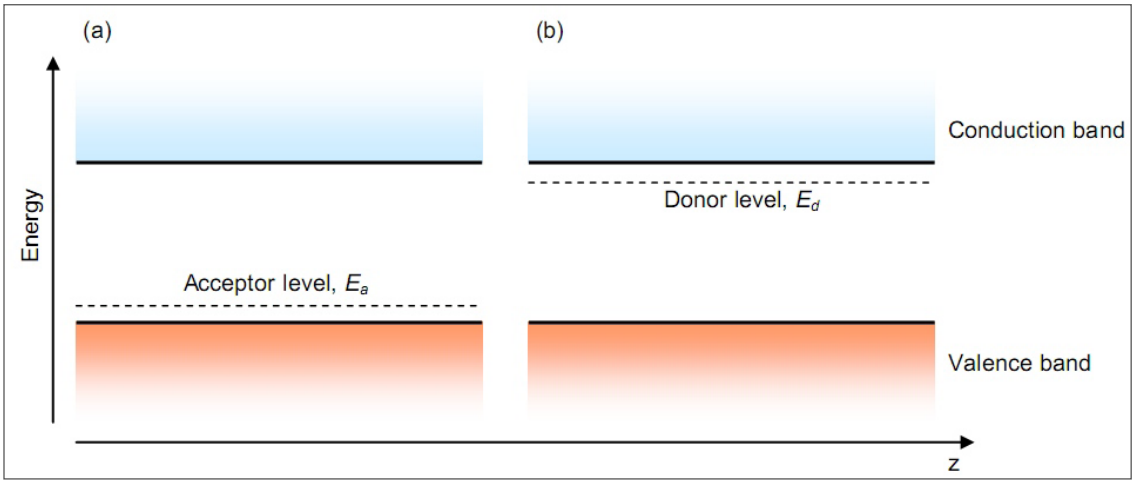

Fig. 2.2 Energy levels in a semiconductor structure: a) acceptor and b) donor energy levels. Z is a spatial co-ordinate; from [7].

These carriers thermalise quickly within the bands, and consequently, the energy released during electron-hole recombination in a doped semiconductor is approximately equal to the energy gap, E_g, of the semiconductor. The energy gap is defined as the difference of the energy of the minimum of the conduction band, E_c, and the energy of the maximum of the valence band, E_v (see Eq. 2.1).

$$E_g = E_c - E_v \qquad (2.1)$$

In semiconductors, the energy of electron-hole recombination can be released as heat (by vibrations of the crystal lattice called phonons) or photon emission. The way in which the energy is released depends on impurities and defects and the character of the bandgap of the semiconductor.

Generally, there are two types of semiconductor bandgap: direct and in-direct bandgaps (Fig. 2.3). The horizontal axis on the Fig. 2.3 (a) and (b) is the crystal momentum, representing the momentum of electrons allowed within the crystal structure. This momentum is directly proportional to the electron wavenumber, k, and is referred as k-space representation. Just before recombination, electrons are close to the minimum of the conduction band energy and holes are close to the maximum of the valence band energy. In a direct bandgap semiconductor, the minimum of the energy of the conduction band and the maximum of the energy of valence band coincide in k-space. Consequently, the recombination can happen without any change of crystal momentum (Fig. 2.3 a). However, in an indirect bandgap semiconductor, the minimum and maximum of the respective energy levels do not coincide in k-space (Fig. 2.3 b). Electron-hole recombination is accompanied by an additional phenomenon: a change in crystal momentum (generation of a phonon - crystal lattice vibration). Thus, the recombination in indirect bandgap semiconductors is less likely to happen. For that reason, most of the efficient light emitting diodes are made out of direct bandgap semiconductors.

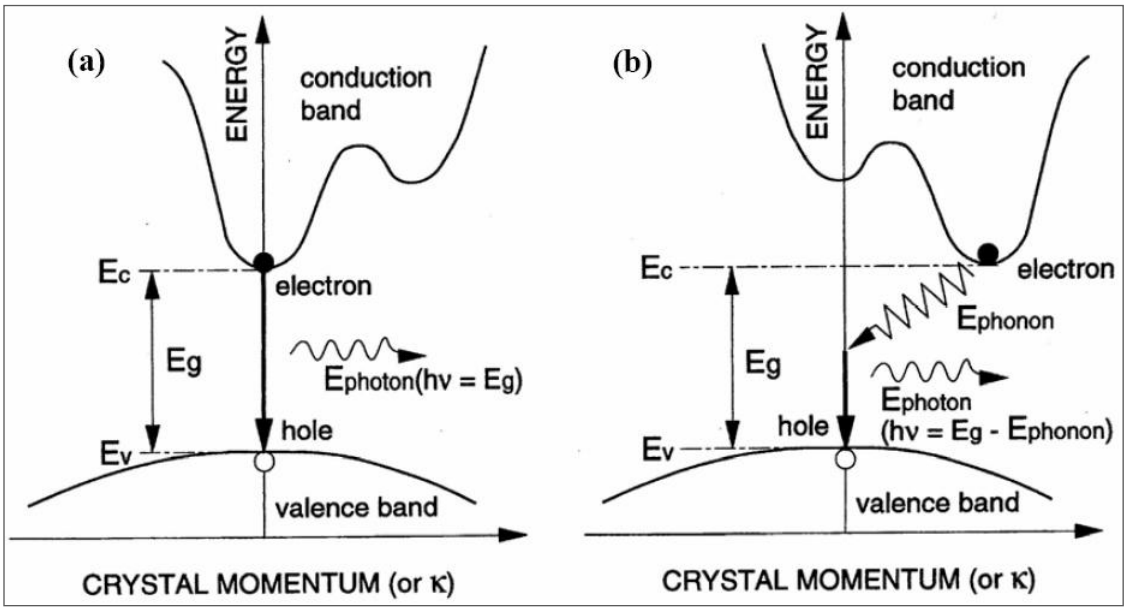

Fig. 2.3 Band structures of (a) direct and (b) indirect bandgap semiconductors; from [8].

Moreover, as seen in Fig. 2.3 a, the photon energy emitted is equal to the bandgap energy. The relationship between the bandgap energy, E_g, and the wavelength, λ of the emitted photon, and hence also its colour, can be described by Eq. 2.2:

$$E = E_g = \frac{hc}{\lambda} \qquad (2.2)$$

Where E is the energy of emitted photon, c is the speed of light in vacuum and h is Planck's constant. Today, the advanced engineering of semiconductor fabrication so-called 'bandgap engineering' allows tuning of the bandgap energy, hence also for tuning emission wavelength.

2.1.4. The p-n junction in a diode

Light emitting diodes (LEDs) are made of a semiconductor having both p and n type doping regions close to each other. Such a semiconductor with the two doping types can be created by controlled ion implantation, by diffusion of dopants or by epitaxial growth

(layer by layer growth on a substrate). When p-doped and n-doped semiconductors are joined together at the so-called p-n junction, electrons from the conduction band are spatially close to holes from the valence band and they recombine more easily. The electron-hole recombination process creates a region in the structure where fixed ions are left uncovered by mobile charges called the space charge region (Fig. 2.4). Since fixed ions are left uncovered in the space charge region, a potential is build up between positive and negative fixed charges, also known as a diffusion voltage V_d, which prevents further mobile charge diffusion and electron-hole recombination. Consequently, an equilibrium state is reached and the material becomes non-conductive at the junction. This non-conductive zone is called the depletion layer. V_d is defined as the potential that needs to be applied externally before the mobile charges can recombine again with the opposite carriers.

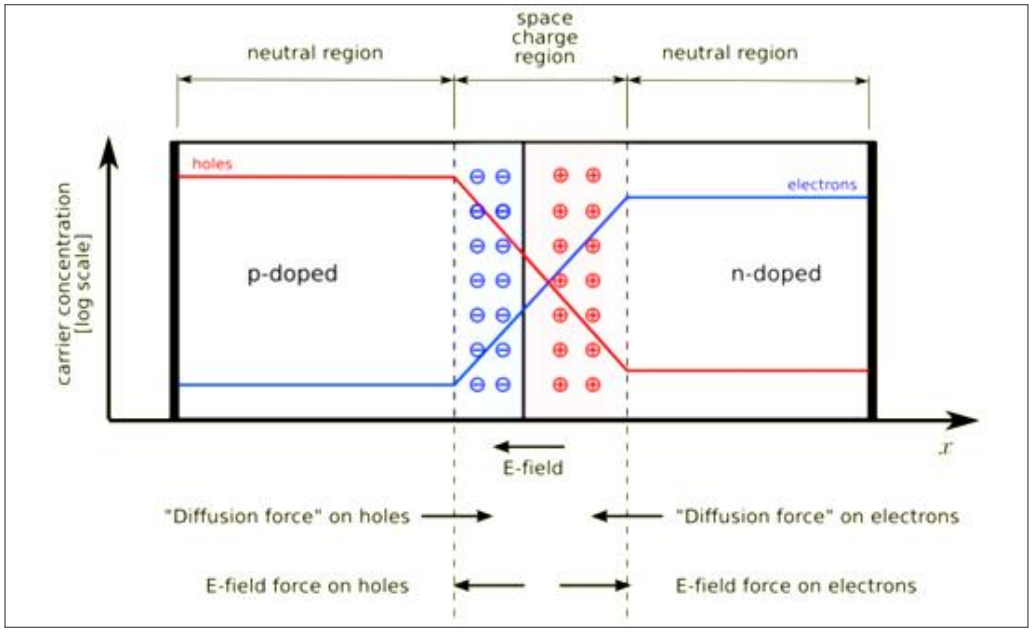

Fig. 2.4 The p-n junction with space charge region; from [9].

When a voltage is applied against the diffusion voltage in a way that p-type material is connected to the positive bias and n-type material is connected to the negative bias (forward bias), holes from the p-type region and electrons from the n-type region flow towards the junction and recombine with opposite mobile charges. The depletion region, i.e. space charge region is then reduced as well as the potential in the p-n junction. When the applied voltage reaches the value of the diffusion voltage, the space charges are fully neutralised. By further increasing the applied voltage, electrons flow into the p-type layer and holes flow into n-type layer and electrons and holes recombine. This electron-hole recombination in light emitting diodes (LEDs) results in photon generation and light emission. Moreover, because the electrons can flow only in one direction in a p-n junction, the p-n junction can also be used to control the current flow and its direction.

2.1.5. LEDs used in this work

Gallium nitride (GaN) based LEDs have attracted particular interest in optoelectronic research and applications. These LED can emit high optical powers in different wavelength ranges. Depending on the AlInGaN alloy composition, the LED emission wavelength will change. As a result, GaN based LEDs can emit light with wavelengths from deep ultraviolet (UV) to amber-red (Fig. 2.5) a range from ~ 240nm to 600nm [10].

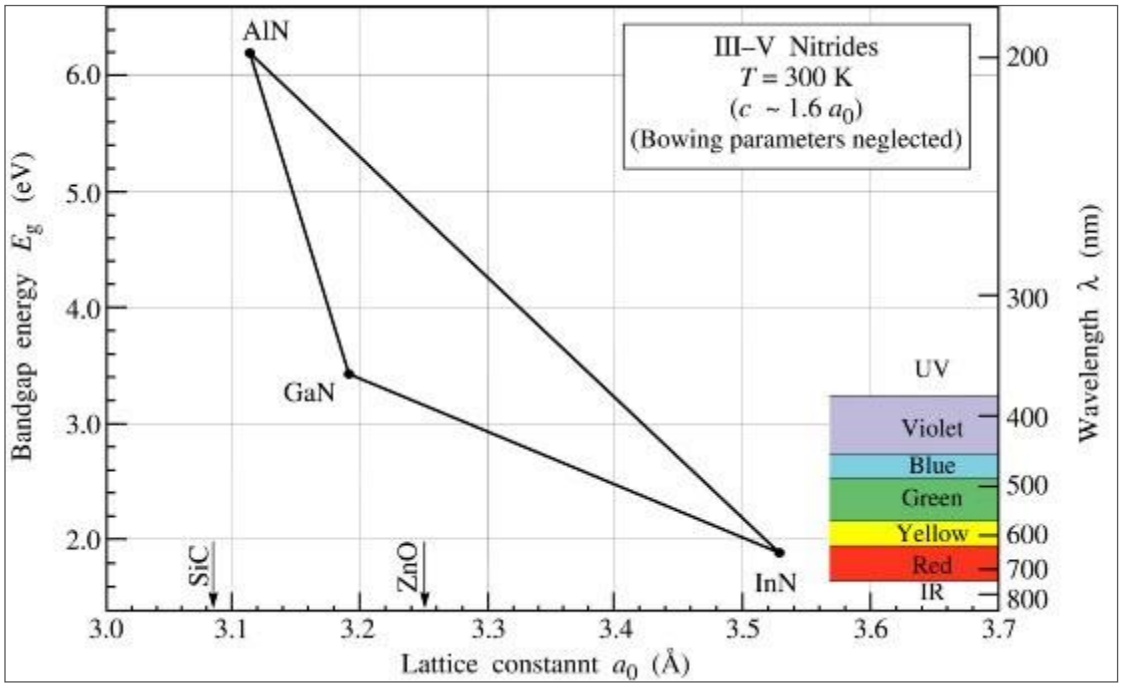

Fig. 2.5 Bandgap energy and emitting wavelength versus lattice constant of III-V nitride semiconductors at room temperature. The lattice constants of certain substrate materials are indicated; from [10].

A typical GaN LED structure is presented in Fig. 2.6. In the structure, there are multi-quantum wells (MQWs) made of InGaN with GaN barriers. A quantum well (QW) is a layer of lower bandgap than the surrounding layers and a thickness of the order of the de Broglie wavelength of electrons in the material (~ 10nm); it provides quantum confinement. These InGaN/GaN layers were grown on a sapphire c-plane substrate. N and p metal contacts were made on the top surface of the LED structure, i.e. on the n type and p type GaN layers because the sapphire is electrically insulating. The p contact was made of a transparent metal layer (Ni/Au). It allowed for current spreading and holes injection to the diode structure. N metal contact allowed for injection of electrons (made of Ti/Al). When a forward bias is applied, holes injected through p doped GaN and electrons injected to n doped GaN layers recombine in the InGaN quantum wells

region, generating photons. To minimise the size of the emitting area, a patterned current blocking layer (insulator such as SiO_2) was deposited on the top of the active region structure.

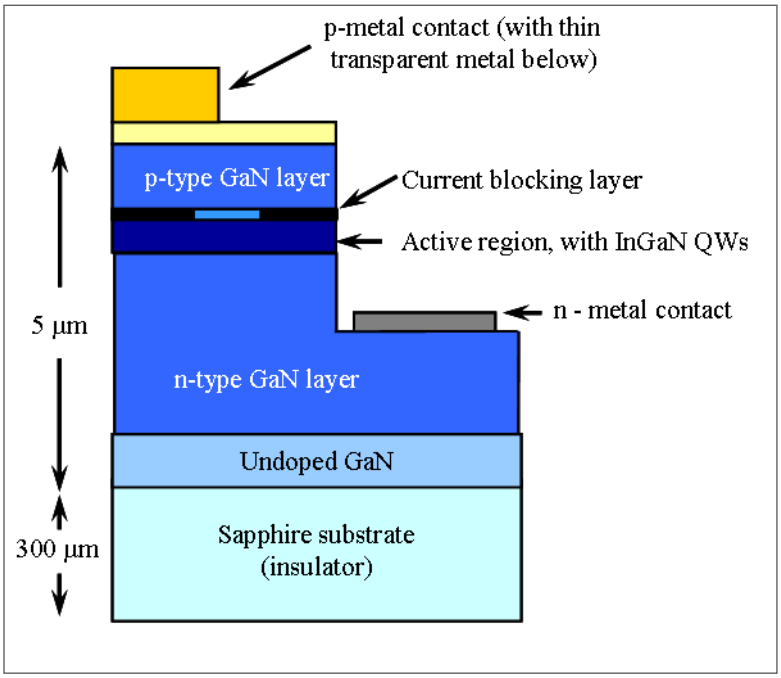

Fig. 2.6 Simplified structure of gallium nitride (GaN) light emitting diode; from [11].

The GaN LED research in the Institute of Photonics (IoP) focuses on the development of pattern programmable micro-light emitting diode (micro-LED) array devices. These GaN micro-LED array devices were fabricated from structures similar to the above, but with the active area processed into high-density arrays of micro-sized pixels, where the pixel diameter ranges typically from a few microns to few tens of microns. Depending on the device format, these micro-LED arrays can be controlled by either a matrix driver [12], or an individual pixel addressable driver [13] or a Complementary Metal-Oxide-Semiconductor (CMOS) driver [14]. In this work, individually and CMOS addressable micro-LED arrays were used. Each of these individually addressable LED pixels had a

separate p contact and all the pixels shared a common n contact. Each LED pixel can be independently controlled via a printed circuit board (PCB) and metal connections (see Chapter 6) or in CMOS controlled micro-LEDs, each LED pixel in the array was bonded directly to its own dedicated individually-controllable CMOS driver. CMOS control allowed precise voltage delivery to the desired pixel, under continuous or pulsed mode. Importantly, CMOS driven micro-LED pixels can emit light pulses shorter than 1ns [14].

The LED devices fabricated at the IoP were prepared in different formats, in either top emission or 'flip-chip' emission configuration, as presented in Fig. 2.7. In the top emission configuration, light was extracted through the top p-doped GaN (Fig. 2.7 a). In the flip-chip configuration light was extracted through the n-doped GaN layer and the sapphire substrate (Fig. 2.7 b). In this case, the upper surface of the sapphire is polished.

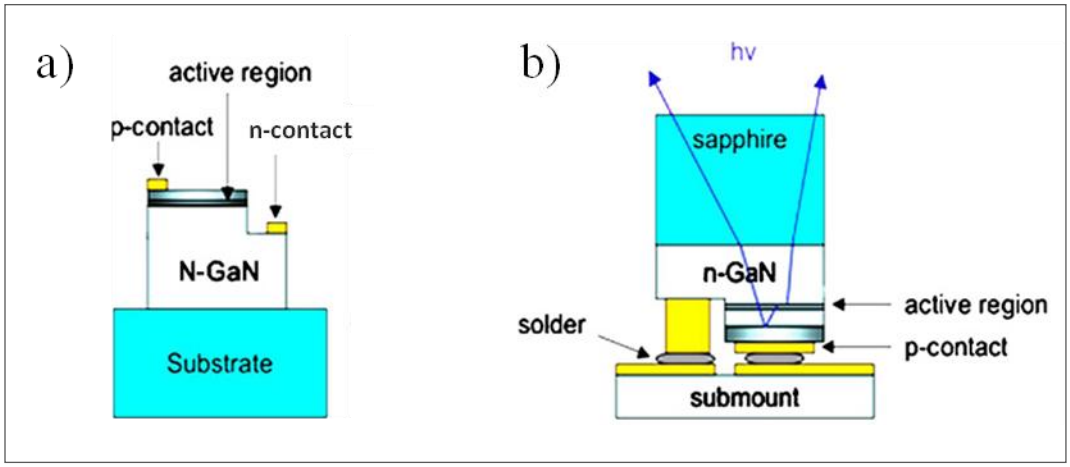

Fig. 2.7 Micro-LED device structures: a) top emission; b) flip-chip device structure; from [15].

The flip-chip configuration has several advantages as compared to the top emitting device. It allows for improved light extraction and light emission uniformity, reduced spreading resistance, better thermal management and it has a flat, inert emission surface which facilitates integration with other components [12]. Fig. 2.8 shows typical I-V (current-voltage) and L-I (power-current) curves of a representative pixel in a 64×64 flip-chip matrix-addressable micro-LED array emitting at blue (470nm) wavelength comparing to a top-emitting device of the same format [12]. The diameter in this case was 20μm. In this thesis work, flip-chip devices were used throughout. Note the high power density of light that can be delivered by such pixels and the high current densities they can withstand.

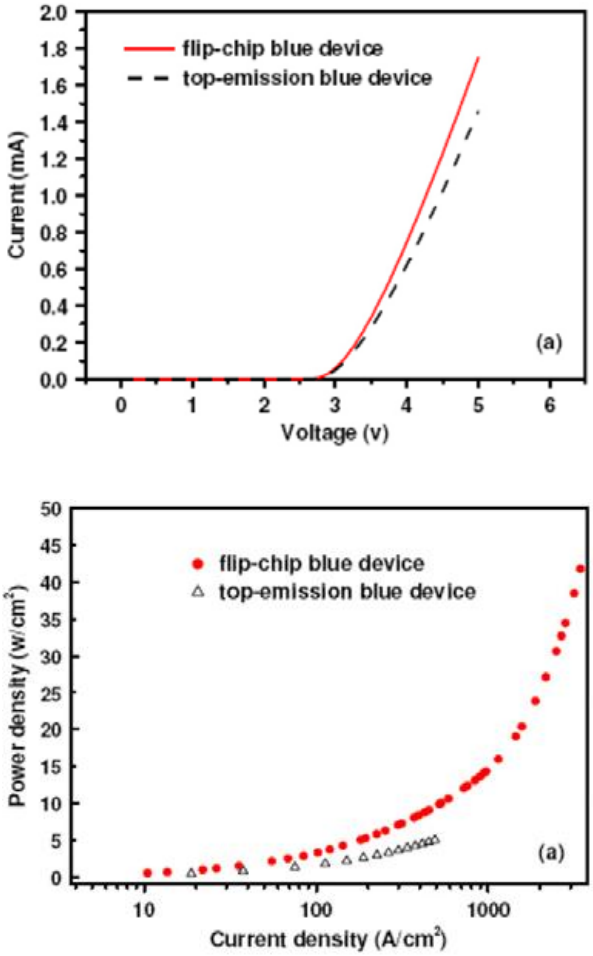

Fig. 2.8 Blue micro-LED pixel operation characteristics: comparison between flip-chip and top emission operation performance; a) current – voltage characteristics; b) power density – current density characteristics; from [12].

In our group, micro-LEDs with different emission wavelengths have been fabricated, from UV emitting devices at 370nm, violet emitting at 405nm, blue emitting at 450nm or 470nm, green at 520nm, yellow at 560nm, to amber-red devices emitting above 600nm. The typical spectra of the devices are presented in Fig. 2.9 [7]. In this work, blue and green micro-LED devices were used. The detailed structures of these micro-LED

devices and the way to control the device for each application will be specified in the following Chapters.

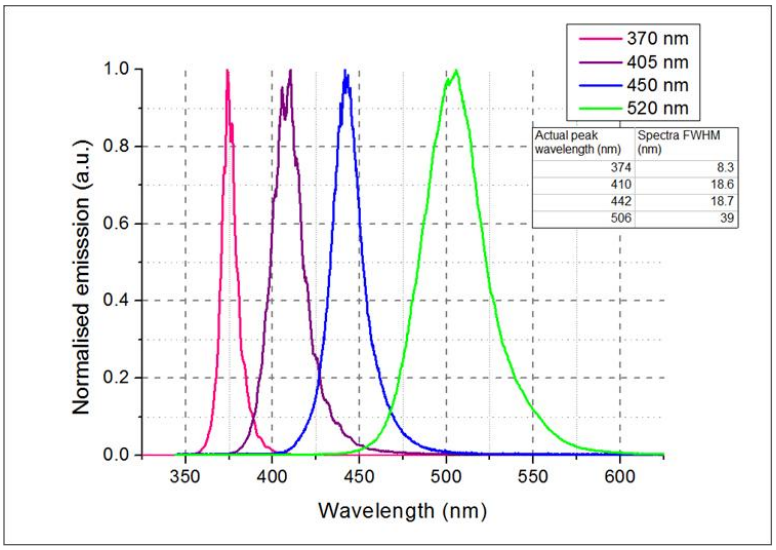

Fig. 2.9 Emission spectra of various micro-LED pixels. Each pixel was 84 μm in diameter and was operated with a DC current of 20 mA; from [7].

Micro-LED devices can be operated in either continuous or pulsed modes. Depending on the emitting wavelength, individually-addressed LED pixels under 25ns pulsed excitation can deliver a power density of 34 W/cm^2 when a 405nm pixel was operated, generating an energy of 85pJ per pulse, and 130 W/cm^2 when 450nm pixel was operated, producing energy of 500pJ per pulse [13]. When operated with a CMOS driver, pulses as short as 300ps were obtained for 370nm emitting devices, 636ps for 405nm and 818ps for 450nm devices, generating energies from 1 to 50 pJ per pulse [6]. Such short pulses are beneficial for fluorescence life-time analysis as well as for high speed light communication.

In this work, the micro-LED devices were used in two new applications: miniaturised optoelectronic tweezers (mini-OET), described in Chapter 3; and local fluorescence excitation in miniaturised format, described in Chapter 6. The originality of this work lies in the system integration with novel micro-LED light sources, both in mini-OET and in the integrated optoelectronic/microfluidic system. The integration makes the micro-systems portable and allows use inside a cell incubator.

2.2. Optoelectronic Tweezers

2.2.1. Background

In biomedical sciences, micro-manipulation techniques allow for investigation of bio-systems on a very small scale by observing interactions between single cells or between cells and their environment [16]. Optoelectronic Tweezers (OET) is a recently developed technique for micro-particle manipulation. Instead of using fixed micro-fabricated electrodes as in traditional Dielectrophoresis (DEP) (details in Chapter 1), OET relies on light-patterned photoconductive electrodes to provide real time control over the positioning of electric fields. As explained below, in response to a projected light pattern, the local conductivity of the photoconductive material is modified, creating non-uniform electric fields in the sample chamber between the photoconductive electrode and a counter electrode [17].

2.2.2. The OET device structure and operating principle

A typical OET device comprises two electrodes made of indium tin oxide (ITO) coated borosilicate glass slides which form a sample chamber [18]. The bottom electrode is covered with a layer of photoconductive material, typically hydrogenated amorphous

silicon (a-Si:H). A top view of the typical OET chamber we used is presented in Fig. 2.10. The typical spacing between two electrodes, i.e. ITO coated glass and a-Si:H/ITO coated glass, is 100μm achieved using sellotape spacers. A conductive liquid, with the micro-particles to be manipulated suspended within it, is placed between the electrodes, and the electrodes are connected to an electrical function generator.

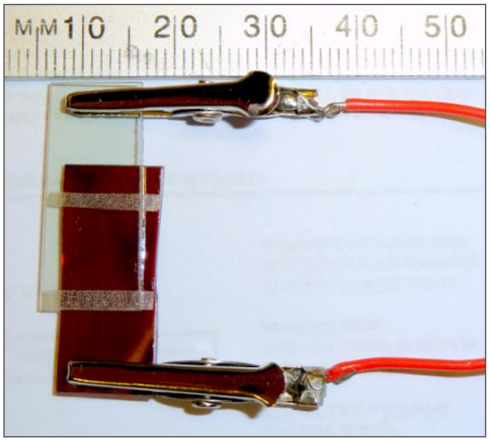

Fig. 2.10 A top view of the OET chamber composed of an ITO and a-Si:H coated glass slide (bottom electrode) and an ITO coated glass slide (top electrode). Crocodile clips connect the electrodes to the AC function generator.

In the dark, the impedance of the photoconductive layer is higher than the impedance of the liquid between the electrodes and almost all the voltage is dropped across the photoconductive layer (Fig. 2.11 a). Under illumination, the impedance of the photoconductor drops dramatically and the voltage is applied onto the liquid around the illuminated area (Fig. 2.11 b). A non-uniform electric field is then generated in that area.

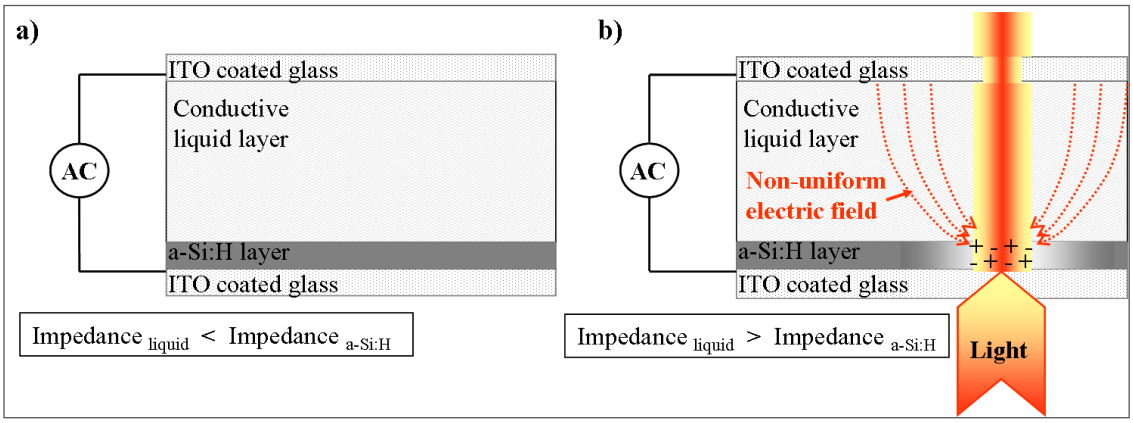

Fig. 2.11 Schematic side-view of the OET device: a) in the dark state – very little voltage is dropped across the liquid layer; b) under illumination, the impedance of the photoconductive layer, a-Si:H, has dropped, the voltage is transferred into the liquid around the illuminated area and a non-uniform electric field is generated between electrodes.

The non-uniform electric field applies a force on polarized particles to move them. This effect is called dielectrophoresis (DEP) [19]. The magnitude and direction of the DEP forces are determined by the relative permittivity of the particle and of the liquid in which it is suspended. Particles with higher permittivity than the liquid experience attraction towards the high electric field region, i.e. positive DEP, while particles with lower permittivity than the liquid medium experience repulsion from the high field region, i.e. negative DEP (Fig. 2.12 a). The DEP force is proportional to the gradient of the electric field squared and reaches its maximum at the edges of the illuminated area where it dominates the particles' motion.

In addition, small quantities of ions exist in the liquid and they are attracted by the opposite charges (ions) appearing at the solid (electrode) surface, forming an electric double layer (EDL). The electric double layer appears at the interface between a liquid

and an object. The object might be a solid particle, a gas bubble, a liquid droplet, or a porous body. Therefore, in this double layer, one is a surface charge layer composed of ions adsorbed near to the solid or liquid surface. The second charge layer is composed of ions in the liquid of opposite charge which are attracted to the surface by Coulomb force. The second layer is also named the diffuse layer as it is susceptible to move under external cues, such as electric fields and thermal motion.

When a low frequency AC bias is applied, the ions in the diffuse layer at the liquid/solid interface are driven by the electric-field-induced force which is stronger at the illuminated region of the device. The movement of the ions drags the bulk of the liquid with them. This phenomenon is called light-induced AC electroosmosis (LACE) [17]. In an OET chamber, this liquid movement is towards the illuminated area close to the a-Si:H surface, and away from the illuminated area above it, and it creates vortices as shown in Fig. 2.12 b. This phenomenon is responsible for particle and liquid movements over relatively large distances (a few millimetres from the illuminated area).

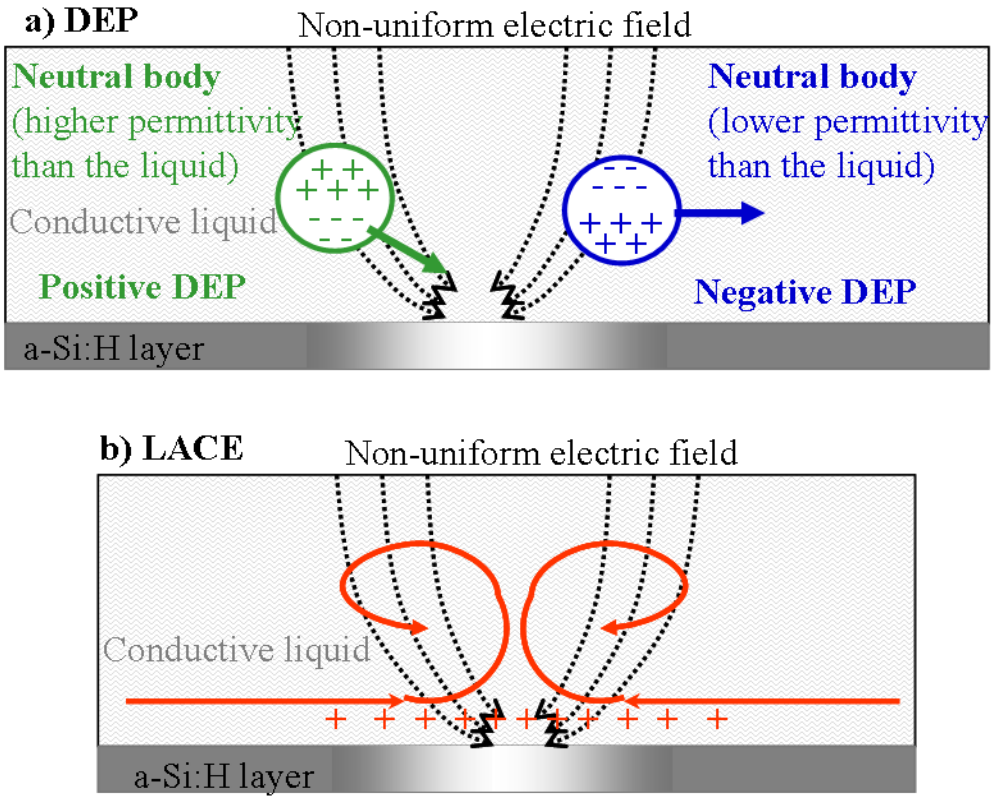

Fig. 2.12 Schematics of a) the dielectrophoresis (DEP) forces generated in OET devices and the resultant particle movement and b) light-induced AC electro-osmosis (LACE) and induced liquid movement.

2.2.3. OET state of art

The optoelectronic tweezing effect was first used by Hayward et al. in 2000 when they used UV radiation to assemble colloidal nanoparticles onto ITO surfaces [20]. At that time the phenomenon which governed the particle motion was not fully explained. Later, Ming Wu's group at UC Berkeley explained the phenomenon and demonstrated that thousands of particles could be manipulated simultaneously thanks to the use of a digital mirror device (DMD) to project a light pattern onto the photoconductive surface [18]. Later, their group developed the OET applications extensively. Some examples of applications developed by them include: controlled single cell lysis [21], guided healthy

embryo selection [22], manipulation of carbon nanotubes [23], nanowires [24], silver nanoparticles [25] and droplets [26]. Today, there are around 13 research groups in the world who have developed OET technique and applications. These include Ming Wu's Group; Chiou's Group at Optoelectronic Biofluidics Laboratory, UCLA; Steve Wereley's Group at Microfluidics Laboratory, Purdue University; Brandt's group at Walter Schottky Institut, Technische Universitat, Munchen, Germany; Steve Neale's group at the University of Glasgow, United Kingdom; Je-Kyun Park's Group at NanoBiotech Laboratory, KAIST, Korea; and two groups at National Tsinh Hua University and National Cheng Kung University, Taiwan [27]. In our optoelectronic tweezing application, performed as collaboration with S.L. Neale, two-dimensional green micro-LED arrays were used for the first time to create light pattern directly without using additional spatial light modulators.

2.3. Microfluidic devices

2.3.1. Background

By using microfabrication technologies, microfluidic devices have been developed since 1970 for applications in optics, mechanics and fluidics [28]. The gas chromatograph developed at Stanford University [29] and inkjet printing heads developed by IBM in the late seventies [30] are examples of early microfluidic devices.

The first microfluidic devices were made out of glass and silicon. However, micro-channel fabrication in these materials required acid or ion etching. In 1993, thanks to the implementation of PDMS (poly(dimethoxysiloxane)) material, a new method of micro-

channel fabrication was developed [31]. PDMS is a cheap, rubber-like material which can be shaped to any form on the pre-formed silicon mould. PDMS is easy to pattern, is optically transparent between 240 and 1100 nm, flexible, gas-permeable, non-toxic and requires fewer skills in fabrication than silicon or glass chips [32]. The method, called soft lithography, allows for faster and cheaper fabrication of micro-channels out of PDMS. PDMS technology was further developed into multi-layer soft lithography by Stephen Quake's group at Stanford University [33] and Richard Mathies at the University of California Berkeley [32] allowing for implementation of micro-actuators inside microfluidic channels. In the middle of 1990s, microfluidic technology was developed intensively.

2.3.2. Principles and applications

In microfluidics, the conditions in which a sample is placed differ from the standard multi-well plate conditions. For example, viscosity and surface tension dominate over gravitational forces and the effect of the momentum of the fluid. This is expressed by a low Reynolds number as defined by Eq. 2.3:

$$\mathcal{R}_e = \frac{\rho V L}{\mu} = \frac{V L}{\nu} \qquad (2.3)$$

Here ρ is the density of the fluid, V is the mean velocity of the object relative to the fluid, L is the travelled length of the fluid, μ is the dynamic viscosity of the fluid and ν is its kinematic viscosity [34].

In microfluidic devices, the viscosity is higher or comparable to the velocity of the fluid and thus the Reynolds number is low. As a consequence, the liquid flows in parallel

lines without vortexes and lateral mixing – the flow is laminar. Thus, the particles transported by the fluid can mix only by diffusion. This effect has been used in the microfluidic device applications, for example to precisely control gradients of the concentrations of the applied chemicals on a micrometre length scale (Fig. 2.13 A) [35]. Moreover, these gradients change when they are subjected to the transversal electrical field thanks to the electrowetting phenomenon. This effect was also used to control and enhance lateral mixing inside micro-channels (Fig. 2.13 B) [36].

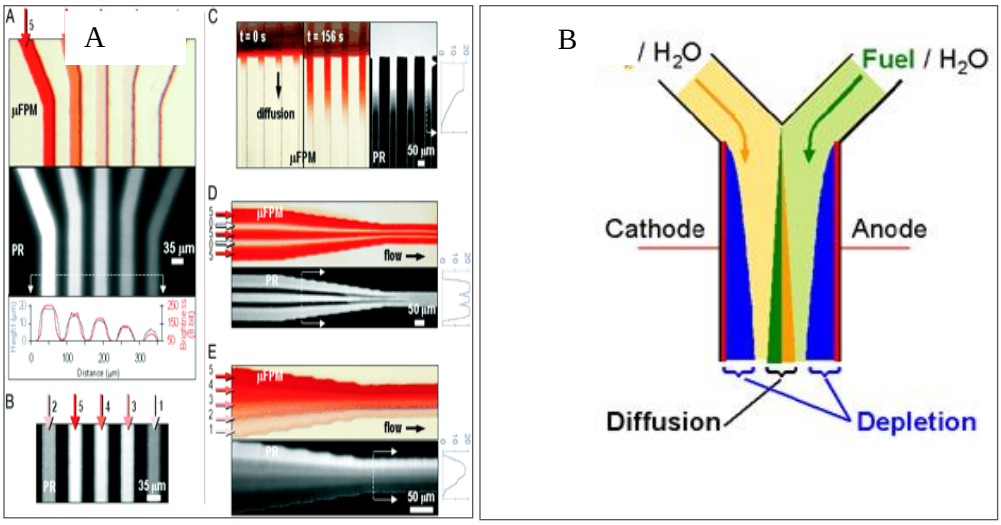

Fig. 2.13 Gradients of chemicals in microfluidic channels: A) Gradients of photoresist obtained in a microfluidic device resulting in different height of created features, from [35]; B) Schematic of the Y-shaped microfluidic channels with applied transversal potential to enhance mixing; from [36].

Also, high surface tension and high fluid viscosity as well as the differences of the latter between different fluids allowed for creation of droplet based fluidics [37]. Droplets allow for controlled sample encapsulation, for example cell encapsulation for efficient viability assays (Fig. 2.14) [38]. Biochemical analysis was substantially enhanced by encapsulation of samples in droplets. Not only was the reaction controlled better, but

also the thermal relaxation was much faster than in microlitre volumes of sample (relaxation in the order of 15ms). Fast thermal relaxation of such small fluid volumes allowed for creation of ultrafast miniaturised polymerase chain reaction (PCR) on chip [39].

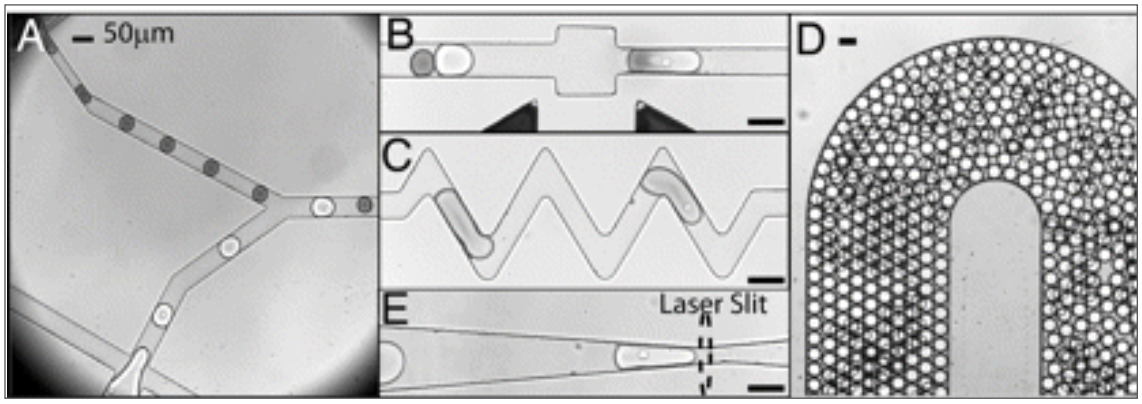

Fig. 2.14 Droplet in microfluidics for on-chip viability assay. A) A set of 2 nozzles: encapsulated cells and viability dyes respectively. The Y junction enabled alternation of cell-containing droplets with dye-containing droplets; B) Fusion module which delivered an AC field and permitted electrically-controlled merging of dye-containing droplets and cell-containing droplets; C) Mixing module which facilitated rapid mixing of cells with dyes; D) Delay line optimised cell staining; E) Detection module confining droplets laterally and vertically to collect the fluorescent signals excited with a laser slit; from [38].

For analysis applications, microfluidic devices, having a lot of advantages as compared to traditional analysis techniques, were developed intensively in the last 20 years. They allowed for easier application and more effective removal of reagents. The time to obtain results in micro-channels was shorter as the diffusion lengths were shorter. Laminar flow inside microfluidic devices created gradients of concentrations on the length scale of a single cell, allowing for precise application of a defined drug at the desired concentration through the sample. Moreover, microfluidic devices allowed for

reducing the space required for the experiment and making the device portable. Thanks to all these advantages, microfluidic devices offer high sensitivity of detection, high speed serial processing (at a single cell level) and high degree of parallelism at lower cost when compared with technologies used today for commercial testing.

In this work, novel cell patterning and engineering methods have been developed. By using piezoelectric printing, well defined cell micro-arrays were created inside microfluidic devices. Piezoelectric printing technology will be described in the next section of this Chapter. The above micro-LED light sources were also integrated with a microfluidic network to create a miniaturised two dimensional cell analysis tool. This work will be presented in Chapter 5 and 6.

2.4. Piezoelectric printing

2.4.1. Background

In this section the piezoelectric printing technology used to create bio-patterns inside microfluidics is described. The word ’piezo’ derives from the Greek word ’piezein’ and means to squeeze or to push. The piezoelectric effect was discovered by Jacques and Pierre Curie in 1880, when they were studying how pressure generates electrical charge in crystals [40]. In 1953, the first high-speed printer was developed by Remington-Rand for use on the Univac computer. The inkjet printer was invented in 1976, but only in 1988 it become a home consumer item with Hewlett-Parkard's release of the DeskJet inkjet printer [41].

Piezoelectric printing is a very flexible, precise, robotic deposition technique that delivers small droplets with controlled volumes and position in non-contact mode. It offers a high degree of flexibility in pattern layout, in concentration range and in operation sequences. It also offers the possibility of multilayer deposition or superposition of different materials in three dimensions. During deposition, little material is wasted because it is printed only where needed. Most importantly, it is a high throughput technique.

In piezoelectric printers, piezoelectric material is located behind the nozzles filled with ink (Fig. 2.15) [42]. When a voltage is applied, the piezoelectric element changes shape and a pressure is applied on the nozzle. This generates a pressure wave in the liquid and a portion of the ink is pushed out of the nozzle. A droplet is generated outside the nozzle and is deposited onto the substrate.

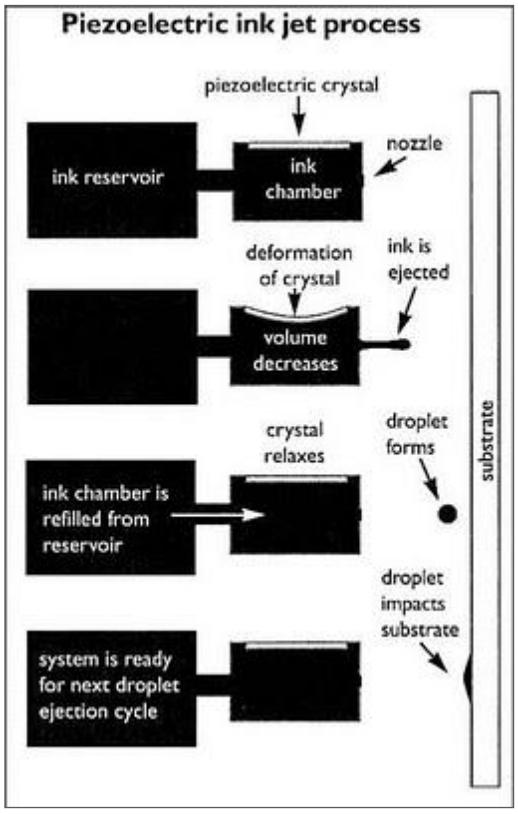

Fig. 2.15 Schematic of the piezoelectric ink jet process; from [42].

Piezolectric printers have advantages over thermal printers as they do not need volatile inks, they do not heat the fluid and consequently the coagulation of the ink is not an issue. However, the printing heads are more expensive to manufacture (the most commonly used piezoelectric material is lead zirconium titanate, abbreviated as PZT).

2.4.2. Printers used in this thesis work

In our study, we used three different printers: a Dimatix® ©FUJIFILM Material Printer DMP-2800, a sciFLEXARRAYER S3 from Scienion AG, Germany, and a PerkinElmer Piezoarray™ micro-spotter.

The Dimatix printer allowed for precise deposition of small droplets, depending on the printing head and nozzles size, of 1pl or 10pl volume (Fig. 2.16) [43]. Besides the small volume of printed droplets, permitting printed features as small as 10µm, another important advantage of using this printing system is the capability of optimising the operating parameters so as to successfully jet bio-fluids (e.g. frequency and structure of the waveform; voltage of individual nozzles). The manufacturer's specification indicates that the drop size repeatability is within 3.5% when the parameters are not optimised and about 0.5% when they are optimised. The positioning accuracy is within 1µm [43, 44]. This system also allowed for printing high quality patterns of function polymers on the top of the micro-LEDs as presented in Chapter 1.

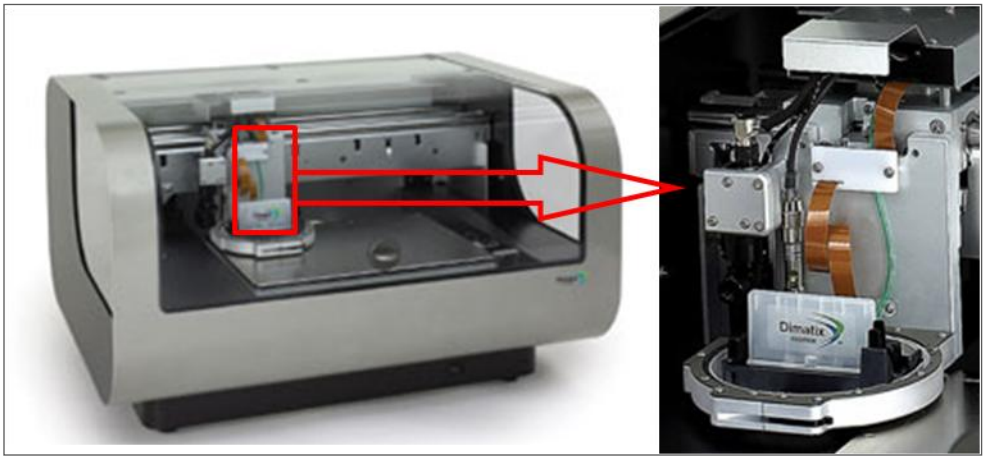

Fig. 2.16 Photographs of the Dimatix DMP 2800 printer. Insert shows the cartridge head. Photographs were taken from [43].

We also used a Piezoarray™ PerkinElmer spotter capable of dispensing droplets of volumes ranging from 330pl to 1nl. An additional advantage of the Piezoarray™ printer was that the nozzles picked up the dispensed fluid from very small volume recipients (100µl) just before printing (Fig. 2.17). Moreover, the resolution of the position of the

printing head was 2µm permitting accurate pattern registration with external devices (e.g. microfluidics) [45].

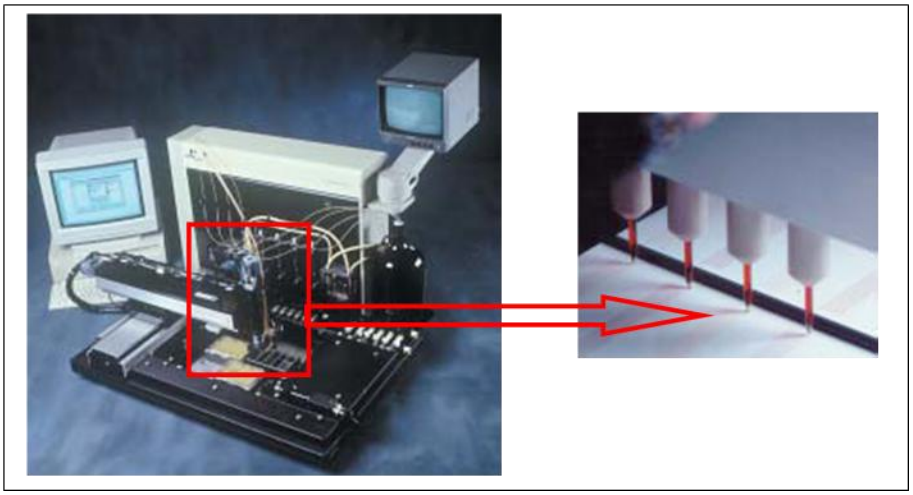

Fig. 2.17 Photographs of PerkinElmer printer. Insert shows zoom on the nozzles. Photographs were taken from [45].

The third printer used, the sciFLEXARRAYER S3 from Scienion AG, was a piezoelectric dispenser specially designed for low volume drop-on-demand printing (Fig. 2.18). The volume of the typical dispensed droplet was 280pl. The diameter of the printed spots, depending on fluid viscosities and concentration, ranged from 120µm to 250µm. The printer had an integrated CCD camera enabling the observation of dispensed droplets. This printer has a resolution of the printing head position of 1µm [46].

Fig. 2.18 Photograph of Scienion printer. Photograph was taken from [46].

In this work, the above piezoelectric printers were used to create micropatterns of proteins. These protein patterns were then used for subsequent cell seeding and cell microarray formation. This work will be presented in Chapter 4 and 5. Thanks to the use of these advanced printing machines, the pattern resolution was higher than previous printed protein patterns. Also, our cell microarrays obtained after seeding on the printed protein pattern were of better quality as compared to the patterns created by other research groups. We have also integrated the microarray of cells created on the top of printed proteins with a microfluidic device for the first time.

2.5. Chapter conclusions

To summarise, four different technologies were used in this thesis work so as to develop three miniaturised cell analysis tools.

The first technology, micro-LED arrays, are capable of generating micro-light patterns. These high power micro-LED pixels emit light with suitable wavelengths for biological and chemical applications. The micro-LED pixels can be individually addressed to precisely control the light pattern. They can also be operated in continuous or pulsed mode. Thanks to these advantages, new tools for biological applications were developed such as miniaturised OET and a small fluorescence cell analysis platform.

The second technology, optoelectronic tweezers (OET), was combined with micro-LEDs to create a miniaturised OET device. This miniaturised OET device is capable of manipulating micro-particles and bio-samples.

The third technology, microfluidics, allowed for precise control of the volume and position of fluid samples. Thanks to the use of microfluidics a miniaturised cell analysis tool integrating micro-LED arrays was created.

The fourth technique, piezoelectric printing, can deposit precise and high-resolution micro-patterns of fluidic samples in a high-throughput manner. In this work, piezoelectric printing was used to create micro-patterns of proteins. Cells have been seeded successfully on these printed protein patterns and the created cell patterns were also integrated inside microfluidic devices.

References

1. H. J. Round, "A Note on Carborundum," Electrical World **19**, 309 (1907).
2. R. D. Dupuis, and M. R. Krames, "History, development, and applications of high-brightness visible light-emitting diodes," J. Lightwave Technol. **26**, 1154-1171 (2008).
3. H. P. Maruska, Stevenso.Da, and W. C. Rhines, "Preparation of Mg-Doped Gan Diodes Exhibiting Violet Electroluminescence," Mater. Res. Bull. **7**, 777-& (1972).
4. H. Amano, M. Kito, K. Hiramatsu, and I. Akasaki, "P-Type Conduction in Mg-Doped Gan Treated with Low-Energy Electron-Beam Irradiation (Leebi)," Jpn. J. Appl. Phys. Part 2 - Lett. **28**, L2112-L2114 (1989).
5. S. Nakamura, N. Senoh, N. Iwasa, and S. I. Nagahama, "High-Brightness Ingan Blue, Green and Yellow Light-Emitting-Diodes with Quantum-Well Structures," Jpn. J. Appl. Phys. Part 2 - Lett. **34**, L797-L799 (1995).
6. J. J. D. McKendry, R. P. Green, A. E. Kelly, Z. Gong, B. Guilhabert, D. Massoubre, E. D. Gu, and M. D. Dawson, "High-Speed Visible Light Communications Using Individual Pixels in a Micro Light-Emitting Diode Array," IEEE Photonics Technol. Lett. **22**, 1346-1348 (2010).
7. J. McKendry, "Micro-pixellated AlInGaN light-emitting diode arrays for optical communications and time-resolved fluorescence lifetime measurements," PhD Thesis in *Physics* (Strathclyde, Glasgow, 2011), p. 182.

8. M. Fukuda, *Optical Semiconductor Devices* (John Wiley & sons, New York, 1999).

9. "Definition of p-n junction," (2007), http://en.wikipedia.org/wiki/P-n_junction.

10. E. F. Schubert, *Light-Emitting Diodes* (Cambridge University Press, Cambridge, 2006).

11. M. Wu, "Hybrid GaN/organic device fabrication by inkjet printing," PhD Thesis in *Physics* (Strathclyde, Glasgow, 2009), p. 203.

12. Z. Gong, E. Gu, S. R. Jin, D. Massoubre, B. Guilhabert, H. X. Zhang, M. D. Dawson, V. Poher, G. T. Kennedy, P. M. W. French, and M. A. A. Neil, "Efficient flip-chip InGaN micro-pixellated light-emitting diode arrays: Promising candidates for micro-displays and colour conversion," J. Phys. D-Appl. Phys. **41**, 094002 (2008).

13. H. X. Zhang , D. Massoubre, J. McKendry, Z. Gong, B. Guilhabert, C. Griffin, E. Gu, P. E. Jessop, J. M. Girkin, and M. D. Dawson, "Individually-addressable flip-chip AlInGaN micropixelated light emitting diode arrays with high continuous and nanosecond output power," Opt Express **16**, 9918-9926 (2008).

14. J. J. D. McKendry, B. R. Rae, Z. Gong, K. R. Muir, B. Guilhabert, D. Massoubre, E. Gu, D. Renshaw, M. D. Dawson, and R. K. Henderson, "Individually Addressable AlInGaN Micro-LED Arrays With CMOS Control and Subnanosecond Output Pulses," Ieee Photonics Technology Letters **21**, 811-813 (2009).

15. P. Degenaar, N. Grossman, M. A. Memon, J. Burrone, M. Dawson, E. Drakakis, M. Neil, and K. Nikolic, "Optobionic vision-a new genetically enhanced light on retinal prosthesis," J. Neural Eng. **6**, 035007 (2009).

16. D. J. Stevenson, F. Gunn-Moore, and K. Dholakia, "Light forces the pace: optical manipulation for biophotonics," J. Biomed. Opt. **15**, 041503 (2010).

17. J. K. Valley, A. Jamshidi, A. T. Ohta, H. Y. Hsu, and M. C. Wu, "Operational regimes and physics present in optoelectronic tweezers," J. Microelectromech. Syst. **17**, 342-350 (2008).

18. P. Y. Chiou, A. T. Ohta, and M. C. Wu, "Massively parallel manipulation of single cells and microparticles using optical images," Nature **436**, 370-372 (2005).

19. R. Pethig, "Review Article-Dielectrophoresis: Status of the theory, technology, and applications," Biomicrofluidics **4**, 022811 (2010).

20. R. C. Hayward, D. A. Saville, and I. A. Aksay, "Electrophoretic assembly of colloidal crystals with optically tunable micropatterns," Nature **404**, 56-59 (2000).

21. J. K. Valley, S. Neale, H. Y. Hsu, A. T. Ohta, A. Jamshidi, and M. C. Wu, "Parallel single-cell light-induced electroporation and dielectrophoretic manipulation," Lab on a Chip **9**, 1714-1720 (2009).

22. J. K. Valley, P. Swinton, W. J. Boscardin, T. F. Lue, P. F. Rinaudo, M. C. Wu, and M. M. Garcia, "Preimplantation Mouse Embryo Selection Guided by Light-Induced Dielectrophoresis," PLoS One **5**, e10160 (2010).

23. P. J. Pauzauskie, A. Jamshidi, J. K. Valley, J. H. Satcher, and M. C. Wu, "Parallel trapping of multiwalled carbon nanotubes with optoelectronic tweezers," Appl. Phys. Lett. **95**, 113104 (2009).

24. A. Jamshidi, P. J. Pauzauskie, P. J. Schuck, A. T. Ohta, P. Y. Chiou, J. Chou, P. D. Yang, and M. C. Wu, "Dynamic manipulation and separation of individual semiconducting and metallic nanowires," Nat. Photonics **2**, 85-89 (2008).

25. A. Jamshidi, S. L. Neale, K. Yu, P. J. Pauzauskie, P. J. Schuck, J. K. Valley, H. Y. Hsu, A. T. Ohta, and M. C. Wu, "NanoPen: Dynamic, Low-Power, and Light-Actuated Patterning of Nanoparticles," Nano Lett. **9**, 2921-2925 (2009).

26. S. N. Pei, J. K. Valley, S. L. Neale, A. Jamshidi, H. Y. Hsu, and M. C. Wu, "Light-Actuated Digital Microfluidics for Large-Scale, Parallel Manipulation of Arbitrarily Sized Droplets," in *Mems 2010: 23rd Ieee International Conference on Micro Electro Mechanical Systems, Technical Digest* (Ieee, New York, 2010), pp. 252-255.

27. A. Jamshidi, "Optoelectronic Manipulation, Assembly, and Patterning of Nanoparticles," PhD Thesis in *Electrical Engineering and Computer Sciences* (University of California, Berkeley, 2009), p. 108.

28. C. M. M. Niemeyer, Chad A., *Nanobiotechnology: concepts, applications and perspectives* (2004).

29. S. C. Terry, J. H. Jerman, and J. B. Angell, "Gas-Chromatographic Air Analyzer Fabricated on a Silicon-Wafer," IEEE Trans. Electron Devices **26**, 1880-1886 (1979).

30. E. Bassous, H. H. Taub, and L. Kuhn, "Ink Jet Printing Nozzle Arrays Etched in Silicon," Appl. Phys. Lett. **31**, 135-137 (1977).

31. D. Mark, S. Haeberle, G. Roth, F. von Stetten, and R. Zengerle, "Microfluidic lab-on-a-chip platforms: requirements, characteristics and applications," Chem. Soc. Rev. **39**, 1153-1182 (2010).

32. R. Mukhopadhyay, "When PDMS isn't the best. What are its weaknesses, and which other polymers can researchers add to their toolboxes?," Anal Chem **79**, 3248-3253 (2007).

33. M. A. Unger, H. P. Chou, T. Thorsen, A. Scherer, and S. R. Quake, "Monolithic microfabricated valves and pumps by multilayer soft lithography," Science **288**, 113-116 (2000).

34. J. Happel, and H. Brenner, *Low Reynolds Number Hydrodynamics: with special applications to particulate media* (Springer, 1983).

35. C. C. Chen, D. Hirdes, and A. Folch, "Gray-scale photolithography using microfluidic photomasks," Proc. Natl. Acad. Sci. U. S. A. **100**, 1499-1504 (2003).

36. P. J. A. Kenis, "Laminar-Flow Micro Fuel Cell Eliminates Membrane, Can Use Alkaline Chemistry," The Hydrogen & Fuel Cell Letter **20**, 384 (2005).

37. S. Y. Teh, R. Lin, L. H. Hung, and A. P. Lee, "Droplet microfluidics," Lab Chip **8**, 198-220 (2008).

38. E. Brouzes, M. Medkova, N. Savenelli, D. Marran, M. Twardowski, J. B. Hutchison, J. M. Rothberg, D. R. Link, N. Perrimon, and M. L. Samuels,

"Droplet microfluidic technology for single-cell high-throughput screening," Proc. Natl. Acad. Sci. U. S. A. **106**, 14195-14200 (2009).

39. D. Issadore, K. J. Humphry, K. A. Brown, L. Sandberg, D. A. Weitz, and R. M. Westervelt, "Microwave dielectric heating of drops in microfluidic devices," Lab Chip **9**, 1701-1706 (2009).

40. "History / Piezoelectricity / Curie / Piezo technology," http://www.noliac.com/History_-6584.aspx.

41. "History of Computer Printers," http://inventors.about.com/library/inventors/blcomputer_printers.htm.

42. "What is PiezoElectric Inkjet Printing?," (2008), http://www.risoprinter.com/2008/06/what-is-piezoelectric-inkjet-printing.html.

43. "Dimatix Materials Printer DMP-2800 User Manual," (FUJIFILM Dimatix, 2007).

44. J. Sumerel, J. Lewis, A. Doraiswamy, L. F. Deravi, S. L. Sewell, A. E. Gerdon, D. W. Wright, and R. J. Narayan, "Piezoelectric ink jet processing of materials for medical and biological applications," Biotechnology Journal **1**, 976-987 (2006).

45. "BioChip Arrayer; Non Contact Microdispensing System," (2002), http://las.perkinelmer.com/Content/RelatedMaterials/Brochures/bro_biochiparrayer.pdf.

46. "Scienion AG; sciFLEXARRAYER S3," http://www.scienion.de/index.php?mid=41&vid=&lang=en.

Chapter 3

3. Miniaturised Optoelectronic Tweezers (mini-OET) device

3.1. Introduction

As described in a previous Chapter (Chapter 2 – Physics background and technologies used), OET devices rely on the light pattern created on the surface of the photoconductive layer inside the sample chamber. To date, to create a suitable light pattern, OET devices have employed bulky light sources such as lasers and lamps or a video-projector. With these light sources, the light patterns are projected into the sample chamber via systems of microscope lenses. The whole setup thus takes up significant space on an optical table as shown in Fig. 3.1. In this Chapter, a novel miniaturised OET device we have developed will be described. The functionalities and capabilities of this miniaturised OET system in particle and cell manipulations will also be presented.

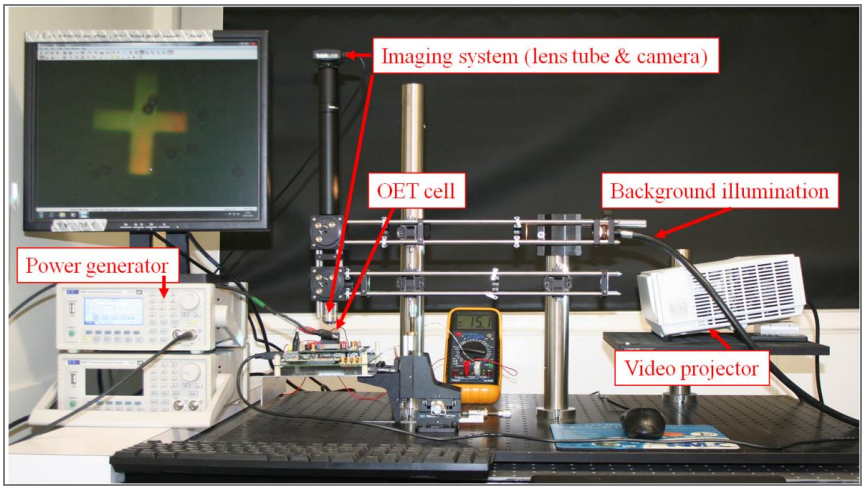

Fig. 3.1 Photograph of a typical OET experimental set up, from the University of Glasgow laboratory.

3.2. Miniaturised OET design and structure

In our miniaturised OET system, the size of the light pattern generation unit was considerably decreased by using CMOS-controlled gallium nitride (GaN) micro-LEDs as an integrated light source. These sources and their CMOS control are described in detail below.

The CMOS/LED unit that has been used for this application consists of a chip containing an array of 8 x 8 GaN LED micro-pixels on a 200μm centre-to-centre pitch, flip-chip bonded to a CMOS control backplane. The microscopic image of a portion of CMOS circuitry (showing four individual CMOS driver pixels) and a representative photograph of the CMOS controlled four micro-LEDs device is presented on Fig. 3.2 [1]. A bump-bonding process was used to electrically and physically contact the micro-LED and CMOS devices. Each CMOS bonding area is connected to a micro-LED pixel by an Au bumpbond, effectively providing an 8 x 8 array of CMOS-controlled micro-LED pixels with a 200μm pitch. Local electrical LED drivers embodied in the CMOS provide direct and independent control of the light output of each pixel, which can be operated continuously or in other modes such as nanosecond pulsing [2].

These sources can thus provide a controllable light pattern directly without using a spatial light modulator and offer the possibility of switching modes of operation, e.g. combined particle manipulation and fluorescence excitation.

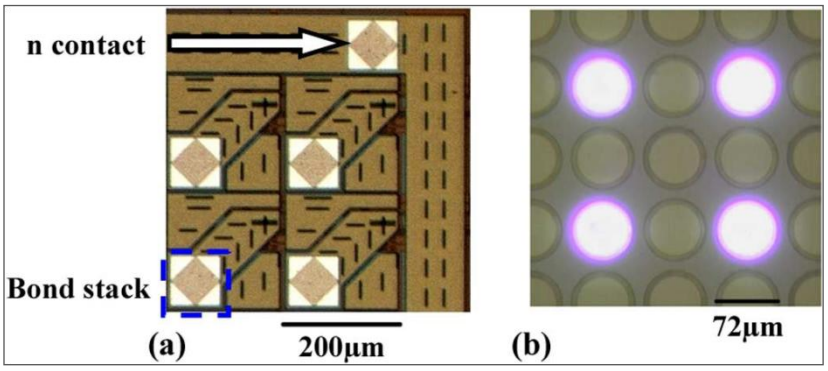

Fig. 3.2 CMOS circuit: a) schematic of the CMOS chip; b) photograph of the CMOS-controlled micro-LEDs; from [1].

Our initial investigations of miniaturised OET were performed using a blue (450nm) micro-LED array device. However, further experiments showed that a green 520nm device was the most suitable. The reason for this and the detailed results will be described below.

In both cases (blue and green devices), to facilitate pixel size dependent investigations, the respective device chips used consisted of 8 rows of LED pixels, each of which had a fixed pixel diameter, but between which the pixel diameter increased at intervals of 10µm (i.e. 14µm row, 24µm row, 34µm row, 44µm row, 54µm row, 64µm row, 74µm row and 84µm row, respectively, as presented in Fig. 3.3).

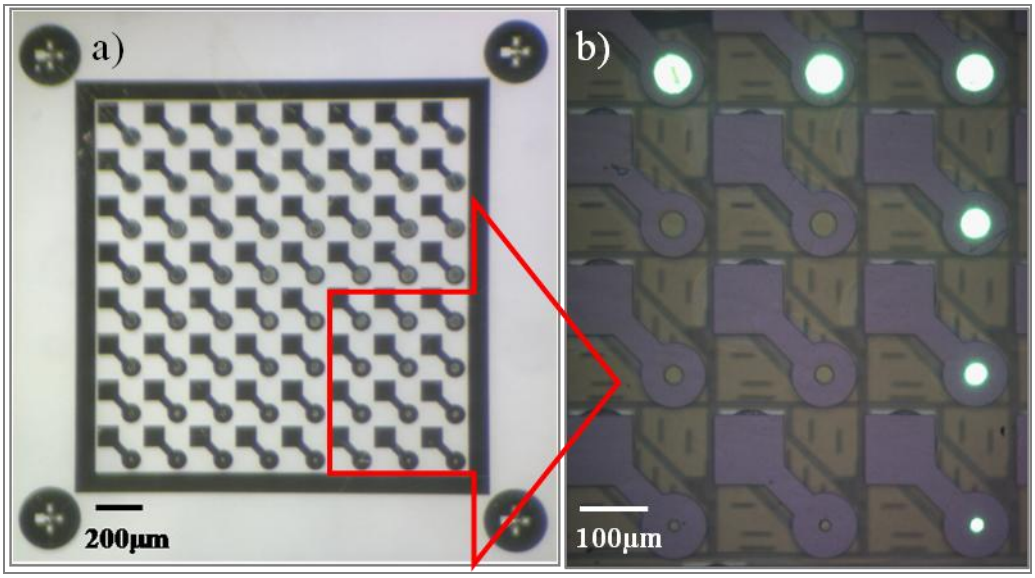

Fig. 3.3 Photographs of the micro-LED array layout showing pixels from 14µm (bottom row) to 84µm (top row) diameter. The LED diameters change in different rows at intervals of 10µm: a) overview of the whole device; b) higher magnification picture with 6 pixels switched on; bottom row has one, 14µm pixel switched on; top row has three, 44µm pixels switched on.

A typical turn-on voltage for a 450nm LED pixel is 3.0V and the pixel can produce an output power up to 4.5mW (as measured for an 84µm diameter pixel at a drive current of 140mA) [2]. At a driving current of 6mA an 84µm diameter pixel of 450nm micro-LEDs emits around 400µW. The 520nm micro-LEDs with an 84µm diameter pixel have a typical turn-on voltage of 4.2V and an average output power of 260µW at 6mA. Fig. 3.4 shows the measured current versus voltage (I-V) characteristics and Fig. 3.5 shows the measured optical power versus injected current (L-I) curves for selected pixels from 450nm and 520nm devices operated with CMOS driver [3]. This CMOS/LED micro-light source is powered and controlled by a computer through a USB connection.

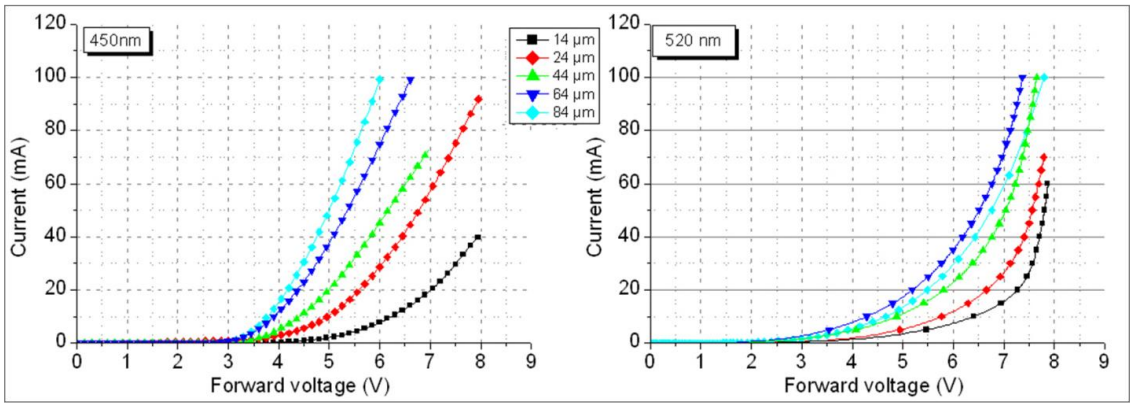

Fig. 3.4 Current versus voltage (I-V) curves for selected pixels of varying diameter in 8 x 8 micro-LED arrays with peak emission of 450nm and 520nm; from [3].

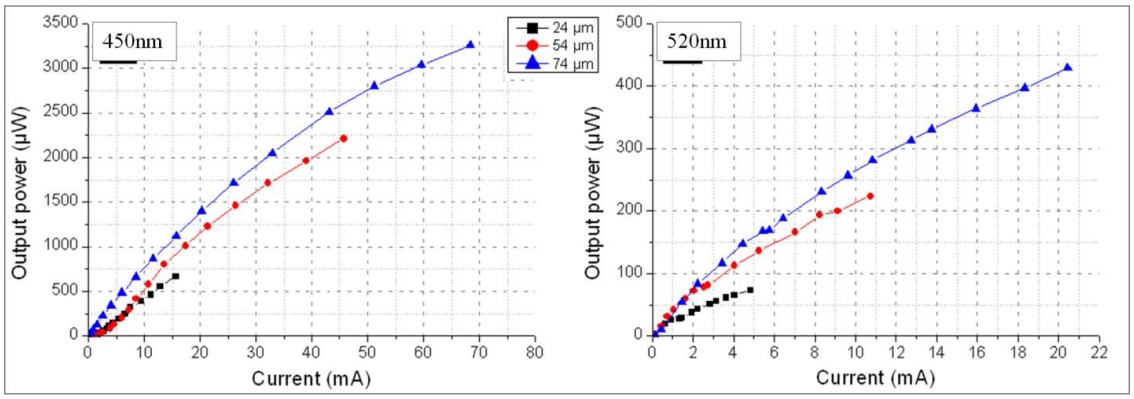

Fig. 3.5 Optical output power versus injected current (L-I) graphs of selected pixels from 8 x 8 arrays with peak emissions of 450nm and 520nm; from [3].

To construct a compact OET device, the CMOS/micro-LED unit was placed underneath the a-Si:H lower electrode allowing for microscope observation of the sample chamber from the top. In addition, a low-cost lens, 6mm in diameter and of NA 0.55 (Geltech™, ThorLabs) was fixed on the top of micro-LEDs to focus the light (1:1 image) onto the a-Si:H surface. We adopted this approach as the light emitted from micro-LEDs is too divergent to be coupled directly to the OET device and without using the lens, the light

power density in the pattern is too low to achieve optoelectronic tweezing. Fig. 3.6 a and Fig. 3.6 b show our miniaturised OET system and its schematic arrangement, respectively.

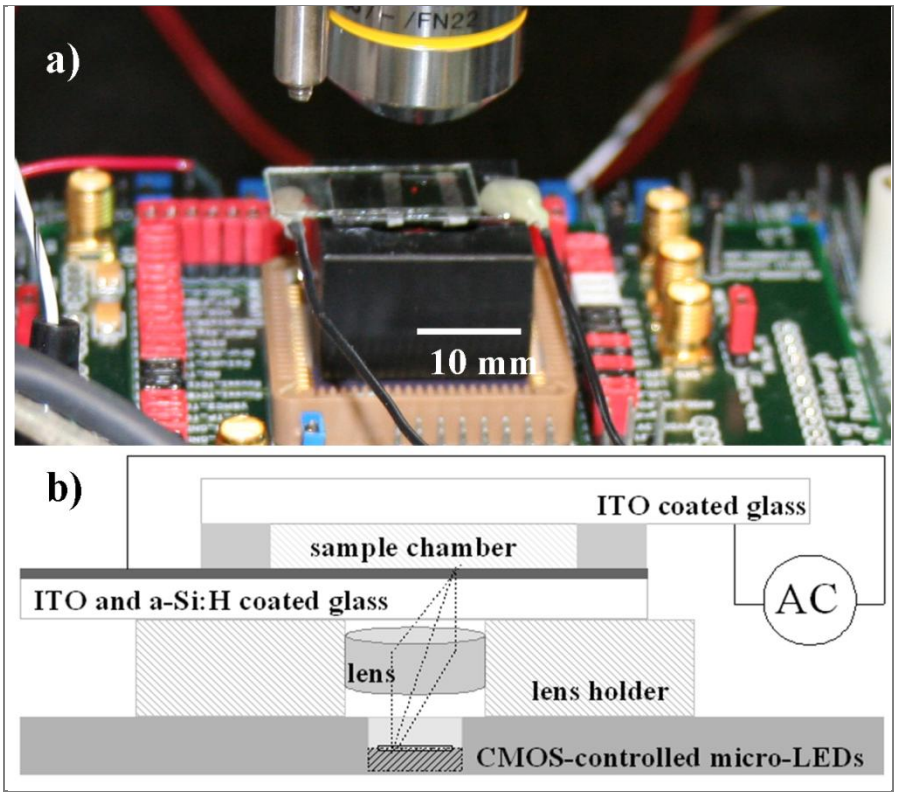

Fig. 3.6 Miniaturised OET: a) Oblique view photograph of the integrated miniaturised OET device under a microscope, and b) the corresponding cross-sectional schematic diagram.

In the visible spectrum, the a-Si:H absorption is lowest at red wavelengths (see Fig. 3.7) [4], and most probably for that reason, red light has been used to create the light pattern onto the photoconductive layer in previous OET studies [5, 6].

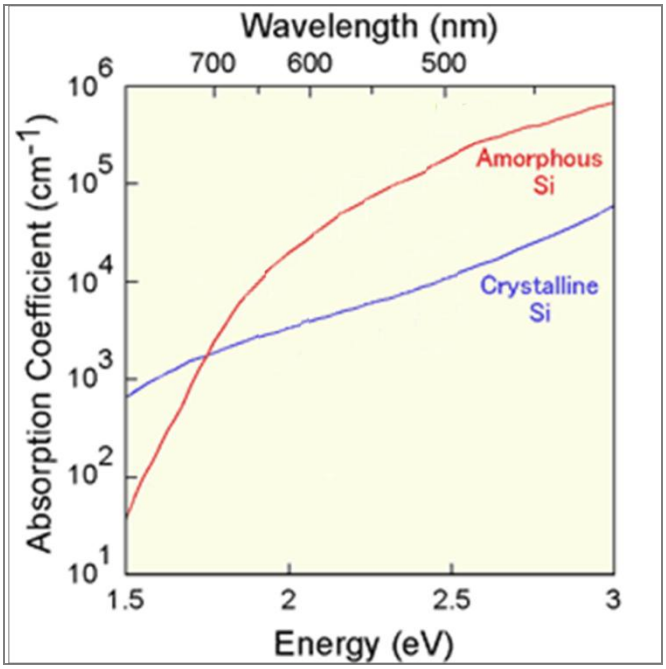

Fig. 3.7 Light absorption coefficient of a-Si:H versus wavelength (from [4]).

However, GaN based visible LEDs have their best performance at blue and green wavelengths. Furthermore, 1µm to 2µm thick a-Si:H layers have been previously used in OET devices, because sub-micron thick a-Si:H layers were not free from defects [5]. However, when integrating the micro-LEDs with an OET device with a 1µm thick layer of a-Si:H, we found that the light emitted from either blue or green LED micro-pixels was fully absorbed before it reached the top a-Si:H surface and thus no DEP effect on the particles was seen. Clearly, this is due to the light absorption of the thick a-Si:H at the blue and green wavelengths. At green wavelength, the light absorption coefficient of a-Si:H is ten times larger than in the red part of the spectrum (the absorption coefficient of a-Si:H, α, is 10^4 cm^{-1} at 625nm, and 10^5 cm^{-1} at 520nm – Fig. 3.7), and being even stronger at the 450nm blue wavelength ($5*10^5$ cm^{-1}) [4, 7].

We found, however, that by optimizing the Plasma Enhanced Chemical Vapour Deposition (PECVD) conditions (work performed in collaboration with University of Dundee), it was possible to produce a high quality thin (300nm) a-Si:H layer almost without defects. Our results demonstrate that by using such high quality thin a-Si:H layers, it is possible to achieve integrated OET with green (520nm) micro-LEDs as a light source. In addition and importantly, by using a thin a-Si:H layer, a small amount of LED light can pass through the a-Si:H layer, allowing the illuminated area to be imaged from above at the same time as the particle trapping.

The high quality a-Si:H was deposited using a modified DP800 PECVD capacitively coupled system (Oxford Plasma technology) with an electrode of 380mm diameter and 30mm spacing. During deposition, the patterned ITO glass substrates were held at the lower grounded plate which was heated to a temperature of 220^{o}C by an upper plate RF source driven at 13.56 MHz with an input power of 10 Watts. The silicon growth rate was 0.8As^{-1} from pure silane at a flow rate of 75 sccm and a chamber pressure of 100mTorr. This deposition was done at the University of Dundee.

For the OET experiments, the output voltage (LED bias) of the CMOS driver was fixed at 4.95V for all 520nm wavelength pixels in a row, giving currents of 0.6mA for the 14µm pixel to 6mA for the 84µm pixel (see Table 3.1). The output optical power density was measured for each pixel size, both at the device and as delivered to the photoconductive electrode. Because of size dependent effects [8], the output power density at each pixel was ~5W/cm^2 almost independent of the pixel size, of which 0.4-

$0.6W/cm^2$ (calibrated independently in each case) was delivered though the package and lens system to the photoconductive electrode (Table 3.1).

Pixel coordinates	Pixel diameter	Pixel current	Output power	Power density	Power density transmitted through the lens (~9%)
	µm	mA	µW	W/cm^2	W/cm^2
A3	84	6.0	255	4.5	0.4
B3	74	4.4	231	5.3	0.5
C5	64	3.3	144	4.5	0.4
D4	54	2.4	96	4.1	0.4
E5	44	1.7	73	4.7	0.4
F2	34	1.5	40	4.5	0.4
G3	24	1.0	26	5.8	0.5
H3	14	0.6	11	7.1	0.6

Table 3.1 Measured LED pixel (520nm) current, output power and power densities before and after the lens at a fixed forward bias of 4.95V.

3.3. Sample materials and preparation methods

For particle and cell manipulation experiments, we chose 10µm polystyrene beads (Thermo Fisher Scientific, UK) in low concentration KCl solution and Chinese Hamster Ovary cells (CHO-K1 cell line from ATCC) in an isotonic sugar solution (0.3% Dextrose, 8.5% Sucrose in DI water). All chemicals were supplied by Sigma Aldrich, UK, unless otherwise stated. CHO cells were cultured at 37°C and 5% CO_2 in Dulbecco's modified Eagle medium containing nutrient mixture F-12 (DMEM/F12, GIBCO) supplemented

with 10% FBS, 2mM L-glutamine and 100 U/ml of penicillin and streptomycin. Prior to the experiment, cells were put in suspension. To detach them from the flask surface, cells were treated with 0.25% trypsin solution. After 3 minutes treatment, DMEM/F12 medium was added to the solution to stop the trypsin acting. Next, cells were spun for 3 minutes at 1400 rpm, the medium was then aspirated and replaced by sugar solution. The washing procedure was repeated 3 times to remove ions which otherwise would increase the solution conductivity and interfere with trapping. Cell solution at a concentration of 2×10^6 cells ml^{-1} was stored in an Eppendorf tube at 4°C prior to the experiment so as to preserve the cells. In order to prevent cell adhesion to the substrate surfaces in the OET chamber, the OET chamber surface was cleaned thoroughly before adding the cells.

The viability of CHO cells was assessed before doing the OET trapping experiment by using trypan blue stain. A small amount of cells was taken from the main cell solution and stained with 0.01M trypan blue. It was confirmed that more than 75% of cells were viable at that stage. The viability of the cells in OET devices during and after trapping has been previously demonstrated by Valley et al. [9]. That work showed that under the light illumination and electric field strength used in the OET devices, cells remain viable.

3.4. Results

To achieve particle trapping, a range of parameters related to the OET device operation, such as AC drive frequency, voltage applied and solution conductivity have been studied. By using green micro-LED illumination, it was found that the best conditions for particle trapping are the following: AC frequency of 10 kHz and solution conductivity of $10mSm^{-1}$ for 10μm polystyrene beads and $1mSm^{-1}$ for CHO cells.

Fig. 3.8 and Fig. 3.9 show examples of polystyrene beads and CHO cells, respectively, trapped by pixels of a green micro-LED array.

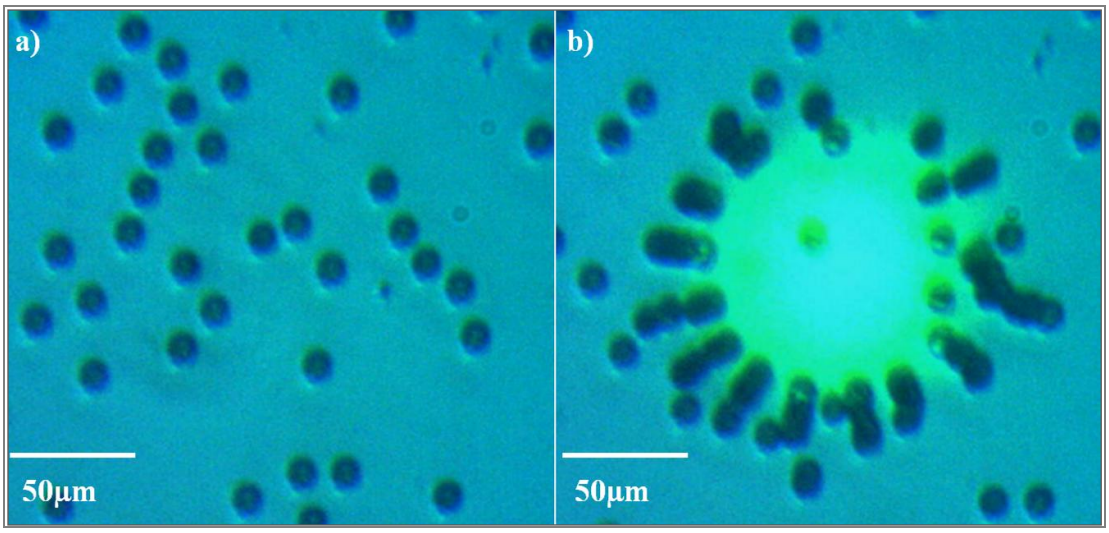

Fig. 3.8 Trapping beads with 74µm diameter pixel, at 20V peak to peak voltage; a) photograph taken with the LEDs turned-off; b) photograph captured 40 seconds after a pixel was turned on.

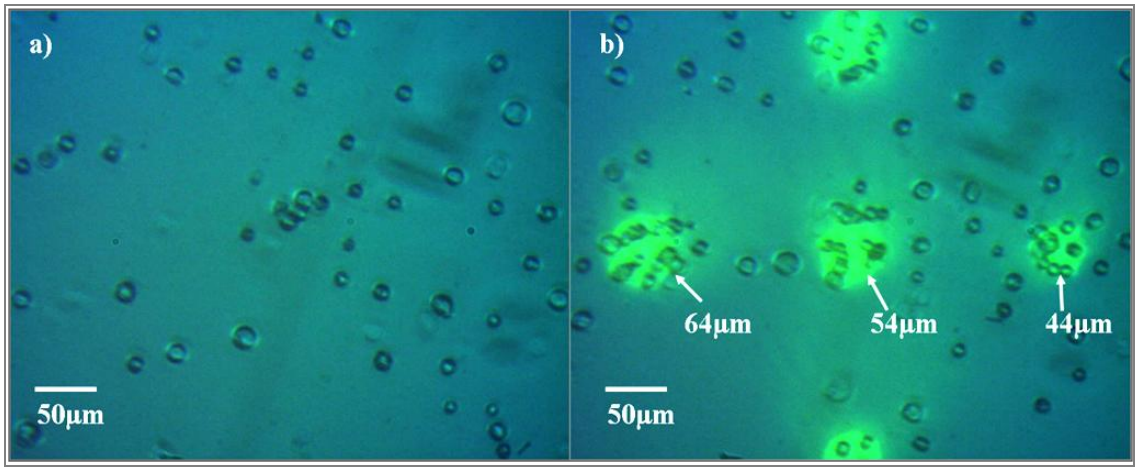

Fig. 3.9 Representative frames of a video showing trapping of CHO cells with 64µm, 54µm and 44µm diameter pixels at 5V peak to peak voltage; photograph a) was taken before any micro-LED pixel was turned-on; photograph b) was captured after 5 pixels had been turned on for 40 seconds. The video can be viewed via http://www.opticsinfobase.org/abstract.cfm?uri=oe-19-3-2720.

The above images clearly demonstrate that the miniaturised OET device with an integrated micro-LED light source is capable of manipulating particles/cells. The results also showed that by operating at a relatively low frequency (10 kHz) in a low conductivity liquid (1 or 10 mSm^{-1}), particles and cells could be attracted to the LED pixel from hundreds of microns away.

We have further investigated how the cell average velocity depends on the LED pixel diameter (via the electric field and field gradient) and AC voltage applied during the trapping. The time for cells to travel a trapping distance of 150μm was measured by using a particle tracker StAT software [10] and the cell average velocity was then calculated. Fig. 3.10 a shows the cell average velocity as a function of the diameter of the micro-LED pixel and how the cell average velocity changes with the AC voltage applied for 4 different pixel sizes is illustrated in Fig. 3.10 b. The reason for the large error bars in Fig. 3.10 is the variation of the cell size (volume) and shape.

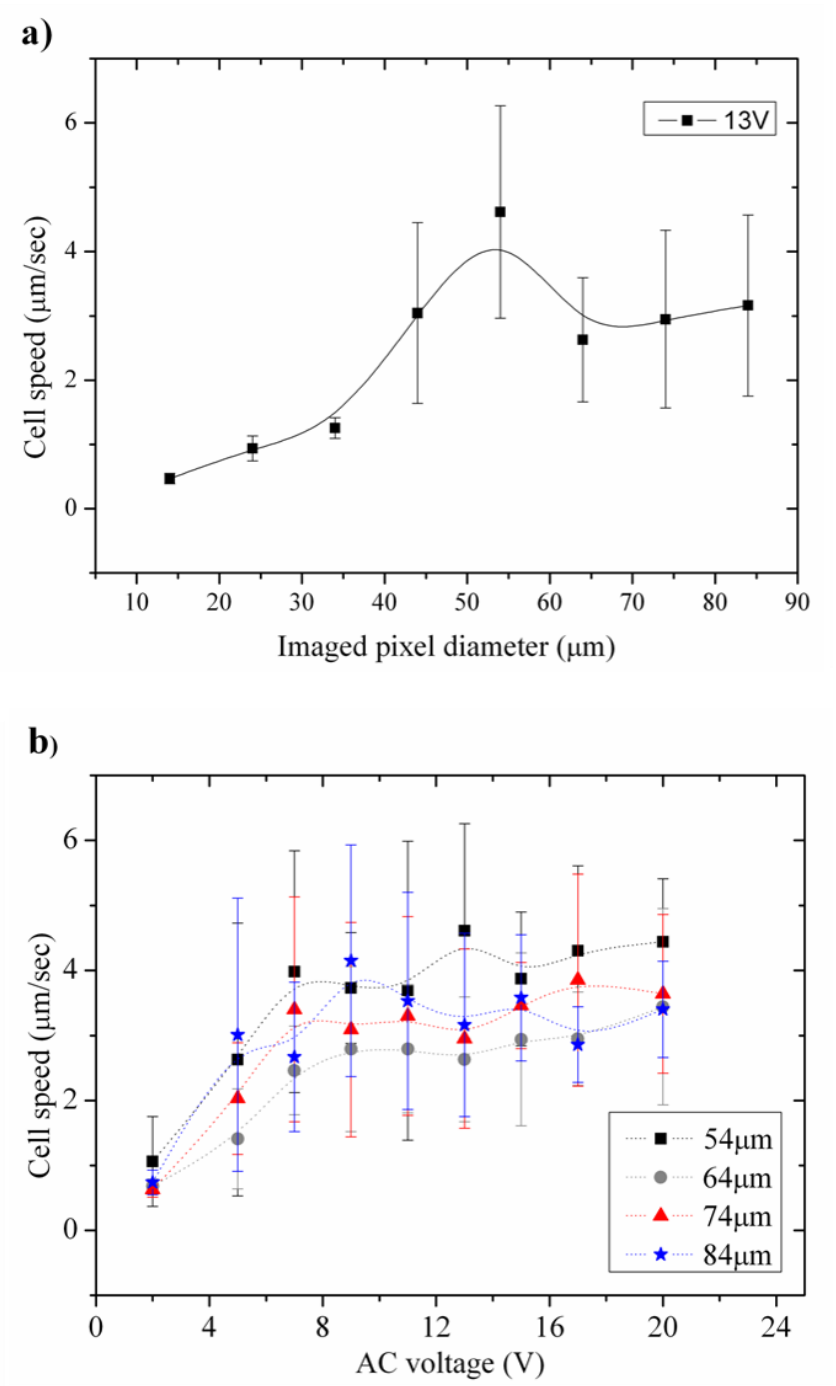

Fig. 3.10 a) A plot of average cell velocity as a function of imaged pixel diameter for one of the AC voltages (13V) applied between the ITO electrodes; b) A plot of average cell trapping as a function of AC voltage for 4 different pixel sizes. Error bars represent +2σ, -2σ.

Fig. 3.10 a shows that the cell average velocity increases monotonically with pixel diameter from 14μm to 54μm, reaching a maximum at 54μm pixel. For bigger LED pixels (>54μm), the velocity is slightly lower with a little increase when the pixel diameter increases from 64μm to 84μm. Fig. 3.10 b shows a roughly linear increase in cell average velocity with an applied voltage between 0 and 8V followed by a further small increase at higher voltages. When comparing the velocities induced by these four LED pixels for each voltage, the 54μm diameter pixel produces the highest cell average velocity. Our measurements have confirmed that all the LED pixels produce very similar optical power densities. Thus a detailed theoretical simulation was required to explain why the bigger LED pixels do not result in the higher cell average velocity. The simulation work and results will be described in section 3.5. Also, the results shown in Fig. 3.10 enable us to find the ideal conditions for cell trapping with the micro-LED system.

3.5. Simulations and discussion

In order to better understand the trapping mechanism and to explain the experimental results, Finite Element Method (FEM) simulations of various OET parameters were performed. The simulated parameters include conductivity profile of the a-Si:H layer, potential and electric field distributions, the gradient of the electric field squared and DEP and LACE forces applied to the particles. During the trapping, a particle's average velocity is determined by the force applied to it. Therefore, it should be possible to explain the measured cell velocity results by the force simulation.

As previously discussed, there are two mechanisms which induce the force placed onto the particles, namely dielectrophoresis (DEP) and Light Activated AC Electroosmosis (LACE).

The DEP force is given by Eq. (3.1);

$$F = 2\pi r^3 \varepsilon_m \mathrm{Re}[k(\omega)]\nabla E^2 \qquad (3.1)$$

where r is the radius of the particle, ε_m is the real permittivity of the medium, Re[k(ω)] is the real part of the Clausius-Mossotti factor and ∇E^2 is the gradient of the electric field squared [11].

The Clausius-Mossotti factor for cells can be given by Eq. (3.2);

$$k(\omega) = \frac{\varepsilon_{eff}^* - \varepsilon_m^*}{\varepsilon_{eff}^* + 2\varepsilon_m^*} \qquad (3.2)$$

The ε_m^* refers to the complex relative permittivity of the medium in which particles are suspended and is defined by Eq. 3.3. The ε_{eff}^* is the effective permittivity of the particles. For cells, the effective permittivity can be approximated by Eq. 3.4.

The relative permittivity of the medium, ε_m^*, can be expressed by the following equation:

$$\varepsilon_m^* = \varepsilon_m + \frac{\sigma}{i\omega} = \varepsilon_m - \frac{i\sigma}{\omega} \qquad (3.3)$$

ε_m is the real part of the permittivity of the medium, σ is its conductivity, ω is the angular frequency of the applied electric field and i is the square root of -1.

For conventional optical tweezers, the latex colloidal bead is a good model for biological cells because they both have higher refractive index than the medium. However, in OET,

the dielectric properties of the object are important, particularly the particle permittivity. The permittivity of cells and latex beads are substantially different. Therefore, they show different OET behaviours: for example, latex beads experience positive DEP and cells experience negative DEP at low frequencies.

A realistic model of a cell consists of a shell of low conductivity material (cell membrane) and higher conductivity medium inside (cytoplasm) [12]. The effective permittivity for a cell is a combination of respective permittivity of the cytoplasm and the permittivity of cell membrane and their radius (see Eq. 3.4) [12].

$$\varepsilon_{eff}^{*} = \varepsilon_2^{*} \frac{(\frac{r_2}{r_1})^3 + 2(\frac{\varepsilon_1^{*} - \varepsilon_2^{*}}{\varepsilon_1^{*} + 2\varepsilon_2^{*}})}{(\frac{r_2}{r_1})^3 - (\frac{\varepsilon_1^{*} - \varepsilon_2^{*}}{\varepsilon_1^{*} + 2\varepsilon_2^{*}})} \qquad (3.4)$$

Here ε_{eff}^{*} defines effective permittivity of the cell, ε_1^{*} and r_1 correspond to the permittivity and the radius of the cytoplasm and ε_2^{*} and r_2 correspond to the permittivity and the radius of the cell membrane. This formula was used to calculate the effective permittivity of cells and to determine the Clausius-Mossotti factor.

The dielectrophoretic force on a particle is determined by the real part of the Clausius-Mossotti factor, while the electro-rotational torque on the particle is determined by its imaginary part [13].

The Clausius-Mossotti factor takes the values between -0.5 and 1 and will change depending on the medium conductivity and frequency used. When this factor changes from positive to negative, DEP interaction changes from attractive to repulsive force (from towards to away from high field regions). Thus, it was important to optimise the

experimental conditions, such as medium conductivity and frequency to assure effective cell and particle manipulation.

To calculate the force due to LACE, the velocity of the ions (the slip velocity) in the liquid was calculated first from Eq. (3.5);

$$v_{slip} = -\frac{\varepsilon_m \zeta E}{\eta} \qquad (3.5)$$

Where ζ is the zeta potential (defined as the voltage drop across the Electrical Double Layer defined in Chapter 2), E is the electric field and η is the liquid viscosity [13].

Once the velocity of the ions is known, the LACE force on a particle could be calculated by considering the Stokes drag at this velocity, Eq. (3.6).

$$F = 6\pi\eta R v_{slip} \qquad (3.6)$$

Where *R* is the radius of spherical objects [13].

From these equations it can be seen that the DEP force is proportional to the gradient of the electric field squared and the LACE force is directly proportional to the electric field. Consequently, simulations of electric field and the gradient of electric field square were performed in order to compare the DEP and LACE forces.

To perform these simulations, the optical intensity profiles of the four large micro-LED pixels were measured at the a-Si:H and these profiles were found to fit well into a profile of two Gaussian distributions with a flat top between them (Fig. 3.11).

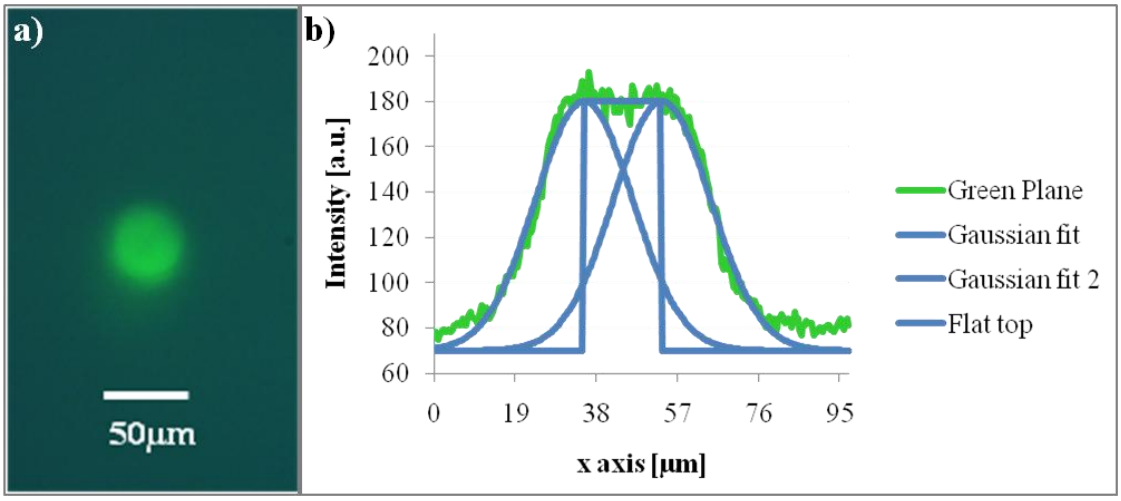

Fig. 3.11 Profiles of the 44µm micro-LEDs pixel on the a-Si:H surface: a) picture of the pixel as seen through the a-Si:H layer; b) illumination intensity profile on the a-Si:H surface with fitted two Gaussians and a flat top.

Based on previous studies [12], it is known that the conductivity of the a-Si:H increases almost linearly with the optical intensity under a range of illumination intensities (10^{-6} ~ 10^{-4} S/cm; Fig. 3.12) [14]. Consequently, the conductivity profiles similar to the intensity profiles were put into the simulations (shown in Fig. 3.13 a).

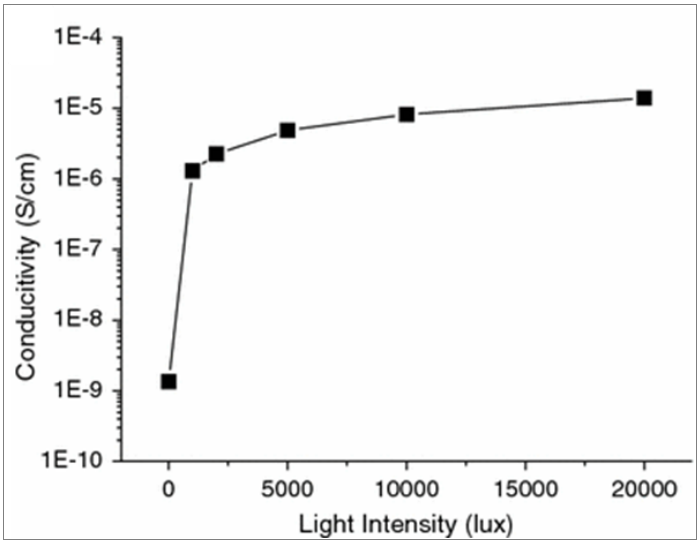

Fig. 3.12 Evolution of the conductivity profile of a-Si:H under illumination; from [14].

The magnitude of the conductivity of the a-Si:H layer was taken at $1x10^{-6}$ Sm^{-1} for the dark a-Si:H and $1x10^{-4}$ Sm^{-1} for the illuminated a-Si:H [15] with a light intensity of $0.5W/cm^2$ [13] ($0.5W/cm^2$ is the light intensity at the a-Si:H layer by micro-LED pixels in our OET device).

Fig. 3.13 b shows the simulation results of the potential drop in the liquid above the a-Si:H in the OET chamber (simulation software: COMSOL Multiphysics). The two-headed arrow dashed lines in Fig. 3.13 a-d indicate the light spot position and diameter of a turned-on LED pixel. The simulations used the quasi-static approximation, which in our case is valid as the device is much smaller than the wavelength of the AC field being applied [12]. The calculated electric field component in the x direction is shown in Fig. 3.13 c and the gradient of the electric field squared is shown in Fig. 3.13 d.

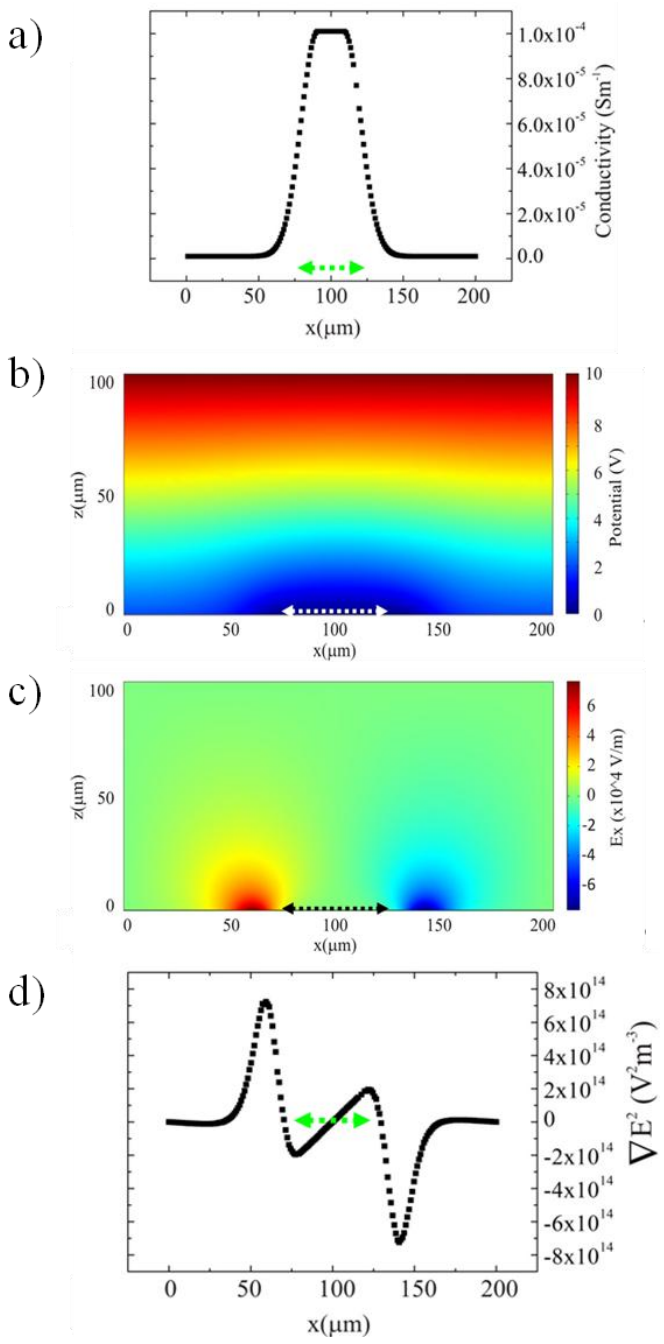

Fig. 3.13 Simulation results. The two-headed arrow dashed lines in all these figures indicate the light spot position and diameter of a turned-on LED pixel. a) conductivity profile of the a-Si:H layer; b) the potential distribution across the liquid above the a-Si:H layer (100μm is the real distance between the two electrodes); c) the electric field distribution (x-component); d) the gradient of the electric field squared in the liquid just above the a-Si:H layer.

From these simulations, the forces experienced by cells due to DEP and LACE can be calculated. To calculate forces we took a particular model of a cell [12]. In this model, cell cytoplasm had radius of 10µm and relative permittivity of 60. Its shell had 10nm thickness and a relative permittivity of 4.4.

Fig. 3.14 a shows the calculated DEP, LACE and total forces induced by a 74µm diameter LED pixel. The insert in this figure shows a magnified section from the left, indicating that the LACE force dominates at a large distance from the light spot and the DEP force dominates when the particle is closer to the light spot. Fig. 3.14 b shows the calculated total forces created by the four large LED pixels, i.e. 74 µm, 64 µm, 54 µm and 44 µm. It can be seen that the total force profiles induced by the three largest LED pixels, 74 µm, 64 µm and 54 µm, are very similar but the 44µm pixel generates a higher force. The optical intensity profiles of the all four LED pixels have varying widths, but the Gaussian decrease in intensity at the sides of the three largest were similar. Furthermore, the optical profile of 44µm diameter pixel was sharper, and fitted a thinner Gaussian, resulting in this larger force. As described before, experimentally it was observed that the three largest micro-LEDs, 84µm, 74µm and 64µm, did not attract cells faster than a 54µm or 44µm diameter pixels (results in Fig. 3.10 a). The small variation on measured cell average velocities attracted by different sizes pixels can be properly explained by our force simulations.

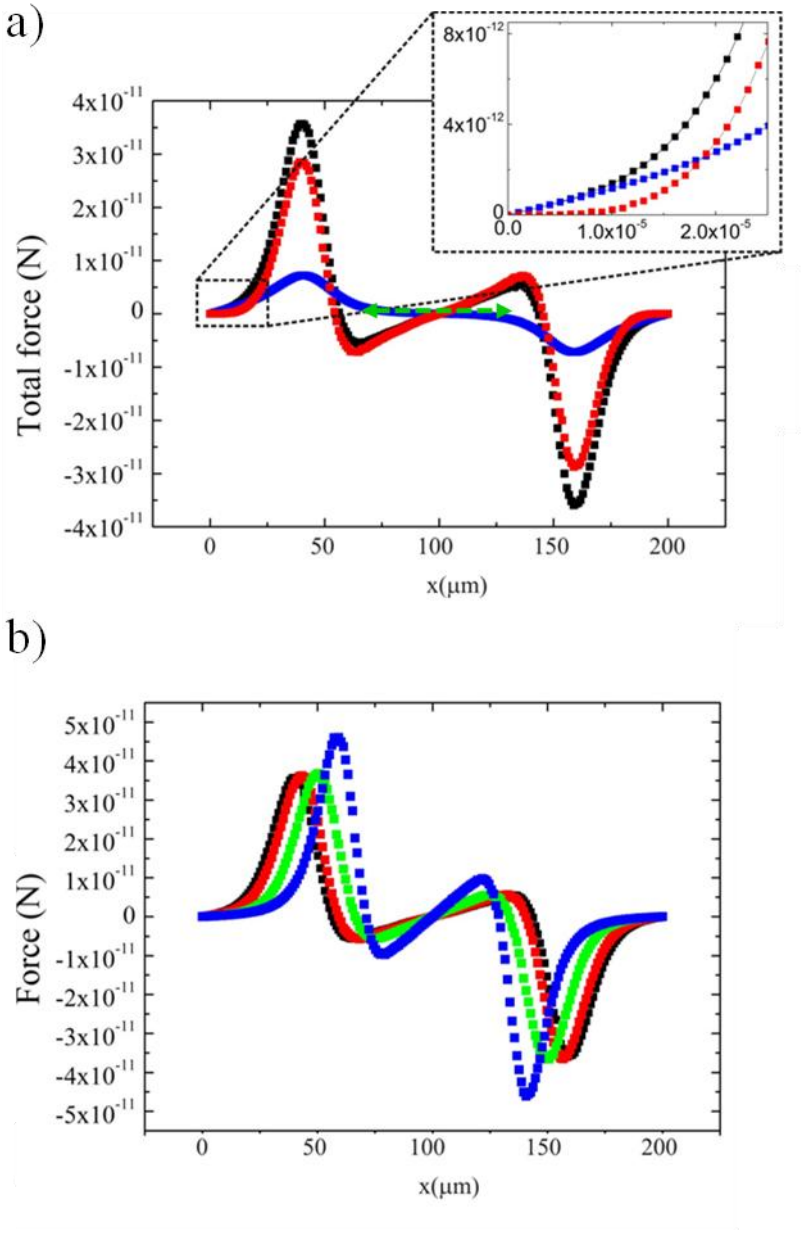

Fig. 3.14 Results of the force simulation: a) the DEP force (red), LACE force (blue) and the total force (black) created by an 74μm LED pixel; green arrow indicates pixel diameter; the insert shows a magnified section where the y axis is in Newtons and the x axis in metres; b) the total force profiles for four pixels, 74μm (black), 64μm (red), 54μm (green) and 44μm (blue). Note: In this simulation the centre of the pixel is not placed at x=0 which results in positive and negative forces for a symmetrical beam.

In our experiments the DEP force dominated particle attraction at a short distance to the pixel. The square of the electric field gradient, which governs the DEP force, was the strongest on the pixels which had the sharpest images on the a-Si:H. The pixels which had 54µm and 44µm diameters had sharper images on the a-Si:H surface than 64µm, 74µm and 84µm pixels, thus smaller pixels were generating slightly higher forces on the particles than bigger pixels despite emitting similar power densities.

For this first miniaturised OET device controlled by CMOS-driven GaN micro-LEDs, the possible maximum optical power output was limited by the imaging optics and the particular CMOS chip used. The CMOS could not provide voltages higher than 5V. The typical turn on voltage of 520nm micro-LEDs was 4.2V and consequently higher optical powers available from the bare micro-LEDs were not used. The next generation CMOS driver currently being tested allows for driving at higher voltages (up to 7V) and scaling the array to 16 x 16 individually driven LED pixels on a pitch of 100µm. Further work will then focus on employing these and even smaller pitch LEDs allowing easy particle/cell control between pixels, and time-resolved micro-fluorescence measurements *in situ* [16] for a multi-function OET system.

3.6. Chapter conclusions

In summary, by using a CMOS-controlled 520nm GaN micro-pixelated LED array as an integrated micro-light source, a miniaturised optoelectronic tweezers system was developed. With the high spatio-temporal and intensity control, the emission pattern generated from the micro-LED array is capable of creating reconfigurable virtual electrodes to achieve miniaturised OET. The average particle velocity, electric field and forces applied to the particles in this system were characterised and simulated. The measurements show that the average cell velocity increases with increasing micro-LED pixel diameters from 14μm to 54μm and then saturates afterward. The simulation indicates that LACE force dominates when the particles are far away from the LED pixel whereas DEP force is much stronger at a short distance. The simulation of the forces generated by using different LED pixels proved that LED pixel image sharpness on the photoconductive layer was the most important factor determining the strength of the forces acting on the cells. The capability of this miniaturised OET system for manipulating and trapping multiple particles including polystyrene beads and live cells was successfully demonstrated. This technique has significant potential to develop portable and low-cost instruments for high throughput manipulation and detection of biological particles. One possible application for mini-OET is to construct a portable diagnostic tool which will allow to separate cancer cells from healthy cells, healthy spermatozoids from unhealthy ones, parasites from human blood, or to distinguish different stages of development of stem cells thanks to the differences in their permittivity [17-20].

References

1. J. J. D. McKendry, B. R. Rae, Z. Gong, K. R. Muir, B. Guilhabert, D. Massoubre, E. Gu, D. Renshaw, M. D. Dawson, and R. K. Henderson, "Individually Addressable AlInGaN Micro-LED Arrays With CMOS Control and Subnanosecond Output Pulses," Ieee Photonics Technology Letters **21**, 811-813 (2009).
2. J. J. D. McKendry, R. P. Green, A. E. Kelly, Z. Gong, B. Guilhabert, D. Massoubre, E. D. Gu, and M. D. Dawson, "High-Speed Visible Light Communications Using Individual Pixels in a Micro Light-Emitting Diode Array," IEEE Photonics Technol. Lett. **22**, 1346-1348 (2010).
3. J. McKendry, "Micro-pixellated AlInGaN light-emitting diode arrays for optical communications and time-resolved fluorescence lifetime measurements," PhD Thesis in *Physics* (Strathclyde, Glasgow, 2011), p. 182.
4. T. Kamei, B. M. Paegel, J. R. Scherer, A. M. Skelley, R. A. Street, and R. A. Mathies, "Integrated hydrogenated amorphous Si photodiode detector for microfluidic bioanalytical devices," Anal. Chem. **75**, 5300-5305 (2003).
5. P. Y. Chiou, A. T. Ohta, and M. C. Wu, "Massively parallel manipulation of single cells and microparticles using optical images," Nature **436**, 370-372 (2005).
6. S. L. Neale, M. Mazilu, J. I. B. Wilson, K. Dholakia, and T. F. Krauss, "The resolution of optical traps created by light induced dielectrophoresis (LIDEP)," Opt. Express **15**, 12619-12626 (2007).

7. R. A. Street, *Technology and Applications of Amorphous Silicon* (Springer, New York, 2000).

8. Z. Gong, S. R. Jin, Y. J. Chen, J. McKendry, D. Massoubre, I. M. Watson, E. Gu, and M. D. Dawson, "Size-dependent light output, spectral shift, and self-heating of 400 nm InGaN light-emitting diodes," J. Appl. Phys. **107**, 013103 (2010).

9. J. K. Valley, S. Neale, H. Y. Hsu, A. T. Ohta, A. Jamshidi, and M. C. Wu, "Parallel single-cell light-induced electroporation and dielectrophoretic manipulation," Lab on a Chip **9**, 1714-1720 (2009).

10. G. Milne, "Labview pattern-matching particle tracker software - StAT," (2007).

11. R. Pethig, "Review Article-Dielectrophoresis: Status of the theory, technology, and applications," Biomicrofluidics **4**, 022811 (2010).

12. S. L. Neale, "Optically controlled microfluidics," PhD Thesis in *Physics and Astronomy* (University of St Andrews, St Andrews, 2007), p. 168.

13. J. K. Valley, A. Jamshidi, A. T. Ohta, H. Y. Hsu, and M. C. Wu, "Operational regimes and physics present in optoelectronic tweezers," J. Microelectromech. Syst. **17**, 342-350 (2008).

14. W. Choi, S. H. Kim, J. Jang, and J. K. Park, "Lab-on-a-display: a new microparticle manipulation platform using a liquid crystal display (LCD)," Microfluid. Nanofluid. **3**, 217-225 (2007).

15. P. Y. Chiou, A. T. Ohta, and M. C. Wu, "Toward all optical lab-on-a-chip system: optical manipulation of both microfluid and microscopic particles," in *Optical Trapping and Optical Micromanipulation*, K. Dholakia, and G. C. Spalding, eds. (Spie-Int Soc Optical Engineering, Bellingham, 2004), pp. 73-81.

16. B. R. Rae, K. R. Muir, Z. Gong, J. McKendry, J. M. Girkin, E. Gu, D. Renshaw, M. D. Dawson, and R. K. Henderson, "A CMOS Time-Resolved Fluorescence Lifetime Analysis Micro-System," Sensors **9**, 9255-9274 (2009).

17. F. Yang, X. M. Yang, H. Jiang, P. Wood, W. Hrushesky, and G. R. Wang, "Dielectrophoresis Separation of Colon Cancer Cell," in *Mnhmt 2009, Vol 1*(Amer Soc Mechanical Engineers, New York), pp. 351-356.

18. J. K. Valley, P. Swinton, W. J. Boscardin, T. F. Lue, P. F. Rinaudo, M. C. Wu, and M. M. Garcia, "Preimplantation Mouse Embryo Selection Guided by Light-Induced Dielectrophoresis," PLoS One **5**, e10160 (2010).

19. E. M. Nascimento, N. Nogueira, T. Silva, T. Braschler, N. Demierre, P. Renaud, and A. G. Oliva, "Dielectrophoretic sorting on a microfabricated flow cytometer: Label free separation of Babesia bovis infected erythrocytes," Bioelectrochemistry **73**, 123-128 (2008).

20. R. Pethig, A. Menachery, S. Pells, and P. De Sousa, "Dielectrophoresis: A Review of Applications for Stem Cell Research," J. Biomed. Biotechnol., 182581 (2010).

Chapter 4

4. Creation of reliable protein patterns by piezoelectric printing

4.1. Introduction

4.1.1. Hepatocyte micro-patterns

High throughput screening of lead components is important for the pharmaceutical industry, particularly at the stage of drug development. One of the steps in drug development is to test every new compound for its toxicity when it is metabolised by the liver. These tests need to be made on liver cells, e.g. primary hepatocytes, freshly extracted from animals. The standard, multi-well format procedure used to test drugs and cosmetics involves using relatively large quantities of cells (tens of thousands of cells) and chemical compounds. Each well has 50µl volume and the tests need to be made in multiple replicas, which requires using several millilitres of reagents. Apart from using substantial quantities of samples, it is difficult to remove and apply reagents uniformly in multi-well plates avoiding edge-effects. The demand to reduce the use of these cells, and thus reduce the use of animals, is very strong as it is fuelled both by ethical issues and the desire to cut costs. Moreover, hepatocytes isolated from animals and kept *in vitro* can lose their functionalities within a few hours, including enzymatic activity important for drug metabolism [1]. Thus, it is important to engineer a test environment which will use much less bio-materials and will support hepatocytes functions better than the standard multi-well plate. The above problems stimulate the

development of miniaturised platforms for drug testing which would (1) decrease the quantities of used samples, (2) assure a cell-friendly environment and (3) allow for efficient and fast tests.

In natural conditions, cells normally reside with other types of cells and with other components, such as proteins. In the liver tissue, hepatocytes are surrounded by different extracellular matrix (ECM) proteins and cells (e.g. fibroblasts). In a real hepatic micro-environment, dominant ECM proteins include type I, III and IV collagens, fibronectin and laminin [2]. One of the approaches to improve hepatocyte functionality *in vitro* is via creation of a micro-array of cells. In a previously published study cell micro-array formation was carried out by first patterning proteins in micro-format and then developing patterned hepatocyte and hepatocyte/fibroblast co-cultures on top of the protein patterned substrates [3]. These results suggested that patterning of proteins first could be a good way to create subsequent cell patterns and ensure a cell-friendly environment.

In our experiment, we chose an alternative method of patterning – piezoelectric printing. The advantages of this method as compared to other protein patterning methods were presented in Chapter 1. Collagen type I was chosen for patterning because it supported hepatocyte adhesion [4]. Poly-L-lysine (PLL) was chosen as a second protein, as it is known to promote attachment of many cell types, but is not as good in promoting hepatocyte adhesion as collagen [4]. Thus, PLL patterns could be used to promote the adhesion of hepatocyte supporting cells, the fibroblasts. The juxtaposition of ECM proteins and cells is important to further enhance the maintenance of hepatocyte

phenotypical functions. Another property of PLL was its smaller size when comparing with collagen which facilitate protein patterning by printing (collagen – 300 kDa, PLL - 150 kDa [5, 6]).

In addition to development of the cell patterning methods as described in Introduction Chapter, in recent years a lot of effort was dedicated to development of miniaturised bio-platforms, the so called "lab-on-a-chip" devices. The latter are micro-sized chambers and channels networks, often assembled on a glass substrate forming a micro-fluidics system. Apart from other advantages, such as easier reagent removal or possibility of high-throughput analysis, their main advantage is reduction in volumes of samples used. In the previous study, done by our collaborator research group, a microfluidic network, integrated on a glass substrate uniformly coated with collagen type I, has been compared with traditional 384 microtitre plate [7]. This study showed that the assay of intracellular Ca^{2+} flux in adherent cells inside microfluidic device gave comparable results to the results from a 384 microtitre plate.

In this work, encouraged by above results, an intermediate approach to create micro-arrays of hepatocytes has been adopted. First, flat micro-patterns of proteins suitable for integration with a microfluidic device have been made by piezoelectric printing; and second, cells have been seeded on these patterns. The integration of these micro-patterns with microfluidic networks has the potential to become miniaturised quantitative cell analysis platform for drug testing, responding to the needs of high-throughput drug screening.

4.1.2. Surface treatment

In *in vitro* conditions, most of the immortal cell lines will grow on any type of surface. Consequently, an effective non-adhesive background on the substrate is essential in order to control cell adhesion spatially in micro-array format [8]. Although thick films, such as acrylamide hydrogels [9], poly-ethylene oxide (PEO) [10] and poly-ethylene glycol (PEG) hydrogels [11], have been used to create non-adhesive backgrounds, their uneven, soft or non-uniform topographies make the leak-free assembly with microfluidic devices difficult. Other methods, reporting creation of cell patterns on a flat non-adhesive substrate that was suitable for microfluidics, consisted in using photolithography and were relatively complex. They involved selective removal of regions of PEG in order to immobilise proteins to exposed substrate or selective protection of protein modified substrate for PEG immobilisation [12-14].

In this work, special PEG treatment was used to create thin non-adhesive layer. Poly(ethylene glycol) (PEG) is well known for its ability to provide a local hydrophilic environment resulting in the reduction of cell adsorption. Different PEGs have been successfully used to create cell adhesion resistant surfaces: thiol-terminated PEG monolayers on gold surfaces [15, 16], thick PEG films formed either by plasma polymerisation on glass and polystyrene surfaces [17, 18] or by UV crosslinking on glass substrates [19]. However, it was found that PEG coupling to the silane-treated glass surfaces has the disadvantages of unreliability and poor reproducibility, while UV treatments required specialised instrumentation and rigorously controlled deposition

conditions [20]. We wanted to develop a relatively easy, accessible and reproducible method to passivate the surface.

We have chosen transparent glass as a substrate because of its minimum interference with conventional optical detection methods. We tested silanisation with Poly-ethylene glycol-chlorosilane (PEG-chlorosilane) which allows for direct one-step procedure to create a non-adhesive background on glass substrates for cell patterning [21]. Excellent performance of this approach in resisting cell absorption has been demonstrated in previous studies [13].

The key property of the PEG treated surfaces – inertness for cell adhesion thanks to resistance to protein adsorption – may influence the binding and stability of the printed proteins on the surface [22, 23]. To overcome this issue, we searched for alternative treatment methods which facilitate the binding of the collagen to the surface with covalent linkage. However, we found that covalent binding involved multistep treatments, caused cross-contamination and did not assure printed collagen attachment on the surface (data not shown). Consequently, we used a simple, one step PEG treatment, which will be described in detail below. Deposited proteins were simply left to dry and physically adsorb on a clean PEG surface. The attachment and stability of the printed collagen and Poly-L-lysine (PLL) patterns on PEG treated surfaces are investigated in detail in this work.

In this Chapter, firstly, the method to generate a self-assembled thin PEG layer on glass will be described. Secondly, a novel technique to generate collagen and poly-L-lysine

patterns by non-contact piezoelectric printing will be presented. Thirdly, characterisation of patterns and methods of controlling pattern formation will be shown. In particular, the influence of the concentration of the proteins in the dispensing liquid and printing conditions on pattern size will be investigated. Also the stability of printed proteins on the PEG treated surface, even after extensive washing and hydration will be presented. The results of the subsequent cell seeding work on these patterns are described in the Chapter 5.

4.2. Materials and methods

4.2.1. Surface treatments

Commercially available PEG-chlorosilane containing 9 to 12 ethylene glycol units (MW=600, Gelest, Inc. USA) was used in this work. Glass microscope slides (VWR international Ltd.) were washed successively with isopropanol, methanol, acetone, and water for 5 minutes, prior to being cleaned using Piranha solution for 10 min (7:1 of sulphuric acid to 30% hydrogen peroxide). Slides were finally washed in RO water and blown dry with nitrogen. The cleaned glass slides were activated in an oxygen plasma chamber at 200W for 5 minutes before immersion in a PEG-chlorosilane (2-trichlorosilane (MW=600, Gelest) solution in anhydrous toluene for 2 hours under nitrogen protection. The slides were then rinsed with toluene and dried with nitrogen. Then, the substrates were further dried at 100°C for 2 hours and stored in a dessicator. All the chemicals were bought from Sigma Aldrich, UK unless otherwise stated.

Modified surfaces have been characterised with contact angle measurements and X-ray photoelectron spectroscopy (XPS).

Contact angle measurement detects changes in surface energy and it is a fast way to check whether the surface reaction occurred. The contact angle is formed at the equilibrium state between a liquid, vapour interface and the solid surface and it is determined by interactions between surfaces. The theory predicting the shape of the droplet is determined by the Young-Laplace equation:

$$0 = \gamma_{SV} - \gamma_{SL} - \gamma_{lv} \cos \theta_0$$

Where γ_{SV}, is the surface energy at solid-vapour interface, γ_{SL} is the energy on solid-liquid interface, γ_{lv} is the energy on liquid-vapour interface (or surface tension) and θ_0 is the equilibrium contact angle (Fig. 4.1). Surface tension is caused by attraction forces between molecules, their tendency to be in the lower state of energy, to occupy the smallest volume and to have the locally lowest surface area possible.

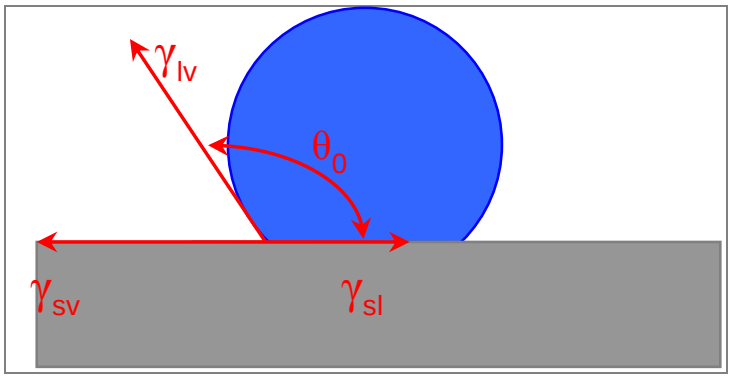

Fig. 4.1 Contact angle schematic: γ_{SV}, - surface energy at solid-vapour interface, γ_{SL} - energy on solid-liquid interface, γ_{lv} - energy on liquid-vapour interface (or surface tension) and θ_0 - the equilibrium contact angle.

Contact angles of the substrates after each modification step were measured using a 3 µL droplet of DI water precisely deposited with an Easy Drop device from KRUSS GmbH. The optical system in this device captured a picture of the profile of a liquid droplet on a solid substrate and DSA Software (also from KRUSS GmbH) was used to calculate contact angles by fitting the droplet contour with the Young–Laplace method (YLM).

XPS provides information on the chemical state of each element which can be correlated with the compound used in treatment. XPS was applied to measure the element composition on the surface to find out what molecules were present and consequently which surface treatment had been effective.

The samples' surfaces were analysed after each chemical treatment. The XPS analysis was carried out at the National Centre for Electron Spectroscopy and Surface Analysis (NCESS), Daresbury Laboratory, UK, using a Scienta ESCA 300 photoelectron spectrometer with analyzer pass energy set to 150eV and slit width of 0.8mm. A flood gun generating low-energy electrons (4eV) was used to eliminate substrate charging. A rotating anode X-ray source and quartz crystal monochromator provided Al Kα radiation (1486.6eV) and electrons were detected at a takeoff angle of 90° (normal to the substrate). To ensure a consistent energy scale for different samples, electron binding energies were corrected so that the Si(2p) peak in SiO_2 was at 103.4eV (this placed the alkyl C-H peak at 285.0eV).

4.2.2. Protein pattern generation by piezoelectric protein printing

Collagen solutions for printing were prepared by dissolving dried collagen fibre (type I from calf skin) in 0.1 M acetic acid. Solutions were subsequently adjusted to pH 7.4 with 0.1 M NaOH solution. The concentrations of collagen solutions used for printing were 0.25, 0.5 and 0.9 mg/ml. PLL used was bought in 0.01% (w/v) liquid solution. All chemicals were bought from Sigma Aldrich, UK unless otherwise stated.

A range of commercial piezoelectric printers are available to deposit droplets of either picolitre (pl) or nanolitre (nl) volumes of proteins. In our study, 330pl and 1nl droplets were printed with a PerkinElmer Piezoarray™ micro-spotter; 280pl droplets have been printed with a sciFLEXARRAYER S3 from Scienion AG, and smaller, 10pl droplets were printed with a Dimatix® Material Printer-DMP-2800.

During all printing, substrates were firmly fixed on the supporting surface via a vacuum mount or clamps to enable pattern registration. The printing voltage and frequency were tuned to minimise satellite droplet formation. After printing, all printed samples were stored at 4°C prior to cell studies.

To eliminate the use of additives that could compromise cell growth, proteins were printed in their physiological solution. Solution parameters, such as viscosity and surface tension, which determine the quality of the pattern, were optimised only by adjusting the concentration of the solution.

4.3. Results and discussion

4.3.1. Generation of reliable non-adhesive surface

In order to routinely monitor the effectiveness of the PEG functionalisation reaction, contact angles were measured. The contact angle of PEG-terminated samples was 39.3 ± 0.2 degrees in comparison to less than 5 degrees for the ultraclean glass prior to silanisation.

XPS analysis of the C (1s) spectrum of the PEG-chlorosilane-modified surface showed a small shoulder at 285.0eV (Fig. 4.2) corresponding to CH_3 groups and a dominant CH_2-O peak corresponding to the ethylene glycol units at 286.6eV. The magnitude of these signals indicated successful attachment of the PEG layer. Most notably, the PEG surface generated in such a way provided excellent repellent properties towards cell attachment. No cells attached to these surfaces for up to 5 days of incubation (more details will be presented in next Chapter).

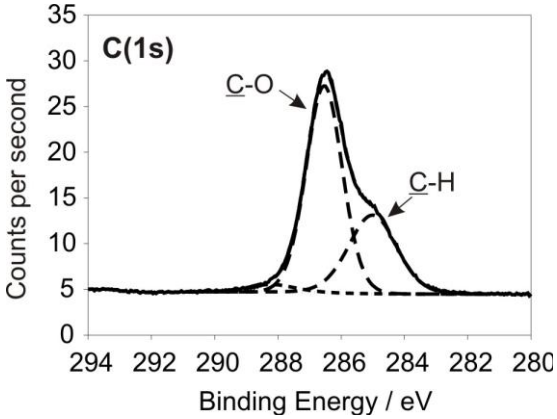

Fig. 4.2 XPS analysis of PEG modified glass: C (1s) spectrum for PEG-chlorosilane on glass. Deconvolution showed the saturated CH_3 peak at 285.0eV and the dominant C-O peak at 286.6eV due to the CH_2-O groups of ethylene glycol. No N (1s) signal was found for PEG-silane coated glass samples.

Moreover, a few routinely used treatments to create cell non-adhesive surfaces were also tested e.g. (3-Aminopropyl) triethoxysilane (APTES) and 3-glycidoxypropyltrimethoxysilane (3-GPS) (data not shown). Comparing with these treatments, we found that the one step PEG-chlorosilane treatment was the easiest treatment and gave non-adhesive background of the best quality for cell patterning, simultaneously allowing efficient protein immobilisation.

The disadvantage of using the PEG-chlorosilane solutions was that stringently anhydrous conditions may have to be used in order to prevent hydrolysis of the chlorosilane group and the formation of a rough multi-layer. Roughness of the surface could enhance cell adhesion as cells tend to occupy rough sites and deteriorate the quality of the assembly with a microfluidic network [24].

4.3.2. Protein printing

4.3.2.1.Collagen printing

Proteins were often not completely dissolved in the solutions and liked to form bundles which made them difficult to print with small printing nozzles. The best performance for collagen printing was achieved by dispensing 330pl droplets with the PerkinElmer® system which could be operated with a high concentration of collagen solutions: 0.25, 0.5 and 0.9 mg/ml. The printed pattern size was limited by both dispensing volume and protein sizes.

The collagen patterns printed with the PerkinElmer™ system are presented in Fig. 4.3. It can be seen that uniform, circular collagen microdots were printed with 0.9 mg/ml solution (Fig. 4.3 A&B). The pattern was imaged before any washing – crystals present on the surface were probably due to the presence of the sodium salt in the solution.

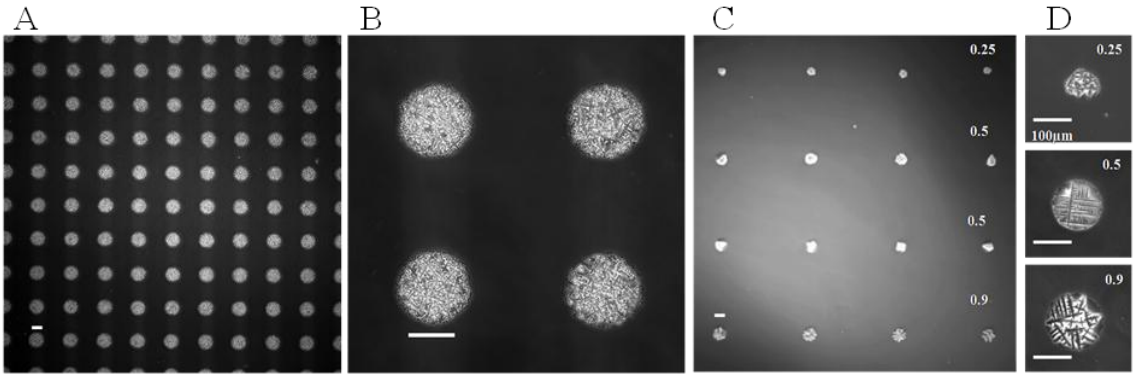

Fig. 4.3 A&B) Representative images of collagen micro-pattern made from 0.9 mg/ml solution shows very good uniformity. C&D) Collagen micropatterns generated from collagen concentrations of 0.25, 0.5 and 0.9 mg/ml respectively. A and C, shows an overview of images at 4X magnification; B&D) shows a portion of A or C at higher magnification (20x). All the scale bars are 100µm.

When comparing the printed arrays for different collagen concentrations, we could see that for the same dispensing volume, 330pl, with increasing concentration of collagen the dot size increased from 95µm to 170µm (Fig. 4.3 C&D and table 1). Moreover, the dots printed with highest concentration showed the smallest deviations in diameter and position. Individual dots printed with 0.9 mg/ml solution had a size of 171.5 ± 4.9 µm (Fig. 4.3 A&B).

Concentration (mg/ml)	Diameter (μm)*	Contact angle
0.25	97.7 ±7.5	$39.0^{o}\pm0.5^{o}$
0.5	154.6±5.6	$36.4^{o}\pm1.5^{o}$
0.9	171.5±4.9	$35.8^{o}\pm0.7^{o}$

*: Average value from 24 dots. Errors – standard deviation.

Table 1: Diameters of dried-out collagen spots from different printing solutions together with contact angle measurements of droplets on PEG surfaces.

To investigate why the microdot dimensions decreased with decreasing concentration, we measured the changes of the contact angle for different concentrations. On the PEG treated glass surface, contact angles for collagen solutions of 0.25, 0.5 and 0.9 mg/ml were 39.0 ± 0.5, 36.4 ± 1.5 and 35.8 ± 0.7 degrees, respectively. Higher contact angle for less concentrated droplets could be related to the higher water content in the solution. Any material adsorbed on solid surface could disturb the equilibrium between liquid and solid phases. Here, wet hydrophilic collagen bundles decreased slightly the contact angle between the PEG and water droplet. The more adsorbed materials were in the solution, the lower the contact angle was. However, this phenomenon did not explain the big difference in dot diameter for different collagen concentrations.

The differences in the dried dot diameter for different concentrations could be related to different wet and dry PEG surface properties and the droplet evaporation processes as described by Willmer et al. and presented in Fig. 4.4 [25].

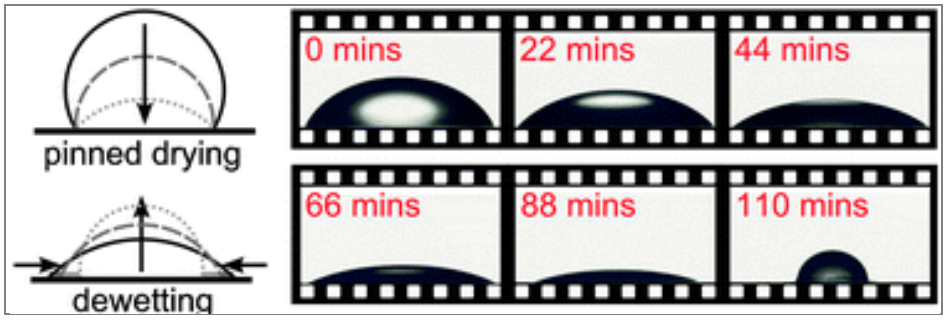

Fig. 4.4 Drying process of the printed dot; from [25].

As presented in Fig. 4.4, when a droplet was deposited on the surface, the evaporation of the water initially caused a decrease of the droplet's height ("pinned drying"), as the surface tension made the water evaporation more difficult at the borders of the droplet where the droplet contacts the surface. During this process, the volume of the droplet decreased and the concentration of the suspension increased. Next, the droplet decreased in diameter ("dewetting"). During this process, the suspended wet particles in the droplet were repelled by the substrate surface. The particles in suspension were then getting closer and closer to each other. The particles stopped moving when their concentration reached saturation. The higher concentrated the solution was, the bigger the dried collagen dot formed and the less deviation of the dot sizes was observed in the printed pattern. This explained why the printed collagen dot size increased with the solution concentration. When water evaporated completely, the surface dried and the collagen dots adsorbed on PEG.

4.3.2.2.Poly-L-lysine printing

PLL solution at a concentration of 0.01% (w/v) was used for printing. Using a Scienion printer at a droplet volume of 280pl, PLL micro-patterns of a dot size less than 50µm diameter were formed, as shown on Fig. 4.5.

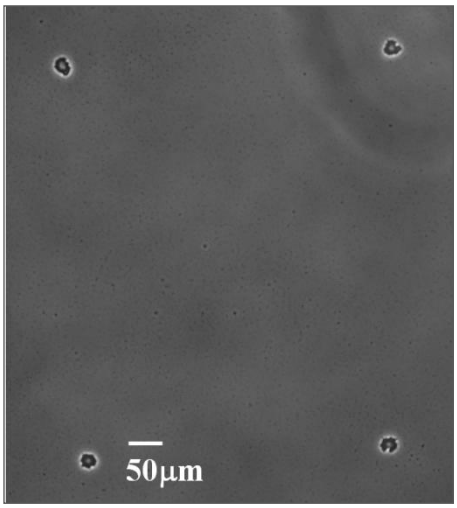

Fig. 4.5 PLL pattern printed with the Scienion printer; 280pl dispensing volume allowed creating patterns with a dot size less than 50µm diameter.

Using the Dimatix® printer at a droplet volume of 10pl, PLL patterns with a dot size of 10µm diameter were generated with one layer of printing (Fig. 4.6 A). Larger dot sizes were easily achieved by successive printing of several layers i.e. printed PLL on top of the dots which had already been printed. For example, 25µm dots were formed by printing 10pl PLL droplets twice (Fig. 4.6 B). Three layers printing generated 35µm dots (Fig. 4.6 C).

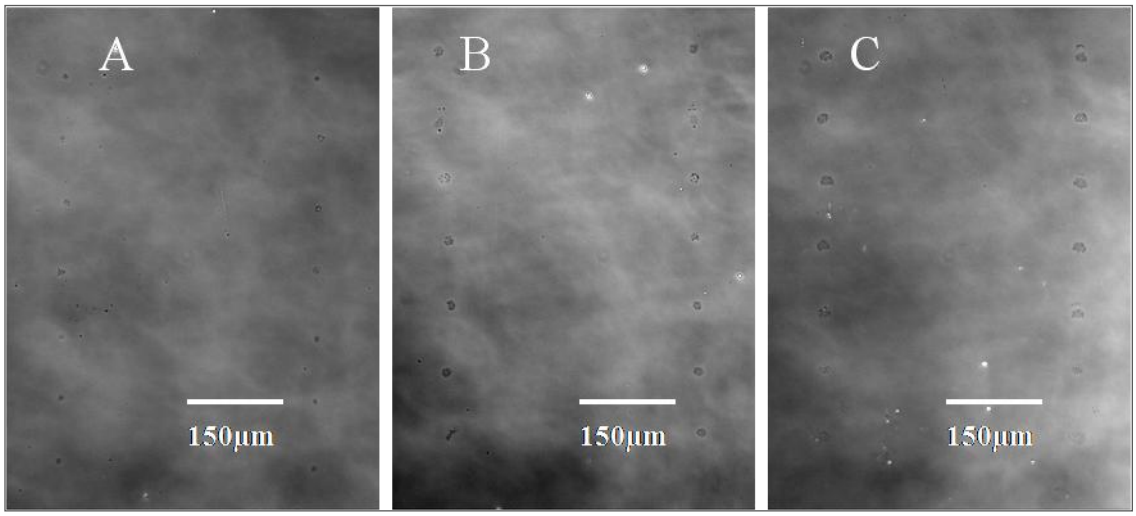

Fig. 4.6 PLL pattern printed with a Dimatix printer; 10pl dispensing volume. A) One layer printing generating a ~10µm dot pattern; B) Two layers printing generating a ~25µm dot pattern; C) Three layers printing generating a ~35µm dot pattern.

The ability to achieve pattern sizes in the range of a few tens of microns simply by varying dispensing volume, concentration and the number of the printing layers demonstrated the potential of piezoelectric printing for generation of versatile and high resolution bio-patterns.

4.3.3. Stability of protein patterns on PEG-surfaces

To immobilise proteins on the PEG surface after printing, the printed pattern was only left to dry and adsorb on the PEG surface at room temperature for 24 hours in sterile conditions. It was tested and confirmed that such printed collagen and PLL spots on a PEG surface remained adsorbed after at least 3 stringent washes with PBS (pH 7.4) Fig. 4.7 shows the bright field and fluorescence images of a printed collagen dot before and after washing (excitation with 488nm laser; emission detected with a 530 ± 20 nm long pass filter). The collagen is composed of molecules such as thyrosine and phenylalanine,

which naturally absorb in the ultraviolet and blue spectral region and emit at higher wavelengths [26, 27]. Thus, using the natural property of these molecules to emit fluorescence, the collagen dot on the surface could be seen. The average auto-fluorescence signal of collagen dot intensity was at least 10% above the background. An image of a washed PLL dot, due to the very weak fluorescence emission, can also be seen as shown in Fig. 4.8

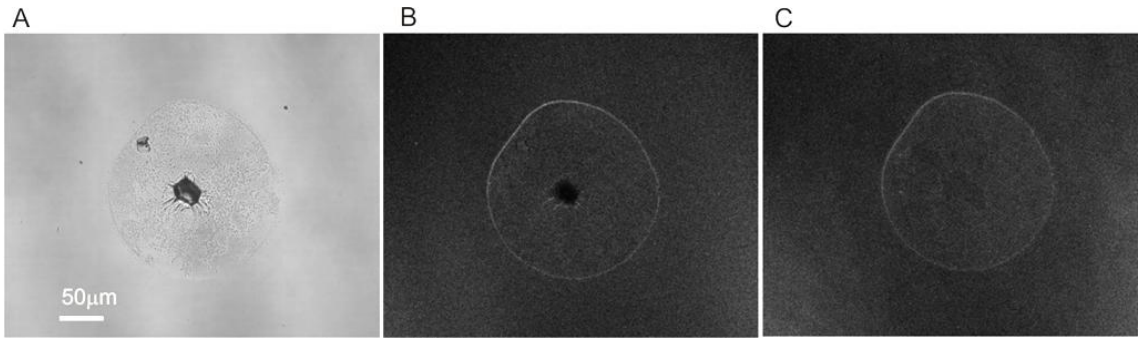

Fig. 4.7 Optical images of a collagen pattern before and after washing: A) bright field image before washing, B) fluorescence image before washing and C) fluorescence images after washing 3 times with PBS. The fluorescence signal is due to collagen auto-fluorescence. The persistence of fluorescence intensity in C (numerical integration shows it to be ~10% above the background glass) indicates that collagen remains on the surface after washing.

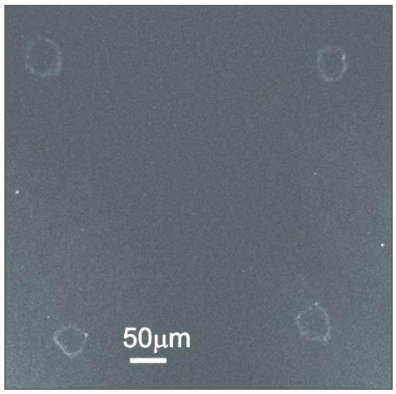

Fig. 4.8 Images of a PLL pattern after PBS washing, showing that PLL dots remain on the PEG treated surface. The rings on the border of the pattern were due to the "coffee stain" effect [28] – accumulation of the particles on the border of drying droplet.

The attachment of collagen on the substrates after washing was further confirmed by XPS measurements (Fig. 4.9). The N (1s) signal for collagen on a PEG-silane-coated glass substrate was clearly observed above the background (Fig. 4.9) (N.B. no N (1s) peak was observed above the noise level from PEG-silane coated glass). Deconvolution of the C (1s) XPS spectrum for collagen on PEG-silane coated glass (Fig. 4.9 B) showed that both the saturated C-H peak at 285.0eV and C=O peak at 288eV were proportionally larger than that found in the spectrum of PEG-silane-coated glass only (Fig. 4.2). These spectra indicated the presence of collagen on a PEG-silane-coated glass. Moreover, the spectrum of Fig. 4.9 B also shows a peak at 286.6eV, in contrast to the spectrum of Fig. 4.2. With the presence of the N(1s) signal, this peak may correspond to both C-O and C-N groups (as found in the ethylene glycol units of PEG and amino or hydroxyl centres in collagen).

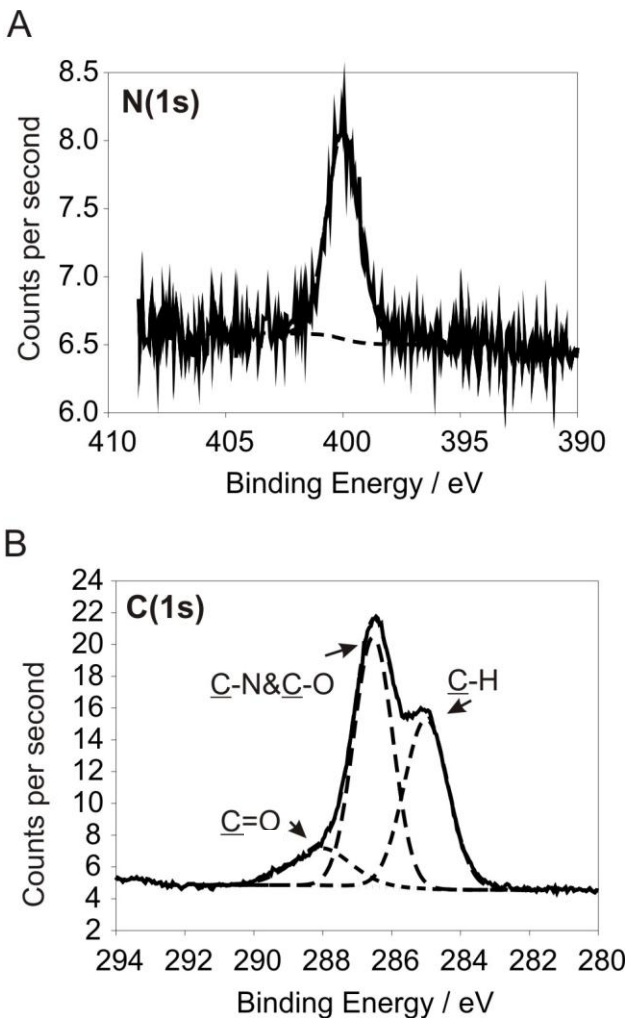

Fig. 4.9 XPS spectrum of collagen on PEG-silane coated glass after washing. (A) N (1s) spectrum. (B) C (1s) spectrum.

We found that the critical step to ensure collagen immobilisation was to dry the PEG surface fully prior and after printing so as to prevent hydration of PEG layers [2, 18]. For that reason, our samples were stored in a dessicator at 4ºC prior to cell seeding. Samples stored in this way were used for cell seeding even several months after printing, indicating a high stability of the patterns produced.

4.4. Chapter conclusions

By using non-contact piezoelectric printing systems, we have developed a simple and robust method to prepare highly uniform protein micro-dot arrays with dot sizes ranging from tens to hundreds of microns. The method used a PEG surface as a background motif, which adsorbed printed protein solution at dried states and was highly protein-resistant in a wet environment. Using this printing technique, patterns of ECM proteins, including collagen and PLL, have been created as an adhesive template for selective cell attachment. The subsequent cell patterning work will be described in Chapter 5. Our works demonstrate that the printing approach is a robust, one-step method to create protein patterns over large surfaces, allowing for high-throughput production of patterned biological materials without the use of masks or stamps and time-consuming procedures. This method is also more adaptable for general use in bio-laboratories.

References

1. M. N. Berry, H. J. Halls, and M. B. Grivell, "Techniques for Pharmacological and Toxicological Studies with Isolated Hepatocyte Suspensions," Life Sci. **51**, 1-16 (1992).
2. G. G. M. Pinkse, M. P. Voorhoeve, M. Noteborn, O. T. Terpstra, J. A. Bruijn, and E. de Heer, "Hepatocyte survival depends on beta 1-integrin-mediated attachment of hepatocytes to hepatic extracellular matrix," Liver Int. **24**, 218-226 (2004).
3. S. N. Bhatia, U. J. Balis, M. L. Yarmush, and M. Toner, "Effect of cell-cell interactions in preservation of cellular phenotype: cocultivation of hepatocytes and nonparenchymal cells," Faseb J. **13**, 1883-1900 (1999).
4. T. Hoshiba, H. Nagahara, C. S. Cho, Y. Tagawa, and T. Akaike, "Primary hepatocyte survival on non-integrin-recognizable matrices without the activation of Akt signaling," Biomaterials **28**, 1093-1104 (2007).
5. "Worthington Biochemical Product Catalog", http://www.worthington-biochem.com/CL/cat.html; .
6. "Sigma Aldrich Catalogue," http://www.sigmaaldrich.com/catalog/ProductDetail.do?D7=0&N5=SEARCH_CONCAT_PNO|BRAND_KEY&N4=P8920|SIGMA&N25=0&QS=ON&F=SPEC.

7. H. B. Yin, N. Pattrick, X. L. Zhang, N. Klauke, H. C. Cordingley, S. J. Haswell, and J. M. Cooper, "Quantitative comparison between microfluidic and microtiter plate formats for cell-based assays," Anal. Chem. **80**, 179-185 (2008).

8. J. W. Lussi, D. Falconnet, J. A. Hubbell, M. Textor, and G. Csucs, "Pattern stability under cell culture conditions - A comparative study of patterning methods based on PLL-g-PEG background passivation," Biomaterials **27**, 2534-2541 (2006).

9. C. J. Flaim, S. Chien, and S. N. Bhatia, "An extracellular matrix microarray for probing cellular differentiation," Nat. Methods **2**, 119-125 (2005).

10. E. Tenstad, A. Tourovskaia, A. Folch, O. Myklebost, and E. Rian, "Extensive adipogenic and osteogenic differentiation of patterned human mesenchymal stem cells in a microfluidic device," Lab Chip **10**, 1401-1409 (2010).

11. A. L. Hook, H. Thissen, and N. H. Voelcker, "Advanced Substrate Fabrication for Cell Microarrays," Biomacromolecules **10**, 573-579 (2009).

12. E. E. Hui, and S. N. Bhatia, "Microscale control of cell contact and spacing via three-component surface patterning," Langmuir **23**, 4103-4107 (2007).

13. D. Irimia, and J. O. M. Karlsson, "Development of a cell patterning technique using poly(ethylene glycol) disilane," Biomed. Microdevices **5**, 185-194 (2003).

14. A. Revzin, P. Rajagopalan, A. W. Tilles, F. O. Berthiaume, M. L. Yarmush, and M. Toner, "Designing a hepatocellular microenvironment with protein microarraying and poly(ethylene glycol) photolithography," Langmuir **20**, 2999-3005 (2004).

15. V. Sivagnanam, B. Song, C. Vandevyver, J. C. G. Bunzli, and M. A. M. Gijs, "Selective Breast Cancer Cell Capture, Culture, and Immunocytochemical Analysis Using Self-Assembled Magnetic Bead Patterns in a Microfluidic Chip," Langmuir **26**, 6091-6096 (2010).

16. M. Hashimoto, H. Kaji, M. E. Kemppinen, and M. Nishizawa, "Localized immobilization of proteins onto microstructures within a preassembled microfluidic device," Sens. Actuator B-Chem. **128**, 545-551 (2008).

17. S. W. Rhee, A. M. Taylor, C. H. Tu, D. H. Cribbs, C. W. Cotman, and N. L. Jeon, "Patterned cell culture inside microfluidic devices," Lab Chip **5**, 102-107 (2005).

18. E. Leclerc, K. El Kirat, and L. Griscom, "In situ micropatterning technique by cell crushing for co-cultures inside microfluidic biochips," Biomed. Microdevices **10**, 169-177 (2008).

19. E. W. Barrett, M. V. B. Phelps, R. J. Silva, R. P. Gaumond, and H. R. Allcock, "Patterning poly(organophosphazenes) for selective cell adhesion applications," Biomacromolecules **6**, 1689-1697 (2005).

20. S. Takayama, J. C. McDonald, E. Ostuni, M. N. Liang, P. J. A. Kenis, R. F. Ismagilov, and G. M. Whitesides, "Patterning cells and their environments using multiple laminar fluid flows in capillary networks," Proc. Natl. Acad. Sci. U. S. A. **96**, 5545-5548 (1999).

21. S. S. Shah, M. C. Howland, L. J. Chen, J. Silangcruz, S. V. Verkhoturov, E. A. Schweikert, A. N. Parikh, and A. Revzin, "Micropatterning of Proteins and

Mammalian Cells on Indium Tin Oxide," ACS Appl. Mater. Interfaces **1**, 2592-2601 (2009).

22. A. Tourovskaia, X. Figueroa-Masot, and A. Folch, "Long-term microfluidic cultures of myotube microarrays for high-throughput focal stimulation," Nat. Protoc. **1**, 1092-1104 (2006).

23. S. W. Lee, and P. E. Laibinis, "Protein-resistant coatings for glass and metal oxide surfaces derived from oligo(ethylene glycol)-terminated alkyltrichlorosilanes," Biomaterials **19**, 1669-1675 (1998).

24. B. Groessnerschreiber, and R. S. Tuan, "Enhanced Extracellular-Matrix Production and Mineralization by Osteoblasts Cultured on Titanium Surfaces Invitro," J. Cell Sci. **101**, 209-& (1992).

25. D. Willmer, K. A. Baldwin, C. Kwartnik, and D. J. Fairhurst, "Growth of solid conical structures during multistage drying of sessile poly(ethylene oxide) droplets," Phys. Chem. Chem. Phys. **12**, 3998-4004 (2010).

26. R. RichardsKortum, and E. SevickMuraca, "Quantitative optical spectroscopy for tissue diagnosis," Annu. Rev. Phys. Chem. **47**, 555-606 (1996).

27. L. Marcu, D. Cohen, J. M. I. Maarek, and W. S. Grundfest, "Characterization of type I, II, III, IV, and V collagens by time-resolved laser-induced fluorescence spectroscopy," in *Optical Biopsy Iii*, R. R. Alfano, ed. (Spie-Int Soc Optical Engineering, Bellingham, 2000), pp. 93-101.

28. R. D. Deegan, O. Bakajin, T. F. Dupont, G. Huber, S. R. Nagel, and T. A. Witten, "Capillary flow as the cause of ring stains from dried liquid drops," Nature **389**, 827-829 (1997).

Chapter 5

5. Cell micro-patterns

5.1. Introduction

As described in the previous Chapter, we were interested in creation of micro-arrays of primary hepatocytes. In this Chapter, the cell pattern creation on the collagen protein micro-arrays described in the previous Chapter will be presented. Reproducibility of the cell array as well as cell viability will be studied. To reduce the usage of primary cells, which are difficult to obtain and expensive as well as fragile to manipulate, the protein arrays were initially seeded with NIH-3T3 fibroblasts or Chinese Hamster Ovary (CHO) cells to optimise the conditions of cell pattern formation and cell maintenance. Following the description of the NIH-3T3 fibroblast cell pattern, the creation of primary rat hepatocyte micro-arrays will be presented. Then, enzymatic activity of patterned hepatocytes will be assessed by a liver-specific assay, 7-ethoxyresorufin-O-deethylase (EROD) assay, measuring cytochrome P450 activity.

The cytochrome P450 super-family, officially abbreviated as CYP, is a large group of enzymes which catalyse the oxidation of organic substances, such as lipids, steroidal hormones, drugs and toxic substances. They take part in metabolism and bio-activation of drugs. Consequently, it is important to test this enzyme activity in drug development [1].

One of the methods to test CYP activity is the 7-ethoxyresorufin-O-deethylase (EROD) assay. The EROD assay allows for measuring the de-ethylation of 7-ethoxyresorufin (non-fluorescent) to its highly fluorescent product resorufin by cytochrome P450 enzymes. When a compound is taken up by a cell, the CYP P450 enzymes, produced inside the cell, metabolise it. Thus, the increase in fluorescence mirrors the metabolic activity of a cell [2]. When a toxic compound is metabolised by a cell, it changes the cell's normal metabolic function. These changes can be observed as decrease or increase in resorufin fluorescence intensity. Because the metabolism is generally highest in hepatic tissue, primary liver cells, hepatocytes, are the target cells for investigating the activity of the cytochrome P450 1A1/2. Also, it was shown already that CYP activity of single hepatocytes could be detected *in situ* and quantified by the resorufin fluorescence intensity [3]. The EROD assay on patterned hepatocytes will be presented in this Chapter.

Furthermore, the coexistence of fibroblast and hepatocyte micro-arrays could improve hepatocyte activity further [4, 5]. To achieve this aim, a collagen pattern and PLL were combined first, and then hepatocytes and fibroblasts were incubated respectively in the following experiment. The different affinities of hepatocytes and NIH-3T3 cells for collagen and Poly-L-Lysine (PLL) patterns were used to develop a simple technique for creating a co-culture of these two types of cells.

Finally, we were interested in developing cell micro-array technology compatible with the microfluidic network. Combining a microfluidic device with the cell pattern allows the creation of a miniaturised, high throughput portable tool for toxicity testing. The

integration of the cell pattern inside a microfluidic device will be presented in the last section of this Chapter.

5.2. Materials and methods

5.2.1. Cell cultures

NIH-3T3 fibroblasts (ATCC) and CHO cells (ATCC) were cultured at 37°C and 5% CO_2 in Dulbecco's modified Eagle medium containing nutrient mixture F-12 (DMEM/F12, GIBCO, UK) supplemented with 10% foetal bovine serum (FBS), 2 mM L-glutamine and 100 U/ml of penicillin and streptomycin. All chemicals were supplied by Sigma Aldrich, UK unless otherwise stated.

Fresh primary rat hepatocytes (LGC Standards, UK) were prepared according to suppliers instructions and cultured in Leibovitz-(L-15) medium (GIBCO) supplemented with 1 µM dexamethasone, 25 mM Hepes (4-(2-hydroxyethyl)-1-piperazineethanesulfonic acid), 0.1 µM insulin, 8mM d-glucose, and 0.1mM gentamicin at 37°C in a normal air atmosphere.

5.2.2. Cell pattern formation conditions

The protein patterned substrates described in Chapter 4 and the control slides (non-treated or treated only with PEG glass slides) were cut into 1.5 cm x 2.5 cm samples. These samples were washed twice with PBS buffer (pH 7.4) and sterilised using UV illumination for 15 minutes within a biological laminar hood immediately prior to cell culture. The substrates were then placed in a 6-well plate and seeded with a cell suspension at a density of 2.5×10^5 cells/cm^2 (unless otherwise indicated). Hepatocytes and NIH-3T3 fibroblast cells were seeded onto the collagen patterns in the same way.

After incubation for 2 hours in the culture conditions suitable for each cell type, cells adhered on the protein patterns. To remove unattached cells, the remaining suspensions were sucked up with a pipette and the substrate surface was washed twice with new cell culture medium. To keep the cells in continuous culture, additional culture medium was supplied for up to 5 days.

5.2.3. Cell viability evaluation

Cell viability was assessed using a fluorescent live/dead cell assay as follows: live cells were labelled using the non-fluorescent compound calcein-AM. Calcein-AM crosses the membrane of viable cells where it is hydrolyzed by esterase enzymes into the strongly fluorescent anion calcein (which is retained in the cytoplasm). Dead cells were stained using the DNA intercalating compound ethidium homodimer-1 (EtD-1). EtD-1 fluoresces red only when it binds to the DNA. This positively charged compound does not cross the cell membrane of living cells and only labels the nucleus of dead cells.

Prior to adding the assay solution, the culture medium was aspirated and fresh pre-warmed stain solution was added. The cells were incubated with 5µM calcein-AM and 10µM EtD-1 solution in PBS at 37°C and 5% CO_2 for 45 minutes in dark conditions, and after the incubation the fluorescence images were collected using a Zeiss 510 confocal microscope. 488 nm Argon laser excitation and a long pass filter 510±20 nm were used for calcein detection and 543 nm HeNe laser excitation and a long pass filter 585±20 nm were used for EtD-1 detection.

5.2.4. Optical imaging and statistic analysis

Bright field, differential interference contrast and fluorescence images of cellular patterns were obtained using an inverted Zeiss Axiovert 200 microscope. Images were

taken at magnifications of 4, 10 and 20 times to provide both a large overview and high resolution images of the patterns. At least three different patterned substrates were examined for each set of the patterning/assay conditions, and several randomly chosen areas on each substrate were imaged. In order to test the reproducibility of individual cell micropatterns, tiles of high magnification images over an area of 5 mm x 5 mm were taken using a Zeiss 510 confocal microscope.

5.2.5. EROD assay

The 7-ethoxyresorufin-O-deethylase assay was used to measure the activity of the enzyme cytochrome P450 in the primary hepatocytes cultured for 24 hours on the patterned protein substrates. Cell culture medium was removed from the cells and replaced with fresh medium containing 20μM 7-ethoxyresorufin and 40μM dicumarol (Invitrogen). The fluorescence intensity was recorded every minute for 30 minutes using a confocal microscope with HeNe laser excitation at 543 nm. The emission was observed at 590 nm using a long pass filter (585±20 nm). The fluorescence intensity (arbitrary units) within defined regions of cells in the field of view was analysed using Image J^{Tm} software.

5.2.6. Assembly with microfluidic device

A special glass substrate of 29.8mm length, 22.3mm width and 3mm thickness (from Dolomite®, UK) was cleaned and treated as described in Chapter 4 with PEG silane. Afterwards, the collagen was printed with the S3 printer from Scienion with 280pl dispensing volume at the concentration of 0.9 mg/ml and the glass was left in sterile conditions as described previously. Next, the pattern was rinsed once in PBS and assembled with sterilized Dolomite microfluidic network.

5.3. Results

5.3.1. Generation of fibroblast cell arrays

2 hours after seeding NIH-3T3 fibroblasts on the collagen micro-patterned substrates, fibroblasts adhered exclusively to the protein pattern. The initial number of cells attached per dot in the pattern increased with an increase of the collagen concentration in printed solutions (Fig. 5.1 A). At a seeding density of 5 x 10^4 cells/cm^2, on average 5, 9 and 15 cells per dot were observed for the collagen dots generated with 330pl of solutions of concentrations of 0.25, 0.5 and 0.9 mg/ml, respectively. After 19 hour culture, near confluent layers were formed on each of the dots but not on the areas between the dots, proving that the collagen patterns promoted cell proliferation (Fig. Fig. 5.1 B). The cell patterns were maintained for 5 days before the overgrown fibroblasts started to bridge between dots. These results also indicated that the PEG surface has a good stability in resistance to cell adhesion (Fig. 5.1 B).

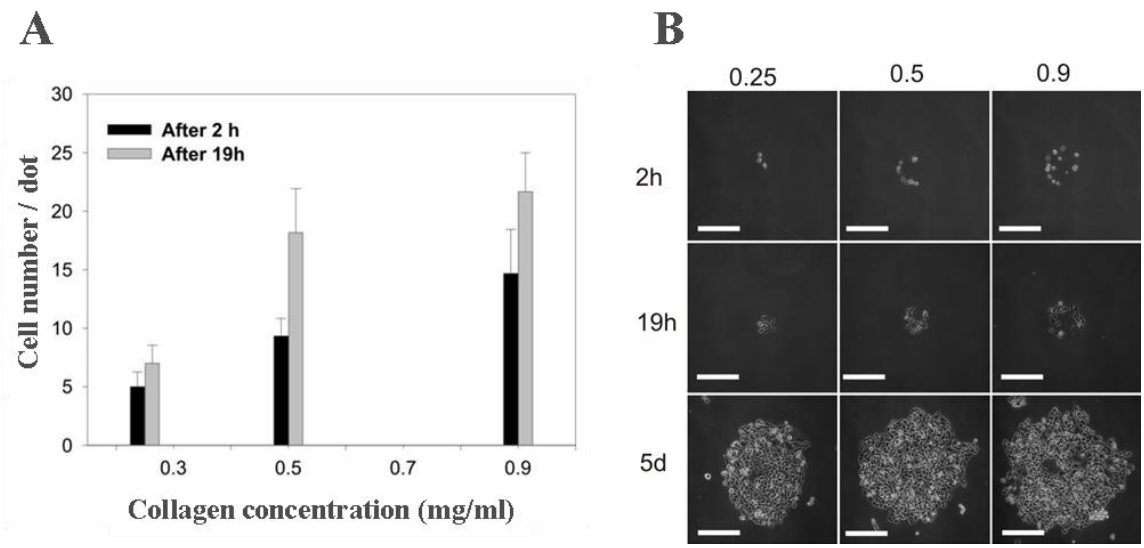

Fig. 5.1 Fibroblast array formation; A) Average number of cells attached per collagen dot for patterns generated from 0.25, 0.5 and 0.9 mg/ml collagen solutions (cell seeding density, $5x10^4$ cells/cm^2). Error bars represent standard deviations from 24 randomly chosen dots at each concentration. B) Phase contrast images of NIH-3T3 fibroblast cells attached and proliferated on collagen patterns printed from collagen solutions with different concentrations (as listed on the top row in mg/ml). Images collected 2 hours, 19 hours and 5 days after seeding (cell seeding density, $5x10^4$ cells/cm^2). All scale bars represent 150µm.

With a higher seeding density of 2.5 x 10^5 cells/cm^2, more cells were attached to each collagen dot. Taking the collagen pattern prepared with 0.9 mg/ml collagen solution as an example, 2 hours after seeding, an average of 30 cells adhered per dot (Fig. 5.2 (I)). 24 hours after seeding, a confluent layer of cells was formed (Fig. 5.2 (II)). Moreover, the cells near the edge of the dot aligned with the edge line, demonstrating that they exhibited a cellular response to their microenvironments (Fig. 5.2 (II)). When stained for live/dead assay, green fluorescence was observed from all of the cells on the dots which demonstrate high viability of cells on the printed arrays (Fig. 5.2 (III)).

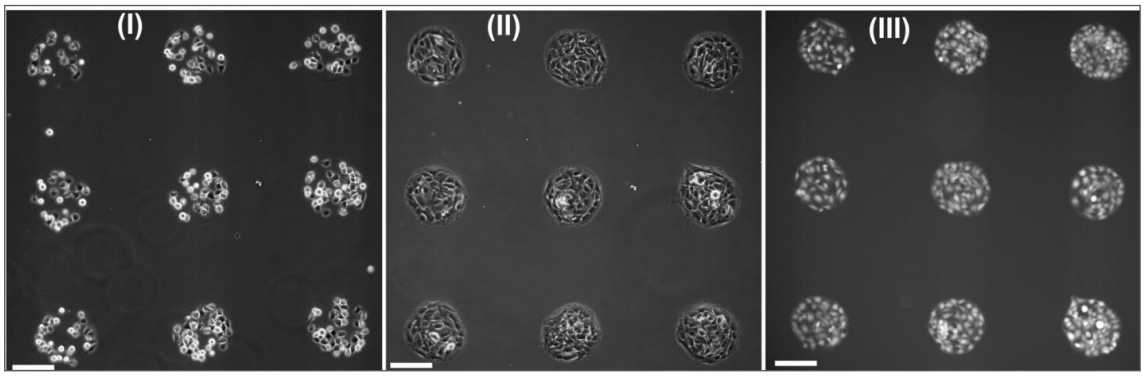

Fig. 5.2 Fibroblast array formation on a collagen pattern printed from 0.9 mg/ml collagen solution at a cell seeding density of 2.5 x 10^5 cells/cm^2. Phase contrast images of cells on the pattern after (I) 2 hours after seeding; (II) 24 hours after seeding, and (III) the fluorescence image of cells from (II) after the calcein-AM assay. Cells emit strong fluorescence showing a high viability of the cells on the array. All of the scale bars are 150µm.

PLL dots of less than 50µm diameter were also tested with cell seeding of density 2.5 x 10^5 cells/cm^2. Initially, 2 hours after seeding, 5 to 7 NIH-3T3 fibroblasts were found to adhere on each PLL dot (Fig. 5.3 (I)). Confocal microscopy measurements showed that the NIH-3T3 fibroblasts proliferated into three dimensional structures after 24 hour culture with a height of 50µm (Fig. 5.3 (II)). The NIH-3T3 fibroblast aggregate exhibited high viability as confirmed by the green fluorescence from calcein-AM staining and the absence of the red fluorescence from Etd-1 staining (Fig. 5.3 (III)).

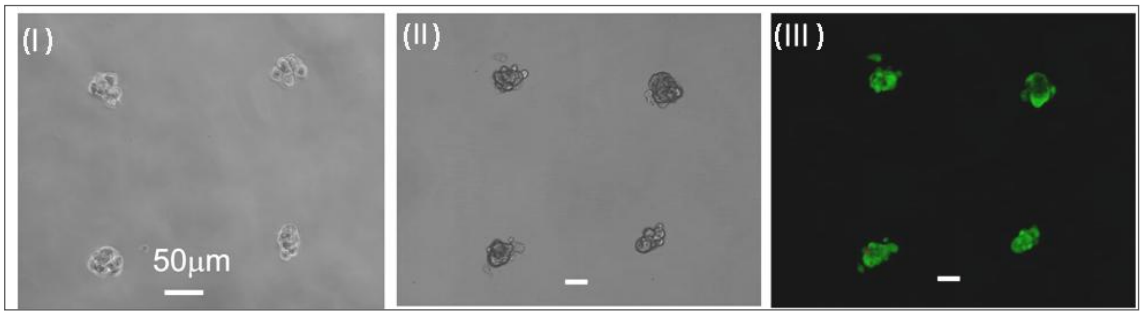

Fig. 5.3 Cell array formation on PLL patterns. NIH-3T3 fibroblasts attached and proliferated on a PLL pattern with a dot size of 50µm. (I) bright field image of fibroblasts 2 hours after seeding - fibroblasts occupy the whole area of the dots; (II) and (III) bright field and fluorescence images of a fibroblast aggregate after 24 hour culture. The fluorescence image is a combined live (green) and dead (red) assay, taken using the z-stack mode of a Zeiss 510 confocal microscope. The slice in the middle of the fibroblast aggregate is shown. The lack of red fluorescence shows the high cell viability. The scale bars represent 50µm.

The PLL dots in patterns created by the Dimatix® printer with 1, 2 and 3 layer printing had size of 10µm, 25µm and 35µm, respectively, as shown in Chapter 4 (Fig. 4.6). When looking at the cell adhesion on 1 layer printing, 2 hours after seeding only single cells adhered per dot, and not on all the PLL dots (Fig. 5.4 A). On double layer printing one or two cells adhered per each PLL dot under the same conditions (Fig. 5.4 B). On triple layer printing on most of the PLL dots two or three fibroblast cells attached 2 hours after seeding (Fig. 5.4 C). After 24 hour culture, on the small 10µm dots, only a few cells proliferated which proves again the non-adhesive property of PEG surface (Fig. 5.4 E). The proliferation of fibroblasts was restrained because the surface on which they adhered was very small. Nevertheless, the green fluorescence from these cells stained with calcein-AM showed that these cells were alive after 24 hour culture (Fig.

5.4 F). The cells stayed confined on the pattern for around 4 days. After 4 days, cells gradually lost their viability, detached from the surface and subsequently died.

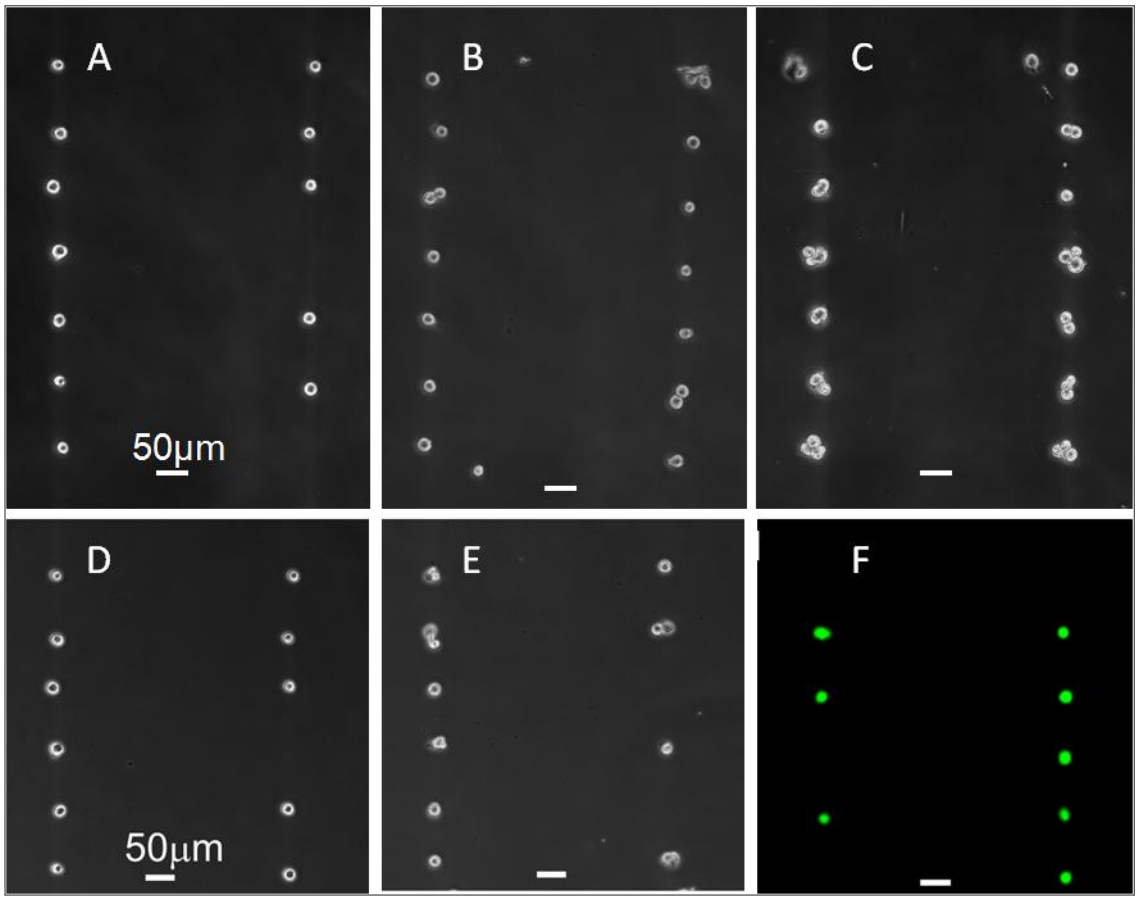

Fig. 5.4 Bright field images of fibroblast arrays formed on PLL printed with Dimatix printer: A) fibroblasts on 10µm dots generated with 1 layer printing, 2 hours after seeding; B) fibroblasts on dots generated with 2 layer printing, 2 hours after seeding; C) fibroblasts on dots generated with 3 layer printing, 2 hours after seeding; D) fibroblasts on 10 µm dots 2 hours after seeding; E) the same pattern as in D after 24 hour culture; F) fluorescence image of the cells stained with calcein-AM from E after 24 hour culture. All scale bars represent 50µm.

The above tests of NIH-3T3 cell adhesion on created patterns showed good stability of the cell arrays. On one hand, collagen patterning allowed for creation of reliable cell

patterns stable in culture for several days. Printed collagen dots had diameter of ~ 100 μm, which were perhaps the smallest collagen dots realised so far by printing [6, 7]. These collagen dots provided enough area for a small group of cells to adhere, spread and proliferate. On the other hand, patterning of the smaller molecule, PLL allowed for creation of smaller cell arrays – a single cell adhered per dot. However, the limited adhesive area prevented cells proliferating, leading to early loss of cell viability. Moreover, for both proteins and patterns generated by all printers, the number of cells adhered per dot depended on the protein concentration and the number of consecutive printings.

5.3.2. Large scale formation of functional primary hepatocytes arrays

Our results show that the collagen arrays printed by a PerkinElmer Piezoarray™ spotter with 0.9 mg/ml protein solution are the best substrates for long term NIH-3T3 fibroblast cell patterning. Thus, these collagen patterns were used for investigations of forming primary rat hepatocyte arrays.

At a seeding density of 2.5 x 10^5 cells/cm^2, 2 hours after seeding uniform primary hepatocyte arrays were formed over an area of 1.5 cm x 2.5 cm, mirroring the underlying collagen patterns (Fig. 5.5 A). A high magnification image of a portion of the array is shown in the insert of Fig. 5.5 A. It can be seen that cells adhered only over the collagen patterns, showing the functionality of the collagen arrays. After a 24 hour culture, hepatocytes developed into a number of distinct features generally observed

only in viable primary hepatocytes [8, 9], including a polygonal morphology, distinct nuclei and nucleoli, anisokaryosis and a large number of binucleate cells (Fig. 5.5 B-I).

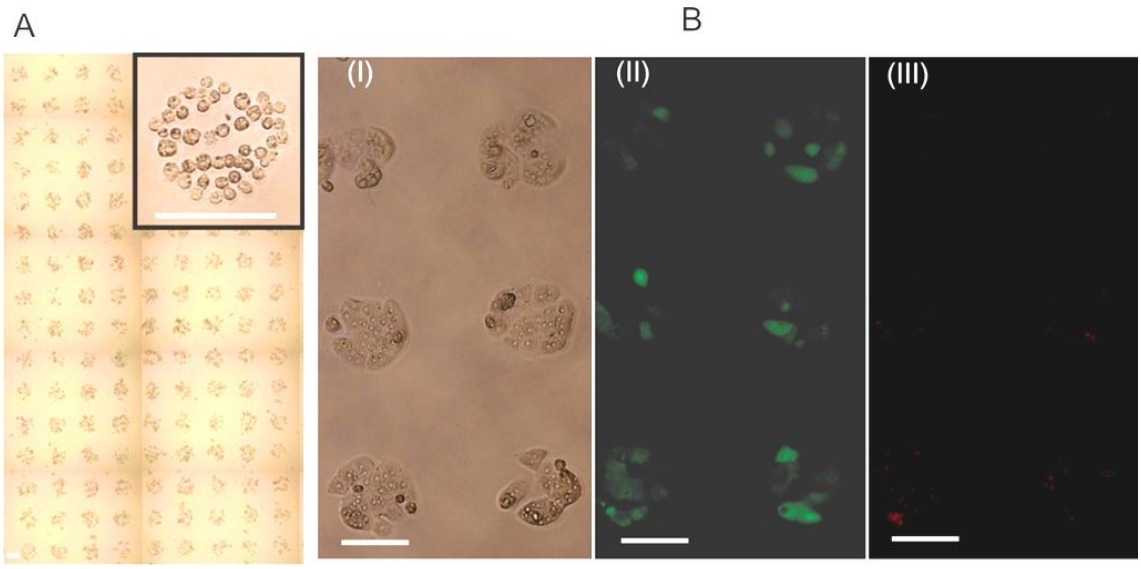

Fig. 5.5 Primary hepatocyte arrays: A) Overview of a large, primary hepatocyte pattern seeded on a collagen pattern 2 hours after seeding. The insert shows one dot at high magnification. The collagen pattern is printed from 0.9 mg/ml collagen solution. B) Images of primary hepatocytes after 24 hour culture: (I): Bright field, (II) and (III): Calcein-AM and EtD-1 emission showing live and dead assays respectively. From image (I), it can be seen that primary hepatocytes have developed into distinct morphologies. All scale bars represent 150µm.

Cell viability after 24 hour culture was examined by measuring green (live) or red (dead) fluorescence as shown on Fig. 5.5-(II)&(III). Quantification of viability (number of life cells/ [number of life cells + number of dead cells]) confirms a higher viability (95%) compared to the cell viability in the seeding solution (determined to be ~75% with trypan blue stain; the live cell membrane is not permeable to trypan blue, thus trypan blue only colours dead cells). These results demonstrate that viable cells adhered

preferentially onto the collagen pattern, which would be beneficial for any subsequent quantitative cell assays on chip.

5.3.3. Toxicity assay – EROD

The next experiment consisted on conducting EROD assay on the micro-array of hepatocytes. For comparison, the same assay was performed on hepatocytes seeded inside a multiwell plate. Fig. 5.6 shows representative results of the fluorescence intensity of resorufin emitted within single cells randomly chosen from within the arrays (n=60 cells). The insert shows fluorescence intensity produced by hepatocytes in a 96 well plate versus time (10^7 cells/well). Each data point represents an average of readings from three wells. This fluorescence intensity reflects the quantity of produced resorufin over the time.

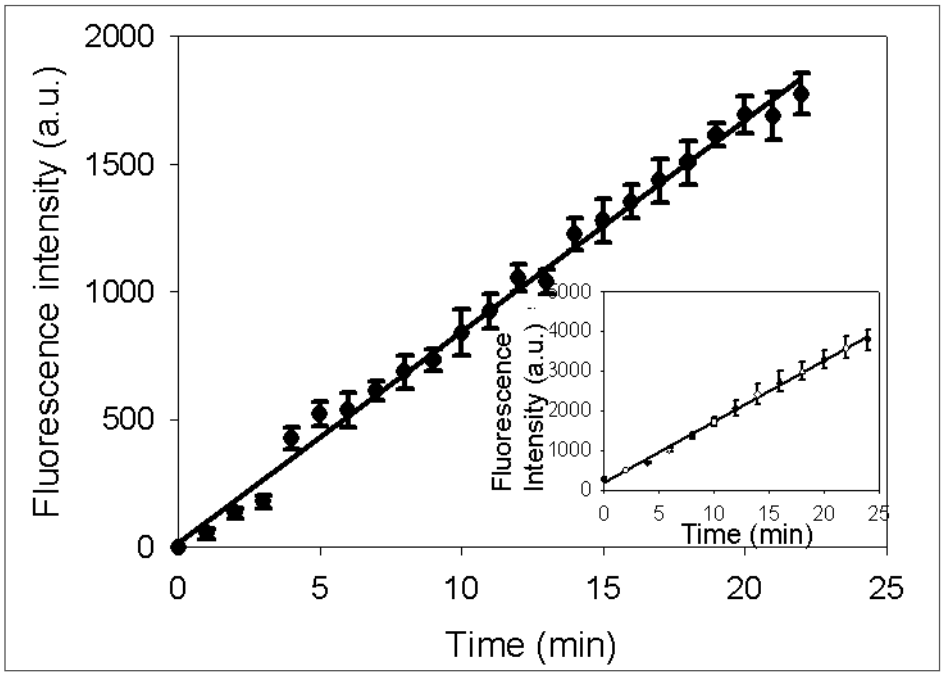

Fig. 5.6 The average intensity of resorufin fluorescence emitted by single cells over the time. Increase in the fluorescence intensity corresponds to the increase in the quantity of produced resorufin which is related to the quantity of metabolised cytochrome P450 (EROD assay). Each data point is an average value from randomly chosen single cells within the array (n=60 cells). Insert: fluorescence intensity of resorufin produced by hepatocytes in a 96 well plate versus time (10^7 cells/well). Each data point represents an average of readings from three wells.

A linear increase of fluorescence intensity for at least 20 minutes was observed from each of the individual cells as well as from the cells in wells. The result suggested that cells grown on the protein substrates expressed high levels of CYP metabolising enzymes and that important liver functions, such as compound metabolism, could be maintained in the cultured single primary rat hepatocyte arrays.

5.3.4. Co-culture of fibroblasts and primary hepatocytes

In the following experiment, patterned microarray of fibroblasts and hepatocytes was prepared. To simplify the procedure, a bigger PLL dot (200µl) was deposited over a collagen patterned area on a glass substrate (prior to any PBS washing) to allow PLL to spread onto the collagen dots and areas between them. Hepatocytes were then seeded. They were incubated on the sample for 2 hours and then the sample was washed once with pre-warmed medium to remove the unattached cells. It was found that the adhered hepatocytes formed distinct micro-islands which occupied only collagen dots. Next, fibroblasts were seeded. They were incubated for 2 hours and the unattached cells were removed from the sample afterwards. The results show that after fibroblast incubation, NIH-3T3 fibroblasts adhered and proliferated on PLL areas, whereas hepatocytes stayed on collagen dots (Fig. 5.7 A). Both cells exhibit high viability after 24 hour culture as shown in Fig. 5.7 B. This method allows for spatially controlled creation of a micro-engineered hepatocyte-fibroblast co-culture and significantly improve the liver cell phenotypic functionalities [4, 5].

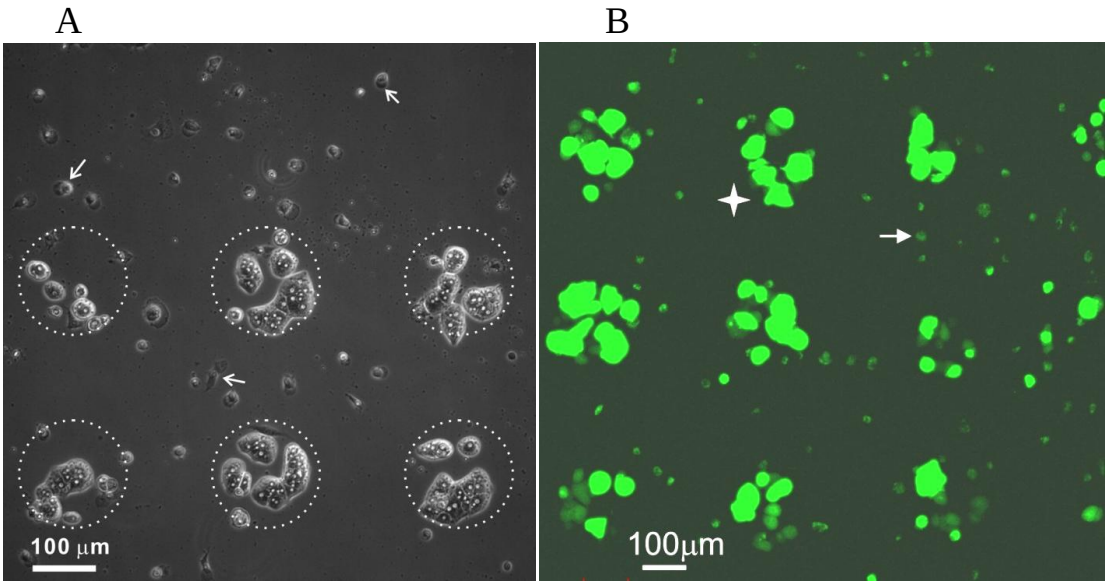

Fig. 5.7 Primary hepatocytes and NIH-3T3 fibroblasts after 24 hour culture: A) Bright field image of a micro-patterned co-culture. NIH-3T3 fibroblasts adhere to the PLL covered PEG area (top of the image) and attached randomly between the hepatocyte array confined to the collagen patterns (indicated by white circles). A small number of representative NIH-3T3 fibroblasts are indicated by white arrows. N.B. The low confluence of NIH-3T3 fibroblasts is due to the low and uneven seeding density; B) Calcein-AM fluorescence images of a micro-patterned co-culture. The fluorescence from the hepatocyte cells, indicated by the white star, is much brighter and covers a larger area than those from the fibroblasts indicated by the white arrow, because hepatocytes metabolise faster than fibroblasts.

5.3.5. Micro-patterns of cells inside microfluidic channels

The following experiment consisted of seeding cells on protein pre-patterned glass slides integrated inside a Dolomite microfluidic device. Fig. 5.8 A shows the assembled microfluidic device. Here, Chinese Hamster Ovary (CHO) cells were used for cell pattern formation inside the microfluidic device to demonstrate the feasibility of combing protein array and microfluidics to form cell pattern in-situ.

CHO cells have been cultured under the same conditions as the NIH-3T3 fibroblast cells. Next, 1 ml of the cell solution at the density of 2.5 x 10^7 cells/ml (which corresponds to 2.5 x 10^6 cells/cm^2) was applied to the microfluidic network with a syringe connected to the analysis chamber with a plastic tube. Once cells reached the analysis chamber they were left to adhere on the collagen pattern for 12 hours at 37°C and 5% CO_2. After that time, fresh medium was applied into the chamber with a syringe connected to a syringe pump. A fresh medium has been continuously pumped into the chamber at the speed of 0.1 µl/min for the following 4 days. A cell pattern created inside the microfluidic chamber after 72 hours of cell culture is shown on Fig. 5.8 B.

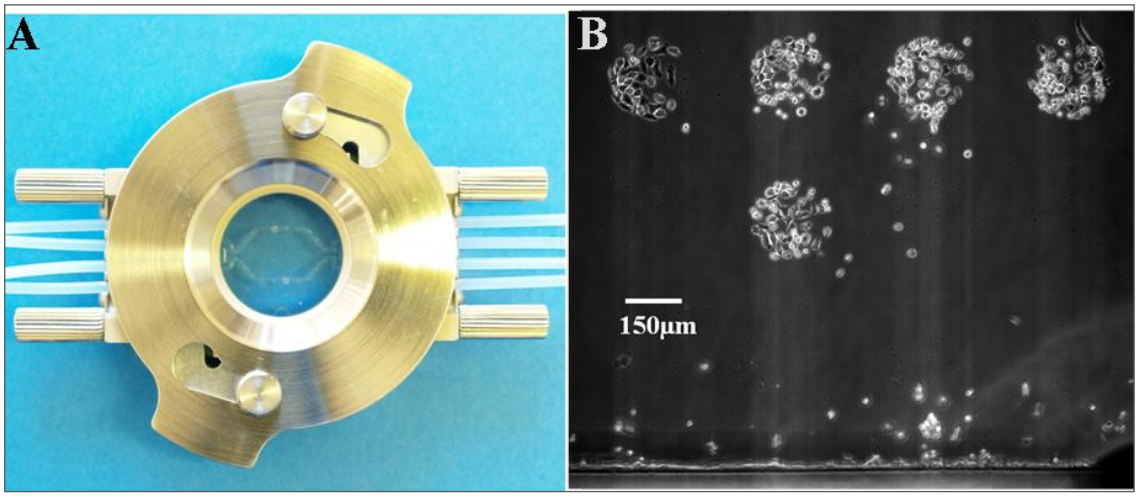

Fig. 5.8 A) A photograph of a microfluidic device (Dolomite®, UK) integrated with a patterned substrate. B) Example of the cell pattern created inside the microfluidic channel 72 hours after seeding.

Fig. 5.8 B shows a successful CHO cell pattern inside the microfluidic network. The seeding conditions are currently optimised for NIH-3T3 fibroblast and hepatocyte culture.

5.4. Chapter conclusions

High resolution PLL patterns have been generated with high fidelity by using a low dispending volume of 10 pl. Our work shows that the regular single cell arrays can be formed on these PLL patterns. Collagen patterns generated with high concentration solutions promoted NIH-3T3 fibroblasts, CHO and primary hepatocytes attachment, growth and long term viability. Cell array formation was dependent on the choice of proteins, the printing method, the substrate surface and culture conditions. PLL patterns promoted the adhesion of NIH-3T3 fibroblasts but not primary hepatocytes (when similarly short seeding periods were used). This permits a simple and flexible method for generation of a spatially resolved co-culture system.

Moreover, primary hepatocytes keep their liver-specific function of cytochrome P450 enzymatic activity, showing the potential of cell arrays for high throughput toxicity *in vitro* analysis. By using the micro-patterned substrates prepared by protein printing, the cell patterning technique developed in this work have advantages of high reproducibility, ease of preparation, robustness, flexibility and low cost. Finally, the micro-arrays of cells were successfully integrated with a microfluidic device. The combination of the cell array with microfluidics allows for precise control of added reagent type and quantities in time as well as its diffusion over the sample. These will assure a correct microenvironment for cell growth and control. In addition, the integrated microfluidic device can be easily adapted for remote control, which allows for precise and repeatable toxicity analysis *in vitro* in a high throughput format.

References

1. "Cytochrome P450," (2011), http://en.wikipedia.org/wiki/Cytochrome_P450.
2. Whyte J. J., and Tillitt D. E., "EROD Activity," http://www.cerc.usgs.gov/pubs/BEST/EROD.pdf.
3. D. K. Hammond, and H. W. Strobel, "Ethoxyresorufin O-Deethylase Activity in Intact Human-Cells," Toxicol. Vitro **6**, 41-46 (1992).
4. S. N. Bhatia, U. J. Balis, M. L. Yarmush, and M. Toner, "Effect of cell-cell interactions in preservation of cellular phenotype: cocultivation of hepatocytes and nonparenchymal cells," Faseb J. **13**, 1883-1900 (1999).
5. S. R. Khetani, and S. N. Bhatia, "Microscale culture of human liver cells for drug development," Nat. Biotechnol. **26**, 120-126 (2008).
6. E. A. Roth, T. Xu, M. Das, C. Gregory, J. J. Hickman, and T. Boland, "Inkjet printing for high-throughput cell patterning," Biomaterials **25**, 3707-3715 (2004).
7. C. N. Jones, J. Y. Lee, J. Zhu, G. Stybayeva, E. Ramanculov, M. A. Zern, and A. Revzin, "Multifunctional protein microarrays for cultivation of cells and immunodetection of secreted cellular products," Anal. Chem. **80**, 6351-6357 (2008).
8. B. J. Kane, M. J. Zinner, M. L. Yarmush, and M. Toner, "Liver-specific functional studies in a microfluidic array of primary mammalian hepatocytes," Anal. Chem. **78**, 4291-4298 (2006).
9. A. Revzin, P. Rajagopalan, A. W. Tilles, F. O. Berthiaume, M. L. Yarmush, and M. Toner, "Designing a hepatocellular microenvironment with protein

microarraying and poly(ethylene glycol) photolithography," Langmuir **20**, 2999-3005 (2004).

Chapter 6

6. Miniaturised microfluidics/micro-LED system for local fluorescence excitation and detection

6.1. Introduction

Light-based bio-analysis - such as fluorescence imaging - requires a high power, tightly focused beam of light of specific wavelength. So far, only big light sources, such as lasers or lamps have met this requirement. Consequently, the miniaturisation and portability of systems for fluorescence imaging and analysis have been restricted. Several attempts were made to resolve the problem of bulky light sources, such as to use waveguide lasers, fibre lasers [1] and vertical cavity surface-emitting semiconductor lasers (VCSELs) [2]. Some examples of such small devices were presented in Chapter 1. However, waveguide and fibre lasers need to be pumped with another laser; therefore the final systems are not portable. An example of using VCSELs as a light source for surface plasmon resonance (SPR) analysis was presented in Chapter 1. VCSELs are small and promising light sources but due to their immature technology are not yet widely tested for bio-applications, and they lack wavelength versatility, especially in the visible.

With the advantages of small size, low energy consumption and low cost, light emitting diodes (LEDs) that are available on the market may be used as compact light sources for a lab-on-a-chip system. As an example, excitation of cells with a LED and fluorescence

detection with a gold plate were demonstrated, but this device was not designed to acquire a fluorescence image [3]. It is important to highlight that the light emission from a commercial LED is inhomogeneous and divergent and thus it is difficult to use LEDs for local fluorescence excitation [4].

In this study, our goal was to integrate a micro Light Emitting Diode (micro-LED) light source with a microfluidic network so as to achieve a miniaturised tool for imaging cell fluorescence. To overcome the problem of LED beam divergence, the micro-LEDs' light emitting surface was placed directly underneath the microfluidic chamber. In addition, when needed, a projection lens was used to create an image of the excitation pixel into the sample chamber. Both adaptations will be described in the following sections of this Chapter.

This Chapter presents first the detailed structures and fabrication of individual components. Second, the integration of a micro-LED device with a microfluidic network is described. Following this, the calibration of fluorescence emission of the integrated device with fluorescein salt solutions is presented. The Chapter will also present the further integration such as with a small lens. Finally, the function of the integrated micro-system is demonstrated by locally exciting green fluorescence from polystyrene beads and Chinese Hamster Ovary (CHO) cells stained with green dye (calcein-AM).

6.2. Preliminary tests

6.2.1. Micro-LED devices used

First, a standard blue (470nm) micro-LED array device composed of 16 x 16 LED pixels was used as an excitation light source. The diameter of a single pixel was 72µm on a

100µm pitch (Fig. 6.1). The active area of the whole array had dimensions of 1.6 mm x 1.6 mm.

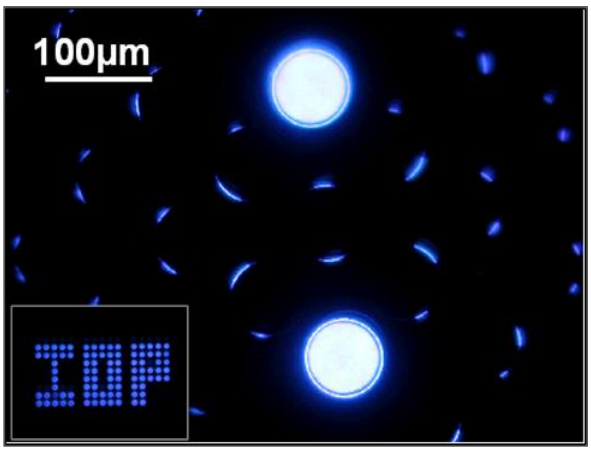

Fig. 6.1 Blue micro-LED device composed of 72µm pixels on 100µm pitch. Two pixels switched on are not adjacent – there is a pixel not switched on between them. The insert shows IOP pattern made with this device.

The micro-LED devices were fabricated in flip-chip format and were glued to a home designed printed circuit board (PCB) as presented in Fig. 6.2 A, leaving top application surface flat. Electric connections through wire-bonding were made on the bottom surface of the device (Fig. 6.2 B). The bottom surface was protected with a plastic frame, a glass slide and silicone glue in order to prevent the possible wire damage by humidity in the cell incubator (37ºC, 5% CO_2, 95% humidity). In this way, the micro-LED devices were robust for several days under the conditions inside a cell incubator.

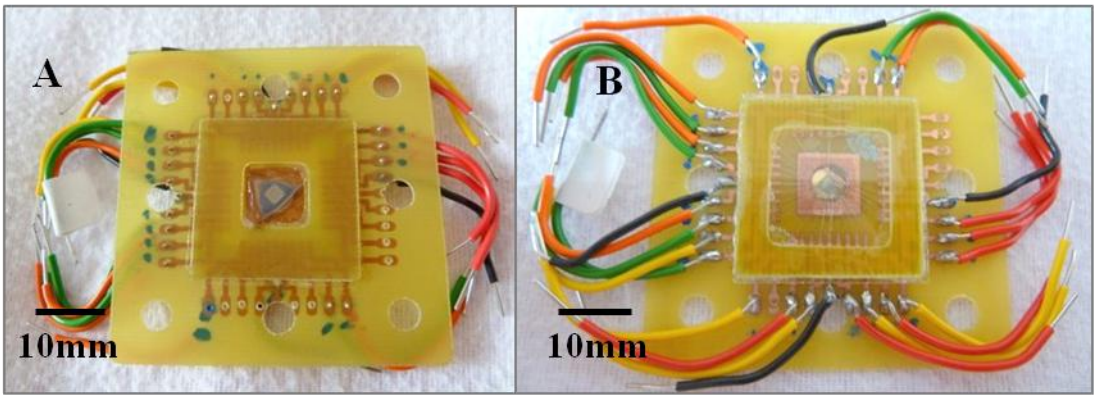

Fig. 6.2 Photographs of the micro-LED array glued onto a PCB board; A) top surface; B) bottom surface.

Metal tracks and connectors were made on the bottom side of the PCB, allowing control of the micro-LED pixels. This configuration was chosen because alternative top electrical connections to the micro-LED device were not optimal for the observation of the bio-sample under a microscope.

6.2.2. First fluorescence detection

The micro-LED device used emits blue light centered at 470nm. The full width at half maximum (FWHM) of this 470nm emission peak is 20-25 nm [5].

For first experiment, fluorescein solution was used as a fluorescent sample. The maximal absorption and peak emission wavelengths of fluorescein are at 490nm and 520nm, respectively. Fluorescein dye (Sigma Aldrich, UK) was dissolved in DI water at concentration of 500µM. The pH of the solution was adjusted to pH 9.0 with NaOH solution in order to obtain the strongest fluorescence signal [6].

When the micro-LED device was tested initially for fluorescein emission, even though efficient emission filters were used to reject all light below 520nm to separate micro-

LED excitation light from the fluorescein emission signal, no fluorescent signal was detected. The fluorescein emission at 520nm was 'covered' by the strong micro-LED tail emission at that wavelength as shown in Fig. 6.3.

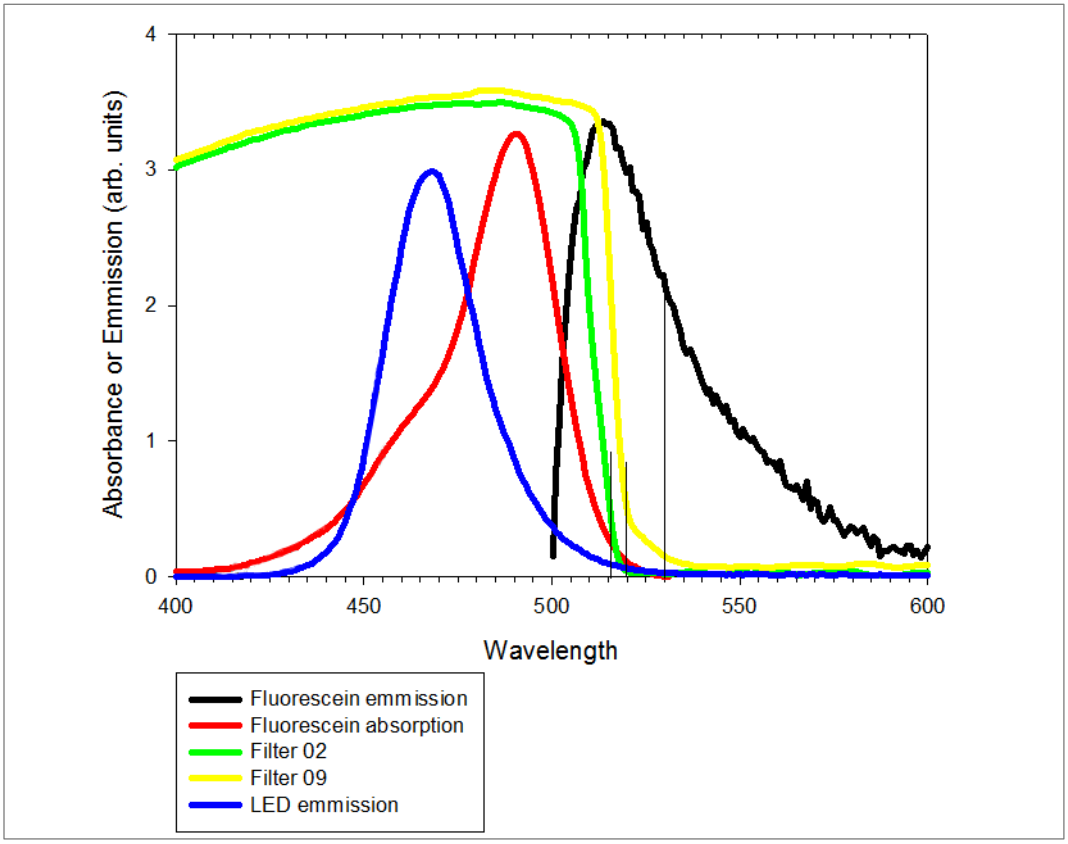

Fig. 6.3 Normalised spectra of fluorescein absorption (red) and emission (black), micro-LED emission (blue) and short pass filters (Zeiss filters number 02 (green) and 09 (yellow)). The fluorescein emission spectrum was not measured but it was calculated from a recorded spectrum composed of micro-LED and fluorescein emissions and then the micro-LED emission spectrum recorded alone was subtracted from the composite spectrum.

To resolve this problem, it was first checked whether the commercial available filters could efficiently reject the micro-LED emission above 500nm and narrow the micro-LED emission peak before it reaches the fluorescent sample (i.e. act as an excitation

filter). Two filters, Zeiss number 02 and 09 with the spectra presented in Fig. 6.3, were proposed for that purpose. 02 and 09 Zeiss filters are short pass filters and reject effectively 95% of light above 520nm and 515nm respectively. In addition, to facilitate the spectral filtration, instead of using micro-LED device emitting at 470nm, a 450nm micro-LED device was used. The 450nm LED gave a better fluorescence signal than the 470nm micro-LED, as it has less tail emission at wavelengths above 500nm. The initial tests with Zeiss filters used as excitation filters and an emission filter rejecting all light below 520nm allowed for fluorescein emission detection (data not shown).

However, adding a commercial filter on the top of micro-LED device made the device more bulky and complicated the further integration of the miniaturised cell analysis system. To minimise the system dimensions, a thin film dielectric filter was designed and commercially coated on the top micro-LED sapphire upper surface so as to narrow down the LED light emission spectral width.

6.2.3. Filter design and performances

In the literature, it was suggested that the cut-off wavelength of the filter, λ_c, should exceed the analytical wavelength, λ, by at least 20nm in the spectrum [7]. The analytical wavelength is the one at which the fluorescence emission is maximal. The cut-off wavelength of a filter was defined as a wavelength at which the filter transmission decreases by 50%. The filter cut-off is not sharp because some spectral width is needed to pass from 95% of transmission to less than 5% of transmission. Consequently, to obtain a filter which would allow for the detection of fluorescein emission at its analytical wavelength, λ (520nm), 490nm was chosen as the filter cut-off wavelength, as

490nm is 30nm below 520nm. Thus 490nm was chosen as a compromise wavelength which allowed for cutting off unwanted micro-LED tail emission below 510nm (10 nm were added for any problems of filter rejection precision) and still allowed a high light output to excite fluorescein [8, 9].

The designed filter was fabricated by SLS Optics Ltd. (Isle of Man, UK). The filter fabrication process consisted of successive depositions of layers of silicon dioxide and zirconium dioxide directly on the surface of the micro-LED chips. The completed device with the thin film filter is shown in Fig. 6.4. A measured transmission spectrum of the filter is presented in Fig. 6.5.

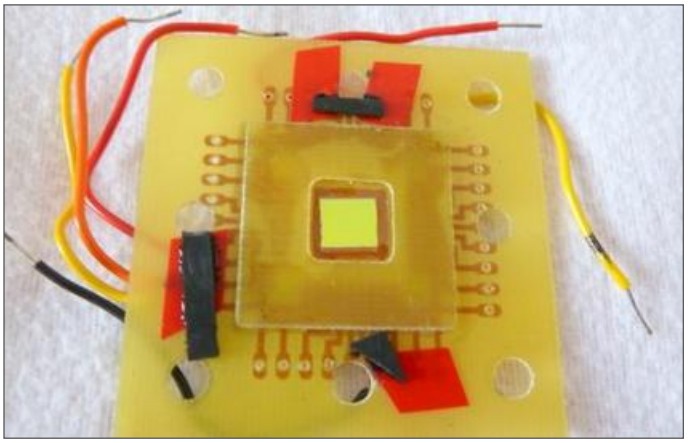

Fig. 6.4 Micro-LED with a thin film filter made by SLS Optics bonded to the PCB.

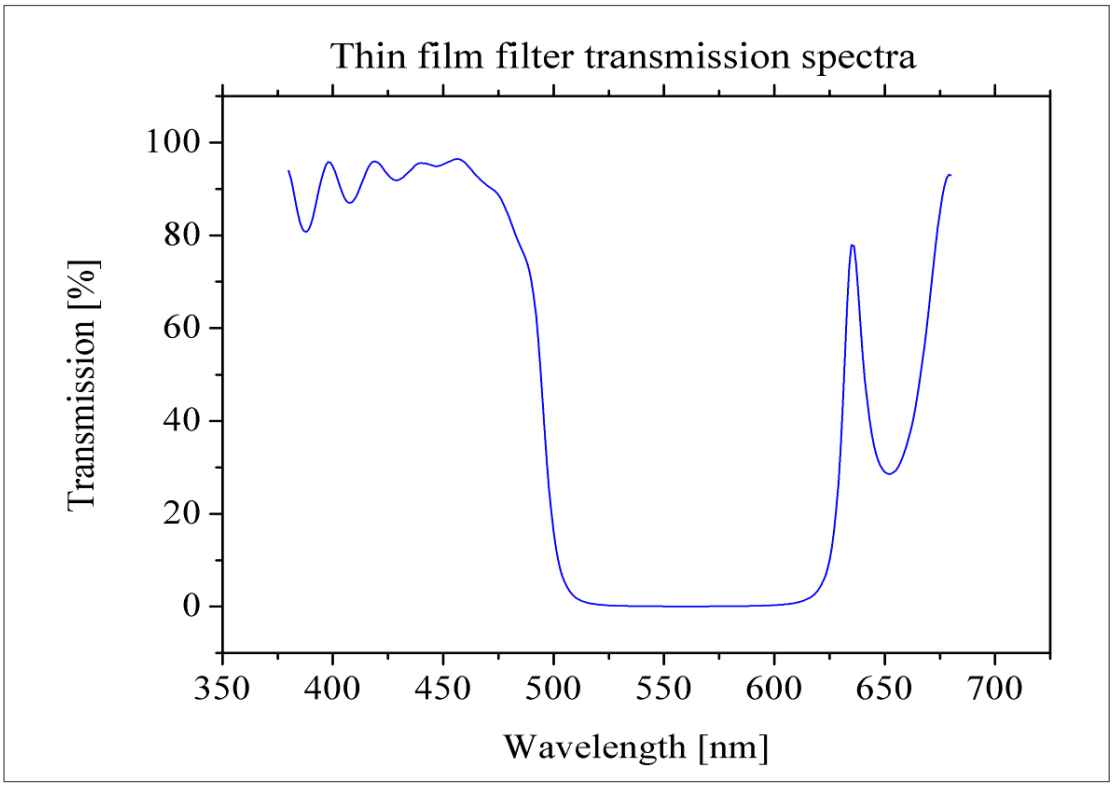

Fig. 6.5 Transmission spectrum of the thin film filter coated on the top surface of the micro-LED device. The spectrum was measured by SLS Optics.

From Fig. 6.5 it can be seen that the light transmission above 510nm should be efficiently rejected by the filter. Fig. 6.6 shows the effect of the filter on 450nm micro-LED emission –light emission above 510nm is effectively filtered. The results of the fluorescence measurement done with this device will be presented in following sections of this Chapter.

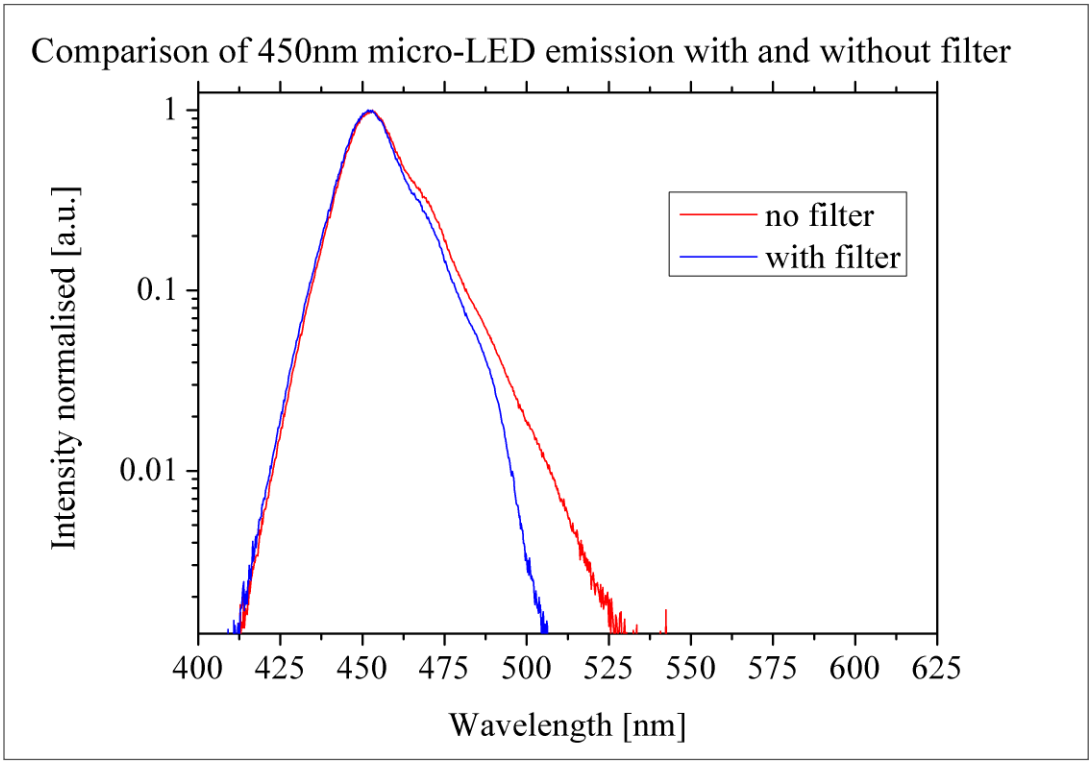

Fig. 6.6 Comparison between filtered and non-filtered emissions of a 450nm micro-LED device (normalised intensity). Both measurements were done on the same pixel: with filter on the front side and without filter on the back side of the device.

6.3. Materials and methods

6.3.1. Fabrication process of the microfluidic network

6.3.1.1. Fabrication of the silicon master

To create a microfluidic network from a transparent silicone elastomer poly(dimethoxysiloxane) (PDMS), (Dow Sylgard®, UK), a silicon master was needed. All chemicals described in this Chapter were supplied by Sigma Aldrich, UK, unless otherwise stated. The substrate for making the master was typically a 4 inch silicon wafer. Before processing, the silicon wafer was cleaned for 5 minutes in the ultrasonic

bath successively with acetone, methanol, isopropyl alcohol (IPA) and rinsed in deionised (DI) water. After cleaning, the silicon wafer was dried with a nitrogen gun. Before applying photoresist, HMDS primer was spun on silicon wafer at 4000 rpm for 5 seconds. Next, the A-Z 4562 photoresist was applied on it at a spin speed of 4000 rpm for 30 seconds. Then, the substrate was soft-baked for 5 minutes at 95°C. In the next step, the wafer with soft-baked photoresist was exposed through a photolithographic mask to the UV radiation (30mW) for 15 seconds in hard contact. For the following experiments, a big microfluidic chamber, 500 µm wide, 100 µm deep and 15 mm long, previously tested for cell seeding [10], was used. This design allowed for using ¼ of the active micro-LED area which had a total dimension of 1.6 mm x 1.6 mm. The acetate masks used here were designed with Corel Draw software, printed by JD Photo, UK and attached to a quartz glass to allow hard-contact exposure.

Next, the exposed pattern on the silicon wafer was developed in A-Z developer/water (1:3) solution for 3 minutes. After the development, the substrate was treated with oxygen plasma for 2 minutes at 100W. Then, the patterned substrate was etched using an STS multiplex inductively coupled plasma (ICP) machine. The etching was made by the Bosch process using alternated SF_6 and C_4F_8 gases for 50 minutes at an etch rate of 2µm per minute to reach a 100µm deep pattern (etch process parameters: coil power @ 600W for etch and passivation; platen power @ 12W; gases flow rates: C_4F_8: 85sccm, SF_6: 130sccm, O_2: 10sccm; etch pressure 35mT; passivation pressure 25mT; chamber temp 50ºC). After etching, the fabricated silicon master was washed successively for 5 minutes in ultrasonic bath in acetone, methanol, IPA and DI water respectively and was then dried with nitrogen gun.

6.3.1.2. PDMS moulding, microfluidic channel fabrication and connection

The microfluidic channel was made from transparent silicone elastomer poly(dimethoxysiloxane) (PDMS). The fabrication involved several steps as described below.

Before PDMS was poured over the patterned silicon master, the master was silanised with 1% Trichloro(1H,1H, 2H, 2H – perfluorooctyl) silane in ethanol solution. Silanisation was indispensable to facilitate the removal of the cured PDMS from the silicon surface. Prior silanisation, the silicon master was treated in oxygen plasma for 20 seconds at 50W. Next, the master was silanised with 1% of above chlorosilane in pure ethanol for 1 hour. After silanisation, the master was ready for PDMS moulding. A mixture of PDMS base with curing agent at a 10:1 ratio was prepared in dust-free conditions and was poured over the silicon mould. The prepared liquid PDMS mixture was placed under vacuum so as to remove air bubbles. When the air bubbles were completely removed, the mixture was cured at 60ºC for at least 2h. Next, the cured PDMS mixture was cut to the required dimensions and removed from the silicon mould.

The next fabrication step of the microfluidic device consists of making connections between the PDMS channels and supplying tubes. This process involved making holes in PDMS channels with blunt metal needles, putting blunt needles into the holes and connecting the channels via blunt needles with polyethylene tubes and syringes. The hypodermic needles and BD syringes used were supplied by Agar, UK and Fisher Scientific, UK. Tubing and the valves were supplied by Cole Parmer, UK.

Before assembling all connections, the PDMS microfluidic device was washed in ethanol and DI water for 5 minutes in ultrasonic bath and dried with a nitrogen gun to remove any dust and to ensure a good seal between the cured PDMS and the surface supporting the device from the bottom (e.g. glass coverslip). The washed microfluidic network with connectors was placed on glass coverslips, washed in a similar way, supplied by VWR Scientific, UK. To ensure good sealing, the cured PDMS device was pressed against the glass coverslip with custom made metal or plastic holders, assembled with screws. Next, plastic tubes were connected to the syringe. Then, liquid was introduced into the PDMS channel with the syringe. On the exit of the channel, the tubing was connected to the waste recipient which was an Eppendorf tube. The fully assembled microfluidic system is shown in Fig. 6.7. The integration of these microfluidics and micro-LED array is described in the following section.

The biggest problem in using this microfluidic device was uncontrolled formation of air bubbles. An air bubble would interfere with cell adhesion inside the micro-chamber because it induces high pressure. Air bubbles could be formed by evaporation of the liquid from the channel through porous PDMS or by involuntary movement of the connections, which introduced pressure inside the plastic tubes. Evaporation was prevented by good sealing and continuous liquid flow. Prevention of moving connections was assured by using a ‘T’ valve and fixing the device, tubing and valve to a plastic holder (Fig. 6.7).

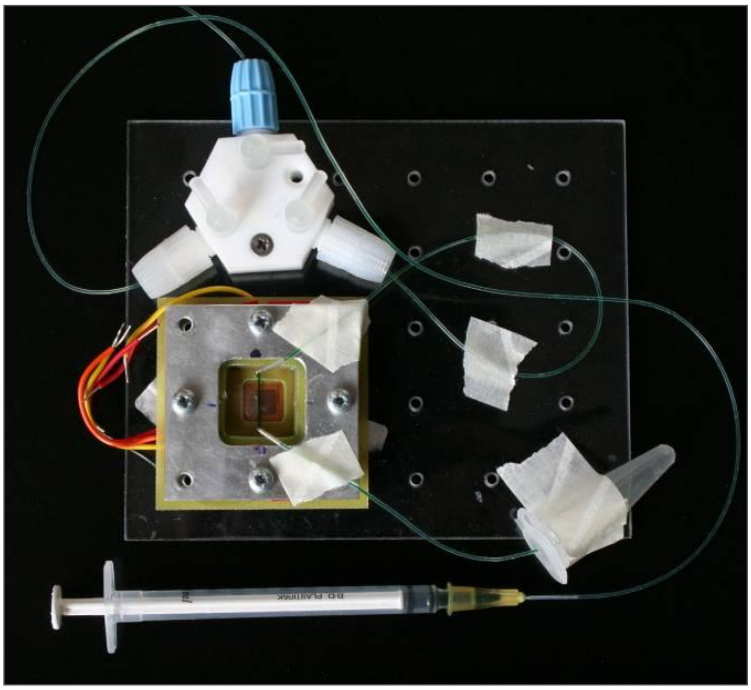

Fig. 6.7 Fully assembled microfluidic system.

The ‘T’ valve was used to separate physically the tubing connecting the fluid supply (syringe) and microfluidic device. The ‘T’ valve inlet was connected to the supplying syringe. Two ‘T’ valve outlets were connected: one to the waste and one to the fixed microfluidic device. The way in which the liquid flowed through the valve was directed by an ‘L’ switch between the three arms. Only two of three arms - (1) syringe fluid supply, (2) microfluidic device or (3) waste - were connected at the same time depending on how the ‘L’ switch was positioned. When carrying out the experiment, the syringe was connected and the fluid was first pushed through the valve to the waste recipient so as to push away remaining old fluid and any possible air bubbles. Then, the switch position was changed and the fluid was directed to the microfluidic network. When the syringe needed to be changed, the switch connecting to it was closed, to avoid

pressure changes in the microfluidic channels. This configuration allowed for changing syringes without introducing air bubbles inside the microfluidic channels.

6.3.2. Microfluidics/LED integration

The microfluidic network, prepared as described above, was assembled with a micro-LED array. In order to construct a fully integrated device, an attempt was made to integrate a microfluidic PDMS network directly on the micro-LED top application surface i.e. sapphire substrate surface. However, as the sapphire surface of micro-LED device is very inert [11] the thin film filter adhered stronger to the PDMS material than to the sapphire surface. Thus, when the PDMS channel was removed, the filter peeled off from the micro-LED substrate surface, or the whole device detached from the PCB, destroying the device. Consequently, a thin glass coverslip (~200μm thickness) was added on the bottom of the PDMS microfluidic device prepared as described in the previous section, to prevent the micro-LED device from damage.

The micro-LED array was placed directly underneath the microfluidic chamber so as to shorten the light path to reach the sample and to obtain the fluorescence image of the sample (Fig. 6.8). The micro-LED light source was in flip-chip format and the filter was deposited on the top of the LED substrate surface, consequently the fluorescence detection was made from the top of the excitation source as shown in Fig. 6.8. This configuration allowed for acquiring two dimensional images of the fluorescence.

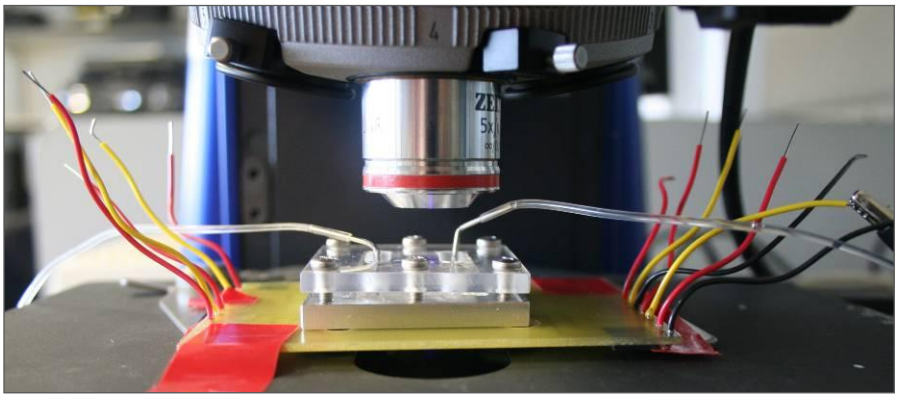

Fig. 6.8 Micro-LED device bonded to PCB circuit assembled with microfluidic network under an upright microscope.

Ideally, to get high resolution images, the base of microfluidic device should be thinner, because high magnification lenses usually have short working distance. However, a microfluidic device with a thin base is not so rigid which may cause the problems of leakage from tubing connection. To make the microfluidic device more rigid, a glass slide was added on the top of the cured PDMS microfluidic device. Two holes were then drilled into this glass slide to allow the tube connections to go into the PDMS microfluidic device. Finally, a thin metal frame was used to fix the glass slide and hold the microfluidic network and the micro-LED array as shown in Fig. 6.9.

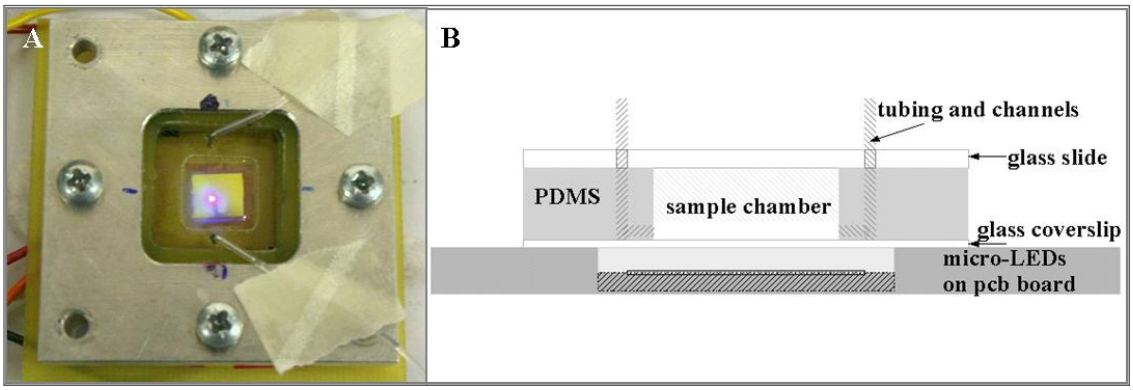

Fig. 6.9 Microfluidic network assembled with a micro-LED device: A) a clos view with one micro-LED pixel switched on; B) schematic diagram showing the cross-sectional structure of the integrated system.

6.3.3. Fluorescein solution detection

Fluorescein salt solutions were prepared for detecting its fluorescence emission with micro-LED excitation in the integrated system. To prepare such solutions, fluorescein salt was dissolved in DI water at different concentrations, from 1 to 1000 µM. The pH of the solutions was adjusted to pH 9.0 with NaOH solution in order to obtain the strongest fluorescence signal [6].

Fluorescein emission in PDMS microfluidic channel was recorded with an HR 800 UV Raman spectrometer with a Synapse detector (both from Horiba Jobin Yvon, UK) and a long-pass filter cutting off all light below 488 nm (± 20 nm). All spectra were recorded with a 10s acquisition time. One LED pixel (72µm in diameter) of the 450nm micro-LED array was used as an excitation source. This LED pixel with an integrated thin film filter was operated at a voltage of 4.0 V (current of 10 mA), producing a power of 670 µW. Despite relatively high emission power for such a small emitter, the power density inside the microfluidic sample chamber was not higher than 0.5 W/cm^2. As explained in

detail in the section below, the light spot inside the microfluidic chamber was increased to 200µm in diameter, due to the divergence of LED light emission.

6.3.4. Integration of the lens

Fig. 6.10 is a 'Z-stack' of cross-section images obtained on Zeiss LSM 510 confocal microscope of emission of one micro-LED pixel. This image shows that the micro-LED emission is highly divergent. The emission divergence of LED devices measured in this way was also reported previously [12, 13].

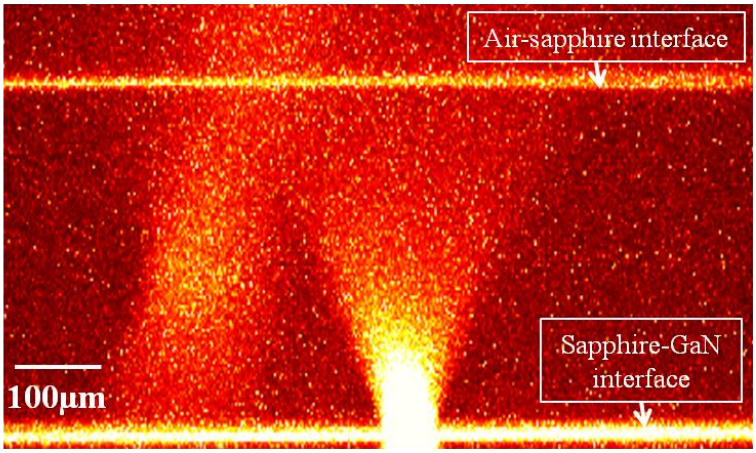

Fig. 6.10 Z-stack (side view) of the blue micro-LED emission imaged through the sapphire substrate and recorded with a Zeiss LSM 510 confocal microscope. The two sapphire surfaces can be clearly distinguished as well as the reflection on the outer sapphire surface. N.B. the vertical scale is different from horizontal one – the sapphire thickness is ~ 300µm.

In order to narrow the light spot inside the microfluidic chamber, the chamber was placed as close as possible to the LED excitation source. In this configuration, the smallest illumination spot for 72µm micro-LED pixel was 200µm in diameter in the sample chamber. This spot size was acceptable for bulk fluorescein excitation, as shown in the results section, but was not suitable for single cell excitation (typical cell diameter

10-20 µm). Also, the quality of the fluorescence image obtained was not comparable with those obtained with current techniques used for cell fluorescence imaging such as standard microscopy using mercury lamps or lasers. In order to obtain a small localised LED excitation spot, a small lens (C230TME-A, Geltech, Thorlabs, Germany) was added on the top of the micro-LED array. This lens projected the LED pixels into the microfluidic sample chamber. The device integrated with the lens and its schematic diagram are shown in Fig. 6.11.

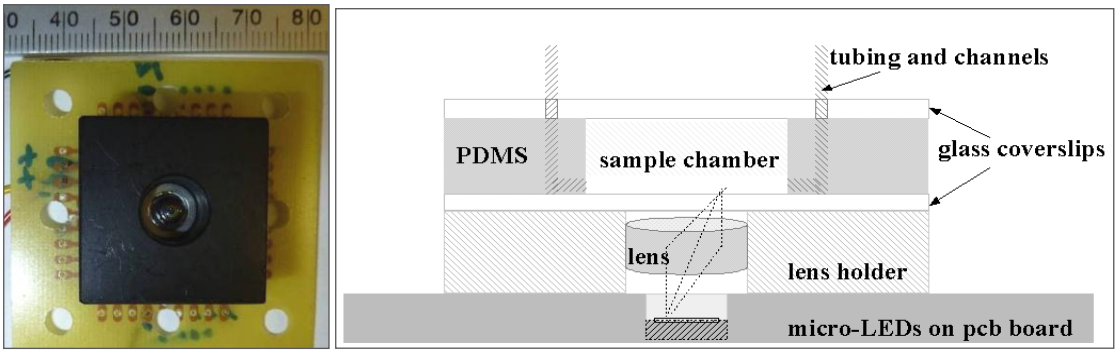

Fig. 6.11 Photograph of the micro-LED array mounted on the PCB and a plastic holder with mounted lens – top view and the schematic diagram of the integrated device with micro-LEDs, lens and microfluidic component.

This lens has a short focal length (4.51 mm) allowing keeping small the dimensions of the integrated system. The lens was placed inside a plastic holder which assured that the LED light emitting plane was placed at 2 focal distances from the lens, creating a 1:1 real image of the micro-LED array inside the sample chamber.

6.3.5. Polystyrene beads fluorescence detection

Polystyrene beads, 1.1 µm in diameter, emitting green fluorescence (F8823, Invitrogen, UK) were used for local fluorescence excitation and detection in our micro-system.

Absorption and emission spectra of these polystyrene beads are similar as respective fluorescein spectra. Polystyrene bead solution in DI water at the concentration of 10^7 beads/ml was used and put inside the PDMS microfluidic chamber.

For this experiment, 450nm blue micro-LED emitters with an integrated filter and lens were used as an excitation light source. For fluorescence excitation, the LED pixel was driven at an injection current of 10mA. Under this condition, the LED light output power was 62μW after the lens, giving a power density of 0.4 W/cm^2 inside the sample chamber. For comparison, the fluorescence images were also taken while the same polystyrene beads in a microfluidic chamber were excited by a fluorescent lamp with a blue filter. The detection was made on an inverted Nikon microscope with a green band pass filter (520nm ± 20nm).

6.3.6. Stained cells fluorescence detection

Chinese Hamster Ovary (CHO-K1 cell line from ATCC) cells were used in the following experiment. These CHO cells were cultured at 37°C and 5% CO_2 in Dulbecco's modified Eagle medium containing nutrient mixture F-12 (DMEM/F12, GIBCO) supplemented with 10% FBS, 2mM L-glutamine and 100 U/ml of penicillin and streptomycin. Stain solution was 5μM calcein-AM in phosphate buffered saline (PBS) solution.

Prior to the experiment, cells were detached from the culture flask and put in the suspension. To detach them from the flask surface, cells were treated with 0.05% trypsin solution. After 3 minutes' treatment, DMEM/F12 medium was added to the solution to stop trypsin acting. Next, cells were spun for 3 minutes at 1400 rpm. The medium was then aspirated and replaced by PBS solution. This washing procedure was indispensable

before staining cells with 5μM calcein-AM dye (calcein-AM stain was explained in details in Chapter 5). The centrifugation was repeated once and PBS was replaced with fresh pre-warmed stain solution. Stained cell solution at a concentration of 2×10^6 cells ml^{-1} was applied into microfluidic chamber with a syringe and incubated at 37°C 5% CO_2 for 45 minutes.

Cell fluorescence was excited and detected in the same way as for the polystyrene beads and the cell fluorescence images were observed by an inverted Nikon microscope. The operating parameters of a micro-LED pixel were also the same as for exciting beads i.e. 10mA driving current, 62μW optical power inside the chamber, and a power density of 0.4 W/cm^2.

6.4. Results

6.4.1. Fluorescein excitation

The measurements presented in Fig. 6.12 and Fig. 6.13 were done in the integrated device without the lens. Fig. 6.12 presents measured fluorescein emission spectra at pH 9 for different molar concentrations of the fluorescein dye. The lowest limit of the detection of fluorescein emission excited with 1 pixel of micro-LEDs was 10 μM (Fig. 6.12 and Fig. 6.13). For a concentration lower than 10 μM, the fluorescence signal was too low to be distinguished from the background. The small peak on the detected spectrum for the wavelengths below 500nm on Fig. 6.12 corresponds to the small fraction of unfiltered LED emission.

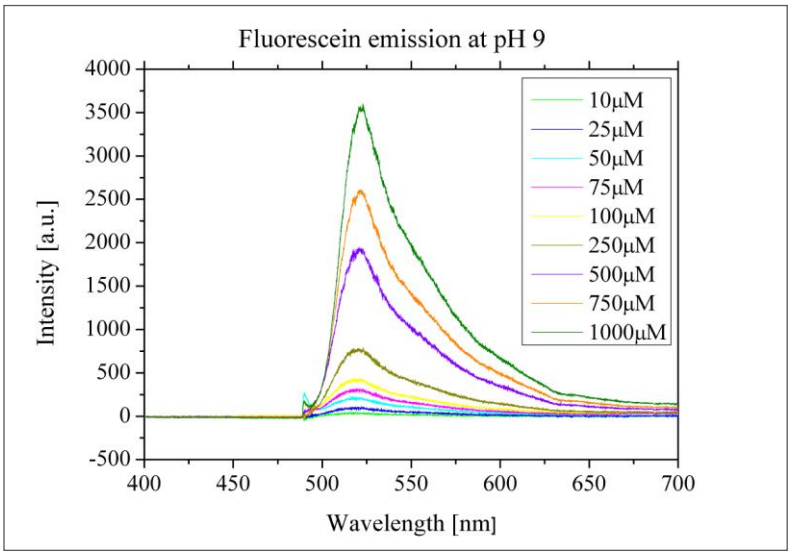

Fig. 6.12 Measured fluorescein emission spectra at pH 9 for different molar concentrations of the fluorescein dye.

Fig. 6.13 shows linear relationship between fluorescence intensity at 520nm and the fluorescein dye concentration. These results demonstrate the integrated device stability in fluorescence excitation.

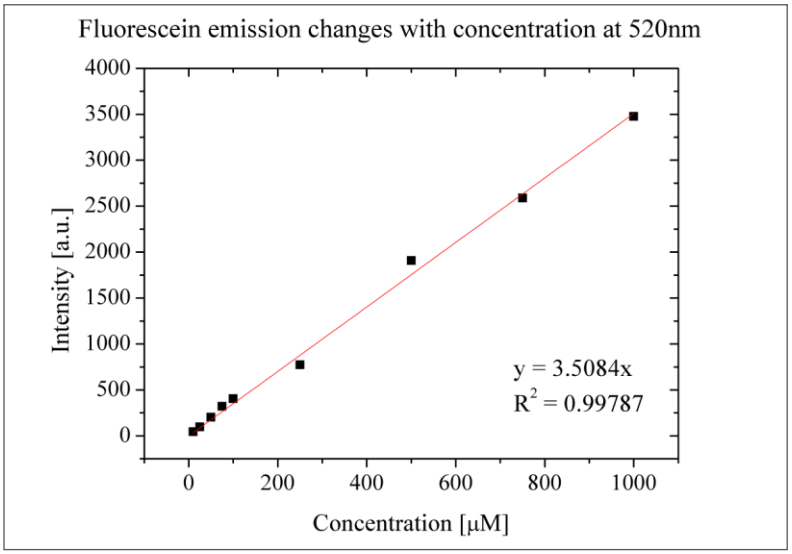

Fig. 6.13 Linear increase of the fluorescence peak intensity at 520nm, the theoretical maximum of fluorescein emission, with increased concentration of the fluorescein dye.

6.4.2. Integration of the lens for localised excitation

By adding a lens to the integrated system, the light spot inside the sample chamber resulted to be ~ 70μm in diameter for a 72μm LED pixel (Fig. 6.14).

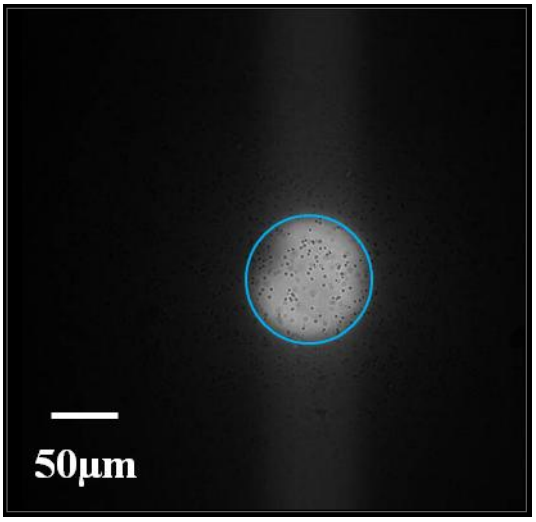

Fig. 6.14 Image of a 72μm micro-LED pixel inside the microfluidic chamber. A schematic of the pixel diameter was added on the picture (blue circle).

It was measured that by adding this simple, small lens on the top of the micro-LED array, 9% of light emission from LED pixels was collected and projected to the sample chamber. Most importantly, this micro-system was integrated with the microfluidic device and was used inside a standard cell incubator. Consequently, this microsystem has a high potential for wide bio-applications.

6.4.3. Local fluorescence excitation and detection

6.4.3.1. Experiments with polystyrene beads

Results: The fluorescence images of polystyrene beads are presented in Fig. 6.15.

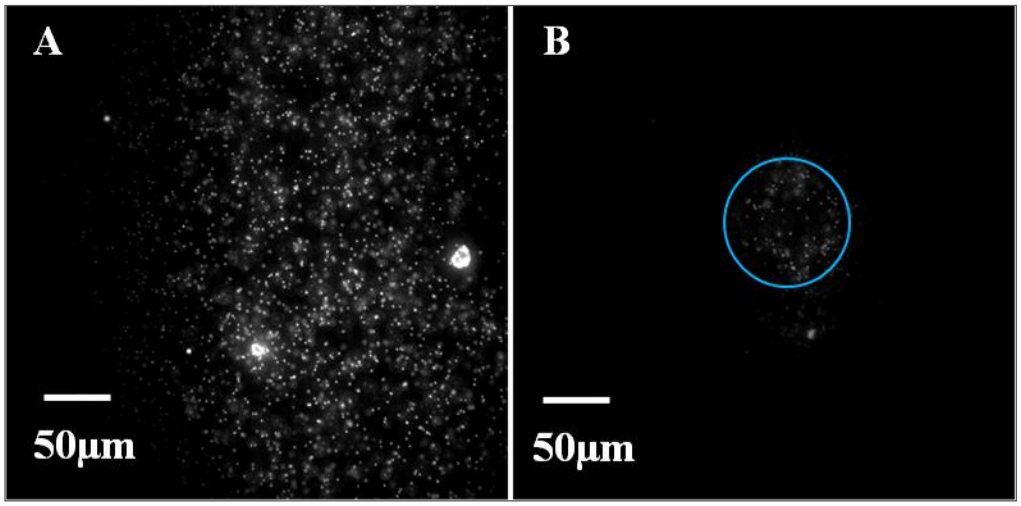

Fig. 6.15 Images of fluorescence of beads taken with a 40x magnification objective; A) fluorescence image excited by a lamp with a blue band pass filter (image acquisition time 10ms); B) fluorescence image excited by a micro-LED pixel operating at 10mA (image acquisition time 10ms); A circle in the image represents the pixel diameter.

From Fig. 6.15 B, a small, localised fluorescence emission can be observed from the polystyrene beads excited by one micro-LED pixel. In contrast, when using a fluorescence lamp, the beads in the whole channel were excited (Fig. 6.15 A). Fig. 6.15 B shows that the fluorescence emission area was slightly bigger than the pixel image because the fluorescence is emitted in all 4π steradians of space [14].

6.4.3.2. Experiments with cells

The cell fluorescence images obtained are presented in Fig. 6.16. For comparison, Fig. 6.16 A shows the CHO cell fluorescence image excited by a lamp. Fig. 6.16 B is the CHO cell fluorescence image excited locally with one micro-LED pixel.

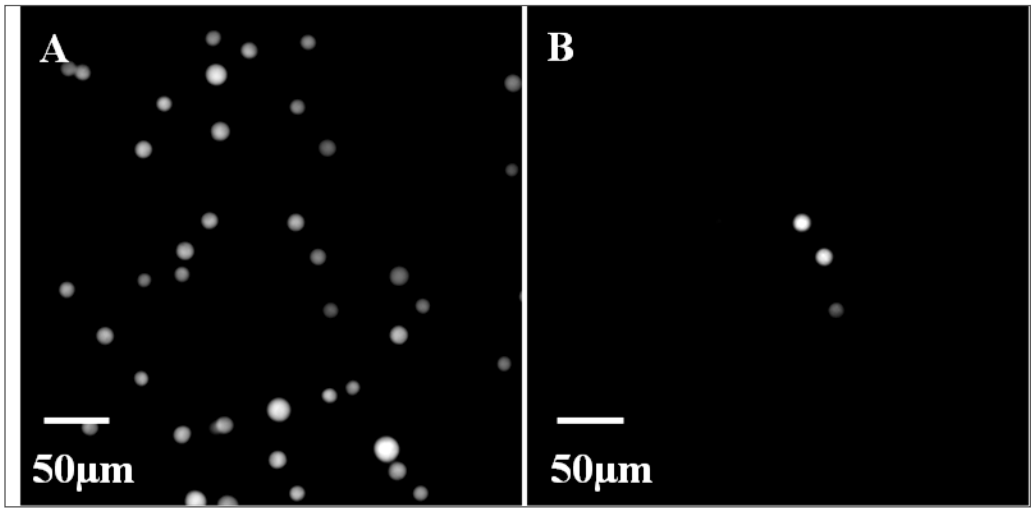

Fig. 6.16 Fluorescence images of CHO cells taken with a 40x magnification objective; A) fluorescence image of CHO cells excited by a lamp with a blue band pass filter (image acquisition time 0.1s); B) fluorescence image of CHO cells excited by one micro-LED pixel operating at 10mA (image acquisition time 5s).

From the above images, one can clearly see the advantages of micro-LED local excitation: in addition to its small size and easy integration with microfluidic network, micro-LEDs allow for fluorescence excitation of just few single cells, reducing the number of cells exposed to the radiation, thus reducing bleaching and cell damage and improving fluorescence contrast.

6.5. Future developments

A second generation of microfluidic devices which matches better with the micro-LEDs dimensions was also designed. The structure of this second generation of microfluidic devices is shown in Fig. 6.17.

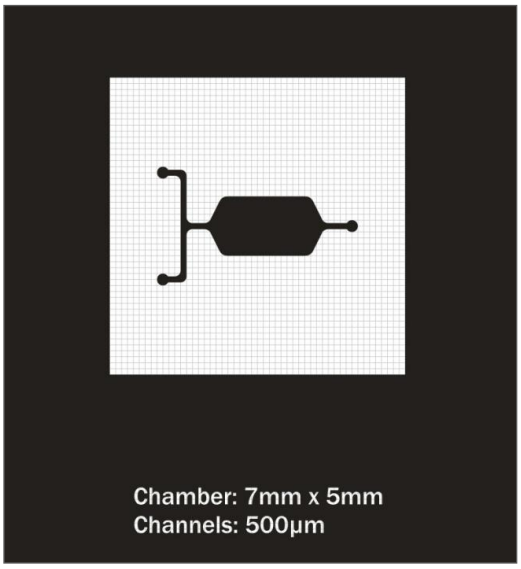

Fig. 6.17 Design of second generation of microfluidic device.

This design was made mainly to host an array of cells for cell assay as shown in Fig. 6.18. Thus, the new microfluidic device can combine the technology of cell patterning presented in Chapters 4 and 5 and localised excitation and detection presented in this Chapter to achieve an integrated miniaturised cell analysis platform.

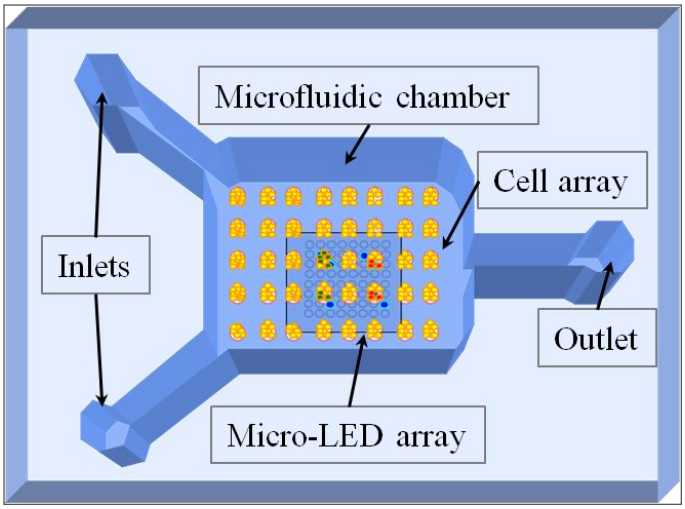

Fig. 6.18 A schematic diagram of the new microfluidic network integrated with a micro-LED array and an array of cells seeded inside it.

However, some problems associated with this new microfluidic device made of PDMS for cell analysis were found. As the PDMS material is flexible, the big 7 mm x 5 mm chamber might collapse due to its size. Moreover, despite its ease of fabrication PDMS microfluidic devices also have some disadvantages, such as absorptions of organic solvents, proteins and other small molecules into microfluidic walls [15]. Therefore, today's trends in commercialisation of microfluidics technology are going into two main streams: towards more reliable and re-usable devices made out of glass or silicone, and towards simpler and cheaper solutions such as 'paper based' tests, which allows for faster diagnostics and are particularly important to implement in developing countries [15, 16]. In spite of its reliability problem, PDMS is still considered as a good testing material to create microfluidic prototypes. The integration of the micro-LED array with glass microfluidic chip and cell array inside it is currently under development in our research group (see Chapter 5).

6.6. Chapter conclusions

A microfluidic network was successfully integrated with micro-LEDs arrays to achieve local fluorescence excitation and detection. The results shown in this Chapter demonstrated that an integrated thin film filter can reject LED emission above 510nm efficiently and a small lens can project LED pixel emission inside the sample chamber accurately. These methods have enabled to achieve high spatial resolution fluorescence excitation and detection. The calibration of the fluorescence with fluorescein salt was demonstrated. Localised fluorescence excitation of 70μm diameter spot size and detection from green fluorescent beads and stained live cells were achieved by using the miniaturised system. There is a further scope to improve the resolution of this micro-system, e.g. by using even small micro-LED pixels (<10 μm in diameter) and de-magnifying the projected light spot.

Results presented in this Chapter show the capabilities of micro-LEDs integrated with a microfluidic device for cell analysis. Such a novel lab-on-a-chip technology will allow for production of entirely new tools with high spatial and temporal resolution for diverse bio-applications.

References

1. B. Lincoln, S. Schinkinger, K. Travis, F. Wottawah, S. Ebert, F. Sauer, and J. Guck, "Reconfigurable microfluidic integration of a dual-beam laser trap with biomedical applications," Biomed. Microdevices **9**, 703-710 (2007).
2. E. Thrush, O. Levi, W. Ha, K. Wang, S. J. Smith, and J. S. Harris, "Integrated bio-fluorescence sensor," J. Chromatogr. A **1013**, 103-110 (2003).
3. K. N. Ren, Q. L. Liang, X. Mu, G. A. Luo, and Y. M. Wang, "Miniaturized high throughput detection system for capillary array electrophoresis on chip with integrated light emitting diode array as addressed ring-shaped light source," Lab Chip **9**, 733-736 (2009).
4. Q. Q. Gan, Y. Wang, Y. H. Sun, S. Tatic-Lucic, and F. Bartoli, "A prototype miniaturized chip for bio-imaging applications," 2008 Conference on Lasers and Electro-Optics & Quantum Electronics and Laser Science Conference, Vols 1-9, 2543-2544 (2008).
5. H. X. Zhang , D. Massoubre, J. McKendry, Z. Gong, B. Guilhabert, C. Griffin, E. Gu, P. E. Jessop, J. M. Girkin, and M. D. Dawson, "Individually-addressable flip-chip AlInGaN micropixelated light emitting diode arrays with high continuous and nanosecond output power," Opt Express **16**, 9918-9926 (2008).
6. "Molecular Probes: The Handbook; pH Indicators—Chapter 20; Probes Useful at Near-Neutral pH—Section 20.2 ", http://www.invitrogen.com/site/us/en/home/References/Molecular-Probes-The-Handbook/pH-Indicators/Probes-Useful-at-Near-Neutral-pH.html.

7. "11.6.1. The use of cut-off filters," http://gratings.newport.com/information/handbook/chapter11.asp#11.6.1.

8. E. P. de Jong, and C. A. Lucy, "Spectral filtering of light-emitting diodes for fluorescence detection," Anal. Chim. Acta **546**, 37-45 (2005).

9. "Interference Filters: The Key to It All," http://www.fluorescence.com/tutorial/int-filt.htm.

10. H. B. Yin, N. Pattrick, X. L. Zhang, N. Klauke, H. C. Cordingley, S. J. Haswell, and J. M. Cooper, "Quantitative comparison between microfluidic and microtiter plate formats for cell-based assays," Anal. Chem. **80**, 179-185 (2008).

11. R. A. Freitas, Jr., "Is Sapphire Biocompatible With Living Cells?," (2002), http://www.imm.org/publications/reports/rep035/.

12. P. Kelm, Massoubre, D., Jessop, P.E, Zarowna, A., Girkin, J.M., Zhang, H., Gu, E., Dawson, M.D., "Beam Intensity Profiles in Flip-Chip InGaN/GaN Micro-LED Arrays," in *UK NITRIDES CONSORTIUM* (University of Strathclyde, Glasgow, 2008).

13. C. Griffin, E. Gu, H. W. Choi, C. W. Jeon, J. M. Girkin, M. D. Dawson, and G. McConnell, "Beam divergence measurements of InGaN/GaN micro-array light-emitting diodes using confocal microscopy," Applied Physics Letters **86**, 041111 (2005).

14. T. Kamei, N. M. Toriello, E. T. Lagally, R. G. Blazej, J. R. Scherer, R. A. Street, and R. A. Mathies, "Microfluidic genetic analysis with an integrated a-Si : H detector," Biomed. Microdevices **7**, 147-152 (2005).

15. R. Mukhopadhyay, "When PDMS isn't the best. What are its weaknesses, and which other polymers can researchers add to their toolboxes?," Anal Chem **79**, 3248-3253 (2007).

16. A. W. Martinez, S. T. Phillips, Z. H. Nie, C. M. Cheng, E. Carrilho, B. J. Wiley, and G. M. Whitesides, "Programmable diagnostic devices made from paper and tape (vol 10, pg 2499, 2010)," Lab Chip **10**, 3428-3428 (2010).

Chapter 7

7. Conclusions and future works

Four different technologies were used in this work to develop three innovative miniaturised cell analysis systems. In the first system, the miniaturised Optoelectronic Tweezers, micro-LED arrays were used as a light source for the first time to achieve micro-particle and cell manipulations. The second system used piezoelectric printing to create micro-patterns of proteins onto the new type of the non-adhesive surface, which is easy to integrate with a microfluidic device. Cells seeded on these patterns formed well defined micro-cell arrays which were successfully used for toxicity study. The third system, a miniaturised cell analysis device, integrates the micro-LED array with a microfluidic network to achieve localised two-dimensional cell fluorescence analysis.

The first Chapter of this thesis presented the background and motivations of this work. An overview of different optical techniques and bio-medical devices was also presented there. Optics and photonics play an important role in the development of new medical technologies, particularly in imaging, surgery and novel diagnostic methods. The 1970s and the 1980s saw major advancements in these fields with the development and application of lasers. Presently, the development of novel light sources such as LEDs enables the further progress in biomedical technologies. Particularly, light emitting diodes offer several advantages as compared to lasers: they are significantly smaller than lasers and have much lower energy consumption, while still being able to emit high

optical powers. Due to their high efficiency, LEDs generate much less heat, which in turn greatly enhances the scope for the development of new bio-instruments and applications. LEDs also have longer life span than lasers and lamps. They can be operated under continuous or pulsed modes and can emit light in different wavelengths. However, only a few bio-micro-systems with a LED light source for bio-analysis have been developed so far. Some examples of such systems were presented in Chapter 1.

In this work, micro-LEDs were used for the first time as a light source to achieve novel miniaturised cell analysis systems. Micro-LEDs have been previously used in different applications, such as fluorescence life-time measurements and mask-less photolithography. In our work, micro-LEDs were used to develop miniaturised optoelectronic tweezers and to construct a miniature cell analysis system with an integrated microfluidic component. In Chapter 1, before introducing the principles of optoelectronic tweezers, other different tweezing techniques were briefly reviewed, including AFM, magnetic tweezers, acoustic tweezers, optical tweezers and dielectrophoresis. The optoelectronic tweezers (OET) method was then described, especially stressing its advantages over other techniques. Moreover, the micro-LED is a low-power light source which thus minimises the interference with cell viability. In both systems, the micro-LED light was projected to the sample chamber with a small lens. As a result, the micro-systems developed were compact and portable. Furthermore, these micro-systems are robust and can withstand standard cell culture conditions, opening a new way for long term bio-study. The previous systems do not have these advantages.

In the miniature cell analysis system, the bio-sample was hosted in the microfluidic chamber. Consequently, the sample does not directly contact the semiconductor material used for making the micro-LED light source and the microfluidic component can be easily separated from the LED light source. This arrangement will protect the bio-samples from possible toxic effect of the semiconductor material and also facilitate the system sterilization and sample residue cleaning. In addition, the microfluidic component is disposable; we can easily dismount it and use the LED light source repeatedly.

Another micro-system developed in this work integrated the cell micro-arrays with a microfluidic component for drug analysis. Today pharmaceutical industry uses a multi-well method for testing efficiency and toxicity of drugs and cosmetics. However, by this way, big quantities of animal-derived cells are used. For ethical reasons, there is a high demand to reduce the quantity of animal-derived cells and thus to make the analysis more effective. The cell micro-array technique coupled with microfluidics can satisfy this demand. For comparison, a short review of the techniques used to create cell micro-arrays was presented. Our new approach to create cell micro-arrays was to pre-pattern selected proteins on cell non-adhesive surfaces. Then, different cell types were seeded on these protein patterns to form well defined cell micro-arrays. So far, different protein patterning techniques such as photo-patterning and micro-contact printing have been developed. However, these techniques involve multistep treatments, use of aggressive solvents or have limited reproducibility. In this work, we chose the alternative piezoelectric printing method which allows creating protein patterns by just one-step

non-contact printing. This technique is reliable with high reproducibility. At the end of Chapter 1, the thesis arrangement and novelty of the work was summarised.

In second Chapter, the physical background and characteristics of different techniques used in this thesis work, such as light emitting diodes, optoelectronic tweezers, microfluidic technique as well as piezoelectric printing, were described in detail. In the first section of Chapter 2, the history and the principles of LED devices were presented. Then, the structure and emission characteristics of the micro-LEDs used in this work were described. The methods developed for controlling each individual LED pixel, such as matrix control, individual control and CMOS control, were also presented in this section. In the second section of Chapter 2, the operating principle of optoelectronic tweezers was introduced. Then, microfluidic technology, its history and applications were described. Finally, the piezoelectric printing technique, its capability in bio-sample printing and the particular printers used in this work were described.

The following Chapters presented the main research results. As described in Chapter 3, the CMOS driven green micro-LED devices were integrated with a photoconductive sample chamber for the first time to form miniaturised optoelectronic tweezers. The functionality of the miniaturised optoelectronic tweezers was successfully demonstrated by manipulating and trapping polystyrene beads and living cells. Previously, only bulky lasers and lamps emitting red or UV light projected onto a pattern generating device or video projector were used for this purpose. Chapter 3 also explained the way in which the OET system was assembled, described the forces induced in the OET and presented the results of manipulating the polystyrene beads and cells. The simulation of the forces

induced in the OET chamber allowed for explaining which forces dominated the particle and cell movement at different distances from the LED pixel. In addition, the simulation of the forces generated by using different LED pixels proved that LED pixel image sharpness on the photoconductive layer was the most important factor determining the strength of the forces acting on the cells.

In Chapter 4, a robust method to create protein patterns by piezoelectric printing was first presented. In order to form the following cell micro-pattern, the protein pattern was printed on a treated substrate surface which is non-adhesive for cells. The excellent stability and uniformity of the printed and washed collagen and the poly-L-lysine patterns were confirmed by microscopic images, XPS analysis and confocal auto-fluorescence images. The methods of controlling the pattern size by multiple printing or changing the solution concentration were also described in Chapter 4.

In Chapter 5, the collagen patterns created by the printing process described in Chapter 4 were used for subsequent cell seeding. The collagen pattern was seeded with NIH-3T3 fibroblasts and primary hepatocytes. The results confirmed the uniform cell micro-array formation, cell growth and proliferation. In addition, a toxicity test, EROD assay, was performed on patterned primary hepatocytes and this test confirmed that primary hepatocytes grown on these collagen patterns kept their enzymatic function. These results demonstrated that our technique is comparable with a standard multi-well test method, showing its potential for high throughput toxicity testing. Co-culture of hepatocytes and fibroblasts on printed collagen and poly-L-lysine patterns was also shown, which is particularly useful for supporting hepatocyte activity. Finally, the cell

pattern was successfully integrated with a microfluidic network. This work is important for the further development of this technology to achieve a miniaturised and high throughput cell analysis platform.

Chapter 6 described the work of integrating a micro-LED light source with a microfluidic component for localised and high resolution fluorescence detection. In this application, a blue, 450nm individually addressable micro-LED was used. In order to detect the weak fluorescence excited by this LED, a set of filters was used, namely excitation and emission filters. Thin film excitation filters were designed and fabricated in order to reject the strong excitation light. The function of the integrated device for exciting and detecting fluorescence of fluorescein solution was demonstrated. The results of projection of the micro-LED light into the microfluidic chamber via a small lens were also presented. It was demonstrated that this micro-system allowed for localised fluorescence excitation of polystyrene beads and stained Chinese Hamster Ovary cells inside the sample chamber. The diameter of an excitation spot in the chamber was the same as the LED pixel used, i.e. 70μm. Fluorescence emission from the excited object remained spatially confined to a similar area. More importantly, this micro-system allowed for excitation and detection of individual cells without interfering with the neighbouring ones.

Future works and prospects

The three micro-systems developed in this work offer exciting opportunities for new and wide applications. In the future, miniaturised OET will continually benefit from further

improvements of micro-LED device technology. The progress in LED materials and micro-LED device fabrication will allow for producing LED pixels with even higher light intensity, which will result in higher electric fields in the OET chamber. Using higher intensity LED devices would enable, for example, to simultaneously trap and excite trapped particle or cells and undertake their fluorescence life-time measurement. Moreover, by developing and using the next generation micro-LED devices with a smaller pixel pitch e.g. 100μm, the tweezing precision and controllability can be enhanced significantly. Furthermore, by using a lens holder with a modifiable focal distance, we will be able to adjust the size of the illumination spot in the OET sample chamber. In the longer term, it is possible to further integrate the OET with micro-LEDs, for example, to share the electrodes.

The miniaturised OET device can be developed to a portable diagnostic tool which is able to carry out dynamic differentiation between different cells thanks to their different electrical properties. It has already been proven that the cancer and healthy cells have different permittivity [1]. Similarly, healthy and unhealthy embryos [2], parasites and lymphocytes in blood [3] and stem cells in different stages of development [4], all have different electrical properties and thus can be sorted and separated by OET devices. Further development of the miniaturised OET devices for these applications is currently under way.

Likewise, further development of the primary hepatocytes analysis system is also ongoing. The next step is to make and place a hepatocyte array inside the microfluidic chamber, optimise the toxicity assay conditions and carry out the toxicity test.

Moreover, there is a scope to combine the micro-systems developed in this work. Indeed, this concept formed the background to this PhD. For example, an integrated micro-LED device could be used to locally excite the cell pattern inside the microfluidic chamber. This will further reduce the size of the cell assay platform and by this way, the number of cells exposed to light radiation will decrease considerably. Last but not least, cell patterns can be integrated with a miniaturised OET device. Then, the patterned-light-induced electric field can be used for reversible electroporation of cell membrane in adherent cell cultures. This will allow for selective gene transfection. Additionally, electroporation could also be used for selective cell lysis for gene analysis, which to date has only been made with laser capture micro-dissection (laser ablation) [5].

References

1. R. Pethig, "Review Article-Dielectrophoresis: Status of the theory, technology, and applications," Biomicrofluidics **4**, 022811 (2010).
2. J. K. Valley, P. Swinton, W. J. Boscardin, T. F. Lue, P. F. Rinaudo, M. C. Wu, and M. M. Garcia, "Preimplantation Mouse Embryo Selection Guided by Light-Induced Dielectrophoresis," PLoS One **5**, e10160 (2010).
3. P. Gascoyne, C. Mahidol, M. Ruchirawat, J. Satayavivad, P. Watcharasit, and F. F. Becker, "Microsample preparation by dielectrophoresis: isolation of malaria," Lab on a Chip **2**, 70-75 (2002).
4. R. Pethig, A. Menachery, S. Pells, and P. De Sousa, "Dielectrophoresis: A Review of Applications for Stem Cell Research," J. Biomed. Biotechnol., 182581 (2010).
5. N. A. Pagedar, W. Wang, D. H. C. Chen, R. R. Davis, I. Lopez, C. G. Wright, and K. N. Alagramam, "Gene expression analysis of distinct populations of cells isolated from mouse and human inner ear FFPE tissue using laser capture microdissection - a Technical report based on preliminary findings," Brain Res. **1091**, 289-299 (2006).

Appendix

Publication list

Publications

[1] “Generation of primary hepatocyte microarrays by piezoelectric printing" A Zarowna-Dabrowska, EO McKenna, ME Schutte et al.; Colloids and Surfaces B: Biointerfaces, Volume: 89 Pages: 126-32 Published: 2012-Jan-1 (Epub 2011 Sep 17)

[2] “Miniaturized optoelectronic tweezers controlled by GaN micro-pixel light emitting diode arrays“, A Zarowna-Dabrowska, SL Neale, D Massoubre et al. OPTICS EXPRESS Volume: 19 Issue: 3 Pages: 2720-2728 Published: JAN 31 2011

[3] “Star-shaped oligofluorene nanostructured blend materials: controlled micro-patterning and physical characteristics”, M Wu, E Gu, A Zarowna et al.; APPLIED PHYSICS A-MATERIALS SCIENCE & PROCESSING Volume: 97 Issue: 1 Pages: 119-123 Published: OCT 2009

Conference Presentations

[1] “Miniaturised Optoelectronic Tweezers Controlled by GaN Micro Light Emitting Diode Arrays“, A Zarowna-Dabrowska, SL Neale, D Massoubre et al.; Oral presentation at 23RD ANNUAL MEETING OF THE IEEE PHOTONICS SOCIETY, Pages: 102-103; Denver, CO, USA; NOV 07-11, 2010

[2] “Micromanipulation of beads and CHO cells using micro light emitting diode arrays to control a miniaturised optoelectronic tweezers device”, A Zarowna-Dabrowska, SL

Neale, D Massoubre et al.; Poster presentation at Photon10 Conference, 22-26 August 2010, Southampton, UK

[3] “Generation of Collagen Micropatterns by Printing”, A Zarowna, ED Gu, EO McKenna et al.; Poster presentation at PGBioMed Conference, 12-14 July 2009, Oxford, UK

[4] “Generation Of Protein Micropattern By Piezoelectric Printing”, A Zarowna, ED Gu, EO McKenna et al.; Poster presentation at Tissue & Cell Engineering Society Conference, 8-10 July 2009, Glasgow, UK; Proceedings in European Cells and Materials Vol. 18. Suppl. 2, 2009 (page 115) ISSN 1473-2262

[5] “Controlled micro-patterning of highly-fluorescent truxene-oligofluorene nanostructured blends” M Wu, D Elfstrom, Z Gong et al.; IEEE Lasers and Electro-Optics Society, 2008. LEOS 2008. 21st Annual Meeting of the; 9-13 Nov. 2008; 634-635; DOI: 10.1109/LEOS.2008.4688778

[6] “Micro-patterning of nano-fluorescing truxene blend materials via drop-on-demand inkjet printing” M Wu, D Elfstrom, Z Gong et al.; The 3rd International Colloquium on Integrated Manufacture by Printing (IMP). 14 - 15 April 2008, Gregynog, Newtown, Powys, UK

[7] “Beam Intensity Profiles in Flip-Chip InGaN/GaN Micro-LED Arrays”, P Kelm, D Massoubre, PE Jessop et al.; Poster presentation at UK NITRIDES CONSORTIUM, Annual Conference, University of Strathclyde, Glasgow, UK; 9th-10th January 2008